VOLUME 36 MAY 1958 NUMBER 5

Canadian Journal of Physics

Published by THE NATIONAL RESEARCH COUNCIL

OTTAWA CANADA

CANADIAN JOURNAL OF PHYSICS

(Formerly Section A, Canadian Journal of Research)

Under the authority of the Chairman of the Committee of the Privy Council on Scientific and Industrial Research, the National Research Council issues THE CANADIAN JOURNAL OF PHYSICS and five other journals devoted to the publication, in English or French, of the results of original scientific research. Matters of general policy concerning these journals are the responsibility of a joint Editorial Board consisting of: members representing the National Research Council of Canada; the Editors of the Journals; and members representing the Royal Society of Canada and four other scientific societies.

Manuscripts for publication should be submitted to Dr. H. E. Duckworth, Editor, Canadian Journal of Physics, Hamilton College, McMaster University, Hamilton, Ontario.

(For instructions on preparation of copy, see **Notes to Contributors** (inside back cover).)

Proof, correspondence concerning proof, and orders for reprints should be sent to the Manager, Editorial Office (Research Journals), Division of Administration and Awards, National Research Council, Ottawa 2, Canada.

Subscriptions, renewals, requests for single or back numbers, and all remittances should be sent to Division of Administration and Awards, National Research Council, Ottawa 2, Canada. Remittances should be made payable to the Receiver General of Canada, credit National Research Council.

The journals published, frequency of publication, and prices are:

Canadian Journal of Biochemistry and Physiology	Monthly	$3.00 a year
Canadian Journal of Botany	Bimonthly	$4.00 a year
Canadian Journal of Chemistry	Monthly	$5.00 a year
Canadian Journal of Microbiology	Bimonthly	$3.00 a year
Canadian Journal of Physics	Monthly	$4.00 a year
Canadian Journal of Zoology	Bimonthly	$3.00 a year

The price of regular single numbers of all journals is 75 cents.

Canadian Journal of Physics

Issued by THE NATIONAL RESEARCH COUNCIL OF CANADA

VOLUME 36 MAY 1958 NUMBER 5

MAGNETORESISTANCE AND FIELD DEPENDENCE OF THE HALL EFFECT IN INDIUM ANTIMONIDE[1]

GASTON FISCHER AND D. K. C. MACDONALD

ABSTRACT

Magnetoresistance and Hall-effect measurements in InSb are described. This semiconductor has charge carriers with sufficiently long mean free paths, l, that it is possible, even at room temperature and with available magnetic fields, to obtain l/r values considerably greater than unity, r being the orbital radius of a charge carrier moving in the applied magnetic field. The classical two-band theory has been found to account rather well for the results up to the highest magnetic fields employed. A review of the underlying assumptions of this theory is presented, and simple formulae are derived which allow the concentrations and mobilities of both types of carriers to be calculated from the magnetic field dependence of the resistivity, ρ_H, and of the Hall-constant, A_H. The parameter $\Lambda \equiv [(A_H - A_0)/A_0]/[(\rho_H - \rho_0)/\rho_0]$ provides a useful means to check the consistency of the theory and can give some indication of the variation of the mobilities with the magnetic field.

1. THE THEORY OF THE TWO-BAND SEMICONDUCTOR

We shall describe experiments carried out on InSb, a semiconductor whose charge carriers have sufficiently long mean free paths l that it is possible, even at room temperature, to achieve l/r values greater than unity* (r is the orbital radius of a charge carrier moving in the applied magnetic field H). Indeed the resistance and the Hall effect are highly field-dependent (see Figs. 1 and 2) and immediately call to mind the theoretical predictions of the two-band model (Wilson 1936). This model has often been proposed to account for the behavior of *metals* where the two bands are usually referred to as s- and d-bands respectively, being first suggested for the transition metals, although in fact it is applied more generally. However, the success of this model with metals has been rather limited, for in most metals the magnetoresistance is found to be rather linear with H and the Hall coefficient shows little dependence on H (cf., for example, Kapitza 1929; Wilson 1936, 1953; Chambers 1956; MacDonald 1957). The discrepancy of experiments

[1]Manuscript received January 14, 1958.

Contribution from the Division of Pure Physics, National Research Council, Ottawa, Canada.

Issued as N.R.C. No. 4683.

*It should be noted that the small effective mass, m, of the carriers contributes to the large values of l/r, remembering that $l/r = -eH\tau/mc = b(H/c)$, where τ is the collision time and b the mobility.

on metals with theoretical predictions was recognized already by Sommerfeld and Bethe (1933) in their well-known Handbuch article. On the other hand, as we shall show, the two-band model appears to account on the whole remarkably well for the conductive behavior of InSb. In view of the very considerable

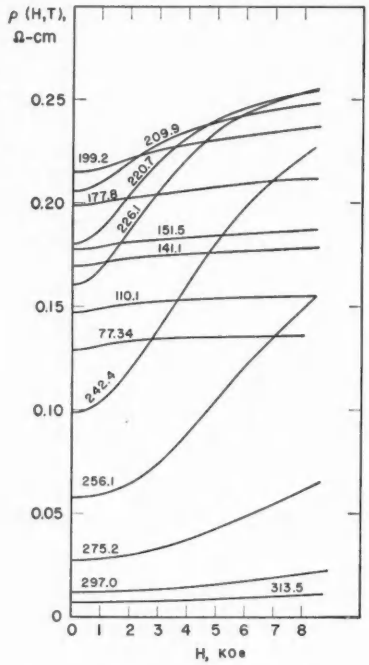

FIG. 1. Resistivity of p-type InSb as a function of the magnetic field. The figures on each curve give the temperature in degrees Kelvin.

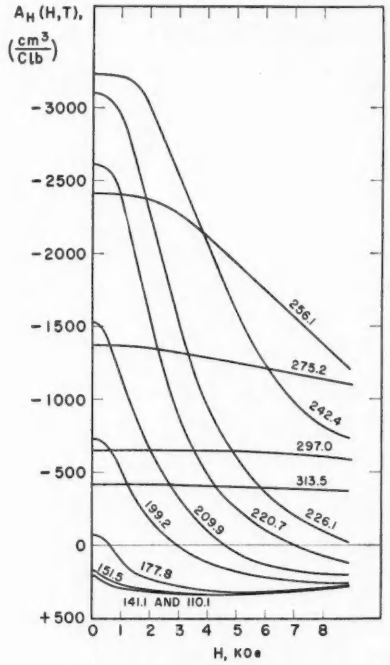

FIG. 2. Hall coefficient of p-type InSb as a function of the magnetic field. The figures on each curve give the temperature in degrees Kelvin.

amount of work already carried out by others on InSb and related compounds, we do not wish to claim any great originality for our measurements, but wish to present a discussion of Wilson's two-band theory and to show that this theory appears reasonably capable of accounting for the galvanomagnetic properties of a semiconductor such as InSb, even in magnetic fields for which l/r is much greater than 1. It thus appears that the basic assumptions of the two-band model are quite well fulfilled in InSb, with possibly one exception: the assumption that the mobilities of the charge carriers are independent of H. The present work does not extend to fields above 8 kOe., but a few measurements at much higher magnetic fields have been presented in an earlier note (Fischer and MacDonald 1957) and the conclusions to be drawn do not differ from those of the present paper. The upper limit of 8 kOe. in the present

work is still well above the critical field giving $l/r = 1$ for the conduction electrons.

To analyze a system of two *non-interacting* and *isotropic* bands, with arbitrary densities of electrons and holes, let us follow Chambers (1952), who has shown that if σ_1 and σ_2 are the conductivities which would be found for each band *separately* in the field H, and A_1 and A_2 the corresponding *separate* Hall coefficients, then the conductivity of the complete system will be:

$$\sigma = \frac{(\sigma_1+\sigma_2)^2+H^2\sigma_1^2\sigma_2^2(A_1+A_2)^2}{\sigma_1+\sigma_2+H^2\sigma_1\sigma_2(\sigma_1A_1^2+\sigma_2A_2^2)} \tag{1.1}$$

and its Hall coefficient:

$$A_H = \frac{\sigma_1^2A_1+\sigma_2^2A_2+H^2\sigma_1^2\sigma_2^2A_1A_2(A_1+A_2)}{(\sigma_1+\sigma_2)^2+H^2\sigma_1^2\sigma_2^2(A_1+A_2)^2}. \tag{1.2}$$

If then we assume constant mobilities b_1 and b_2 in each band (independent of H and energy, so that $\sigma_1 = -n_1eb_1$ and $A_1 = 1/n_1ec$, and correspondingly for band 2), we have

$$\sigma = -e\frac{(n_1b_1+n_2b_2)^2+(H/c)^2(n_1-n_2)^2b_1^2b_2^2}{n_1b_1+n_2b_2+(H/c)^2(n_1b_2+n_2b_1)b_1b_2}, \tag{1.3}$$

$$A_H = \frac{1}{ec}\frac{n_1b_1^2-n_2b_2^2+(H/c)^2(n_1-n_2)b_1^2b_2^2}{(n_1b_1+n_2b_2)^2+(H/c)^2(n_1-n_2)^2b_1^2b_2^2}. \tag{1.4}$$

Note that if we set $n_2 = 0$ or $b_2 = 0$ these results reduce to the single-band formulae $\sigma = -n_1eb_1$ and $A_1 = 1/n_1ec$.

In order to simplify the comparison between theory and experiment we shall transform (1.3) and (1.4) so as to express:

ρ or ρ_H	(the resistivity) in Ω-cm.,
A_H	in cm.^{3}/coulomb,
$n_{1,2}$	in cm.$^{-3}$,
$b_{1,2}$	in cm.^{2}/v-sec.,
H	in oersteds,
e	in coulombs (-1.60×10^{-19} Clb.).

These transformed formulae then read:

$$\rho = -\frac{1}{e}\frac{n_1b_1+n_2b_2+(10^{-8}H)^2(n_1b_2+n_2b_1)b_1^2b_2^2}{(n_1b_1+n_2b_2)^2+(10^{-8}H)^2(n_1-n_2)b_1^2b_2^2}, \tag{1.5}$$

$$A_H = \frac{1}{e}\frac{n_1b_1^2-n_2b_2^2+(10^{-8}H)^2(n_1-n_2)b_1^2b_2^2}{(n_1b_1+n_2b_2)^2+(10^{-8}H)^2(n_1-n_2)^2b_1^2b_2^2}. \tag{1.6}$$

It is of interest to note that if we define the parameter

$$\Lambda \equiv \left(\frac{A_H-A_0}{A_0}\right)\Big/\left(\frac{\rho_H-\rho_0}{\rho_0}\right), \tag{1.7}$$

then on this model

$$\Lambda = (n_1-n_2)b_1b_2/(n_1b_1^2-n_2b_2^2) \tag{1.8}$$

and is thus independent of H. This single parameter Λ gives a very convenient means of checking the validity of the theory proposed. Let us briefly review the assumptions underlying this treatment. The requirement of *non-interaction between the bands* should be fairly well realized, owing to the low concentrations of charge carriers. For the same reason we might expect that the assumption of *constant mobilities in each band* would be acceptable as the electrons will all be near the bottom of the conduction band and all holes near the top of the valence band. With metals, however, these two conditions, or their equivalent, may be less justifiable and this may contribute to the inadequacy of the two-band model when applied to metals. The *isotropy condition* is known to be fairly well realized in InSb (cf. Pearson and Tannenbaum 1953; Hrostovski and Tannenbaum 1954; Dresselhaus *et al.* 1955; Herman 1955). We suppose therefore that the dependence of Λ on H should tell us something about our assumption that *the mobilities are independent of H*. We shall show in an appendix that, with reasonable assumptions, if Λ should vary owing to variations of the mobilities with H, then we expect that

$$\Lambda_{(H=0)} \geqslant \Lambda_{(H=\infty)}. \tag{1.9}$$

2. DERIVATION OF THE CHARGE-CARRIER CONCENTRATIONS AND THEIR MOBILITIES FROM THE FUNCTIONS $\rho(H, T)$ AND $A_H(H, T)$

Starting from the functions described by (1.5) and (1.6) we shall derive n_1, n_2, b_1, and b_2. To do so let us write

$$\rho(H, T) = \frac{1}{-e}\frac{A+(10^{-8}H)^2B}{C+(10^{-8}H)^2D}, \tag{2.1}$$

$$A_H(H, T) = \frac{1}{e}\frac{E+(10^{-8}H)^2F}{G+(10^{-8}H)^2K} \tag{2.2}$$

and we can then set up our problem so as to solve the following system of equations:

$$n_1b_1+n_2b_2 = A\ (=\sqrt{C}=\sqrt{G}), \tag{2.3}$$

$$(n_1b_2+n_2b_1)b_1b_2 = B, \tag{2.4}$$

$$(n_1-n_2)^2b_1^2b_2^2 = D = K, \tag{2.5, 2.5'}$$

$$n_1b_1^2-n_2b_2^2 = E, \tag{2.6}$$

$$(n_1-n_2)b_1^2b_2^2 = F. \tag{2.7}$$

It is seen at once that for the above system to be compatible an additional condition must be satisfied among the coefficients A to K, namely:

$$(AB-D)\sqrt{D}+A^2F-ED = 0. \tag{2.8}$$

Equations (2.5′) and (2.8) express a strong interconnection between the predicted behavior of the resistivity, $\rho(H, T)$, and the Hall coefficient, $A_H(H, T)$. If the two-band model considered here is to account for the behavior of InSb, then these two relations should be satisfied by our experimental results.

Assuming that our sample is p-type, as in the present work, we know that n_1-n_2 is always negative, and the solution of our system may be conveniently written as:

$$n_1 = \frac{A^2}{2\alpha}\left[\frac{2\alpha-\sqrt{D}.(\delta-\beta)}{\delta}\right], \tag{2.9}$$

$$n_2 = \frac{A^2}{2\alpha}\left[\frac{2\alpha+\sqrt{D}.(\delta+\beta)}{\delta}\right], \tag{2.10}$$

$$b_1 = \frac{\delta+\beta}{2A}, \tag{2.11}$$

$$b_2 = \frac{\delta-\beta}{2A}, \tag{2.12}$$

with

$$\alpha = AB-E\sqrt{D}-D, \tag{2.13}$$

$$\beta = E+\sqrt{D}, \tag{2.14}$$

and

$$\delta = \sqrt{(\beta^2+4\alpha)}. \tag{2.15}$$

For an n-type specimen n_1-n_2 is always positive, and the corresponding formulae are obtained by changing the sign in front of $\sqrt{D}$ wherever it appears.

3. EXPERIMENTAL PROCEDURE ON InSb

Our sample was a polycrystalline prism cut from a zone-purified rod of InSb. It appeared to be p-type and was of the following dimensions:

length $d = 1.25$ cm. width $w = 0.37$ cm. thickness $t = 0.095$ cm.

The measurements of the magnetic field were made by an induction method, to an accuracy of about 2%. Resistivity and Hall voltage have been measured to an *absolute* accuracy of about 5% with a bridge described by Dauphinee and Mooser (1955), the error margin being mainly due to uncertainties in the geometry. The *relative* accuracy is raised to 2%, and for many parameters as well as for the calculation of Λ of (1.7) only this relative error matters. To measure the temperature we used a copper resistance thermometer made from wire calibrated by Dauphinee and Preston-Thomas (1954). It was possible to stabilize and measure the temperature within less than one degree, and the range covered extends from about 80° K. to 310° K. Fig. 3 gives a sketch of our sample holders.

Dividing the measured Hall voltage by H yields the Hall coefficient; this greatly increases the uncertainty in the low field values, and as a result the Hall coefficient is less well known than the resistivity. For this reason more experimental data at low magnetic fields would have been helpful; the measurements were performed at the following field values: $H = 0$, 0.125, 1.5, 2.0, 3.0, 4.0, 5.0, 6.0, 7.0, and 8.025 kOe. We have also to mention that below 170° K.

we had some contact difficulties and our results are much less reliable below that temperature.

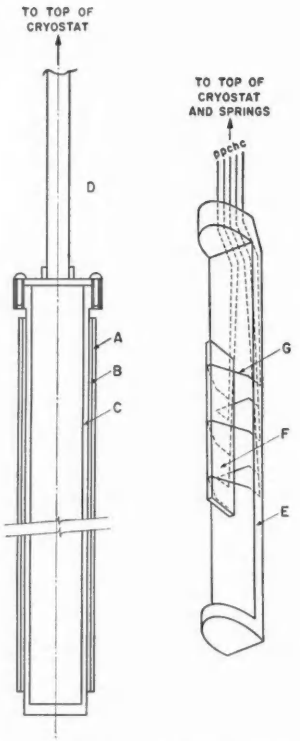

FIG. 3. Sample holder and container. A, non-inductive heater; B, non-inductive resistance thermometer; C, copper container; D, German-silver tubing; E, sample holder (lucite); F, sample; G, current lead; p, c, and h stand for potential, current, and Hall electrodes respectively.

4. DISCUSSION OF THE EXPERIMENTAL RESULTS AND THE COMPUTATION OF THE PARAMETERS A TO K

At first sight one expects the two-band model to account well for the curves displayed in Figs. 1 and 2. One feature for which the theory cannot account, however, strikes one immediately; this is the minimum value observed in A_H which, below 180° K., is found for fields of about 5 kOe. This behavior has also been found by Howarth *et al.* (1957), who have performed very extensive measurements of the Hall coefficient as a function of temperature and magnetic field, and try to account for their results in a somewhat more sophisticated way than we do here. The shape of the function $A_H(H, T)$, as given by (2.2), only allows extremal values of A_H versus H for fields equal to 0 or ∞, and consequently we expect our theory to be inadequate in the low-temperature branch.

Another discrepancy appears on either a plot of A_H versus H^2 (cf. Fig. 4), or of Λ versus H (cf. Fig. 10). Theory predicts behavior according to the *full* line of Fig. 4, while our measurements follow rather the *dashed* curve. Considering a typical set of measurements at 242.4° K. we notice a departure

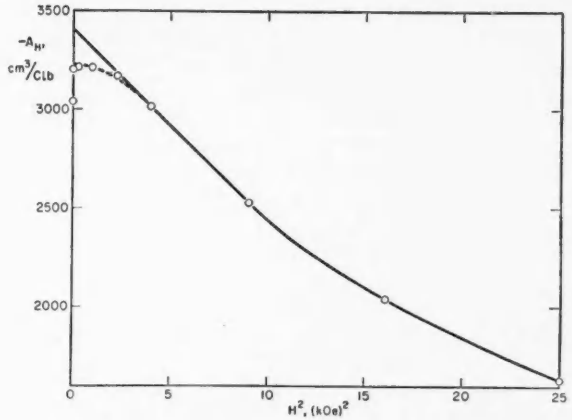

FIG. 4. Hall coefficient at 242.4° K. as a function of the square of the magnetic field. At low field strengths the experimental points fall below the theoretical curve (in full).

from the predicted behavior in the low-field range of 0 to 3 kOe., and it is interesting to compare these field values with those necessary to produce an l_1/r_1 ratio equal to unity for conduction electrons in InSb:

$$l_1/r_1 = H.b_1.10^{-8}, \tag{4.1}$$

where H is expressed in oersteds and b_1 in cm.^{2}/v-sec. Assuming for b_1 a reasonable value of 5×10^4 cm.^{2}/v-sec. (cf. Fig. 8) the field necessary to render l_1/r_1 equal to unity is thus:

$$H = (l_1/r_1)/(10^8/b_1) = 2 \text{ kOe}. \tag{4.2}$$

We have also seen in Section 1 that the parameter Λ defined by (1.7) should be independent of the magnetic field, unless the mobilities are themselves field dependent, and if they are, then we expect (cf. equation (1.9) above):

$$\Lambda_0 \geqslant \Lambda_\infty. \tag{1.9}$$

It is evident from Fig. 10 that a quite significant change of Λ takes place for fields below about 5 kOe. and that above that value Λ is reasonably constant. One might conclude from this behavior that there is a definite variation of the electron mobility when l_1/r_1 varies from zero to around unity, while no further change occurs above that value. We should note, however, that the magnetoresistance (cf. Fig. 5) seems unaffected by this variation. Furthermore, on the same type of plot the Hall-effect measurements of Howarth *et al.* (1957) do

seem to follow quite well the predictions of the simple theory, and we feel that more accurate measurements would be required to settle with certainty this question of mobility variation with magnetic field.

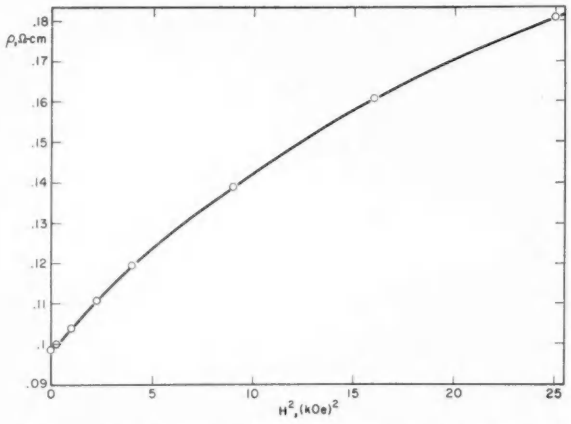

FIG. 5. Resistivity versus the square of the magnetic field at 242.4° K.

We now face the problem of working out the coefficients A to K of the field-independent model, from measurements which are in fact field dependent. One method of approach is to use those measurements in the neighborhood of zero magnetic field. This can be done in a simple manner, using the zero field slopes of the functions $\rho(H, T)$ and $A_H(H, T)$ plotted versus H^2. Let us denote by ϕ and ψ, respectively, these slopes. Using the formulae of section 2 above we then have

$$\phi = -ec^2A^3\left[\frac{\partial\rho(H, T)}{\partial H^2}\right]_{H=0} = AB-D, \tag{4.3}$$

$$\psi = ec^2A^4\left[\frac{\partial A_H(H, T)}{\partial H^2}\right]_{H=0} = A^2F-ED, \tag{4.4}$$

$$\psi/\phi = -\sqrt{D}, \tag{4.5}$$

and the formulae (2.13) to (2.14) can be rewritten as

$$\alpha = \phi+E\psi/\phi, \tag{4.6}$$

$$\beta = E-\psi/\phi. \tag{4.7}$$

In this way we can express n_1, n_2, b_1, and b_2 entirely by quantities corresponding to the field $H = 0$ and thus not directly affected by the field dependence of the mobilities. We have, however, lost the means of checking the *self-consistency* of the measurements by way of the relations (2.5′) and (2.8).

Before we became aware of the possible field dependence of the mobilities we computed the coefficients A to K directly and independently. Two methods

were used, a least mean square approach and the fitting of three arbitrary points. The various sets of parameters which we obtained in this manner did not agree well with one another; for example they were very dependent on the choice of the three arbitrary points when the latter method was used. In addition it was found that these parameters were not very consistent with the relations (2.5′) and (2.8). Several attempts to use them to calculate the n_j and b_j would often lead to imaginary hole mobilities b_2. It now appears clear why this may happen. On the other hand, using the parameters valid in the immediate proximity of the field $H = 0$ gives of course a poorer representation of the actual behavior of $\rho(H, T)$ and $\Lambda_H(H, T)$ over the whole field range.

When the ratio l/r increases beyond about unity it is known that the geometry of the sample can play an important part in magnetoresistance and Hall effect (Welker 1954; cf. also MacDonald 1957). We have not checked this point directly in the present work by using samples of different sizes, but it is possible that our rather short specimen exhibits geometry-dependent results. This might explain—at least in part—the apparent inconsistency of our parameters A to K with respect to the equations (2.5′) and (2.8).

5. COMPUTATION OF THE CHARGE-CARRIER CONCENTRATIONS AND THEIR MOBILITIES

With the parameters determined as described in the preceding section and the formulae (2.9) to (2.12), (4.6), (4.7), and (2.15) we obtain the results displayed in Figs. 6 to 9. The uncertainty of the parameters in the low and high temperature regions, due to the smaller variation with H, reflects itself in the greater uncertainty of the results. Nevertheless our results are in general agreement with the usual findings for InSb. Even the normally difficult, or often ignored, determination of b_2 turns out satisfactorily, and it is interesting to note that we find an increase of electron mobility with temperature, below 300° K., which appears to be characteristic of p-type InSb (Welker 1954).

6. THE BEHAVIOR OF Λ

Let us consider only that range of temperatures where reasonably accurate values of the parameters of $\rho(H, T)$ and $\Lambda_H(H, T)$ can be derived (say from 180° K. to 280° K.). As we have mentioned, it seems fairly definite, in spite of the considerable error margins, that all Λ-curves of Fig. 10 bend ultimately toward smaller absolute values when H tends toward zero. Thus we find, from our measurements, $\Lambda_0 > \Lambda_\infty$. And this limiting behavior is what one would expect if any change of the scattering mechanism takes place when the magnetic field increases. No marked change of Λ occurs above about 5 kOe. for fields up to some 40 kOe. The influence of holes, if their scattering cross section is field dependent, would appear only at very high fields because of their much lower mobility, and the change would presumably be spread over such a wide range that it might hardly be noticeable. In fact a value of $b_2 = 1500$ cm.^{2}/v-sec. gives 67 kOe. as the field for which $l_2/r_2 = 1$. Moreover, it appears that

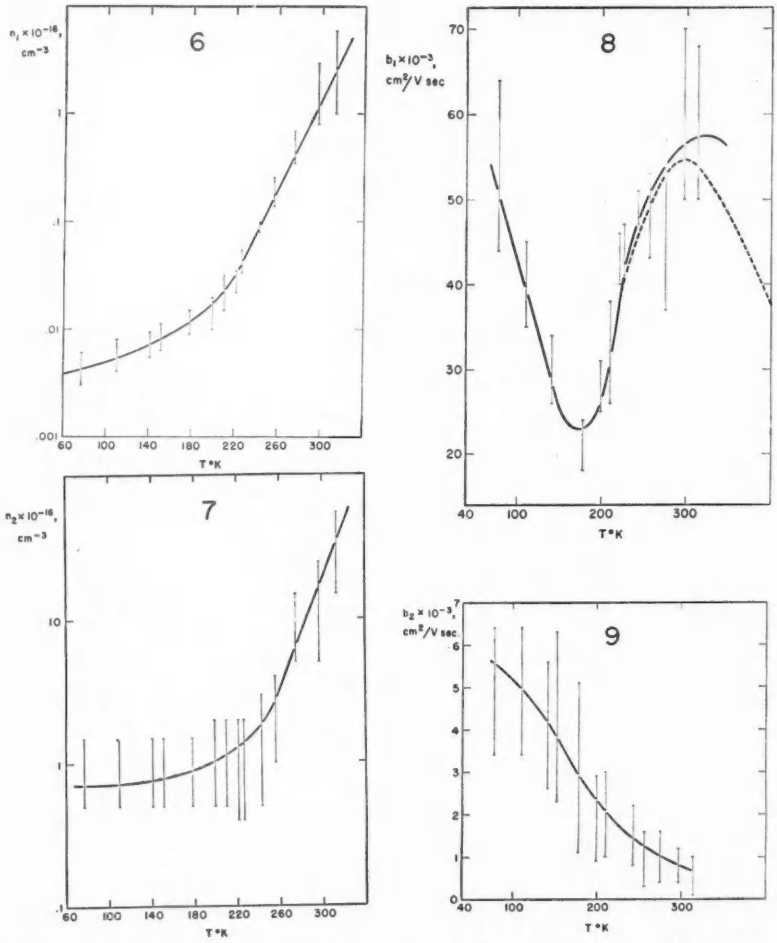

FIGS. 6, 7, 8, and 9. These graphs show respectively the electron concentration, the hole concentration, the electron mobility, and the hole mobility versus temperature. Possible error margins are indicated by vertical lines. The dashed curve of Fig. 8, above 220° K., indicates results published by Welker (1954).

significant changes in the energy gap and effective masses occur at such high fields (Burstein *et al.* 1956; Keyes *et al.* 1956), and it would then be difficult to distinguish between the many causes affecting the behavior of Λ.

7. CONCLUSIONS

1. Broadly speaking the simple two-band model of Wilson accounts well for the behavior of InSb.

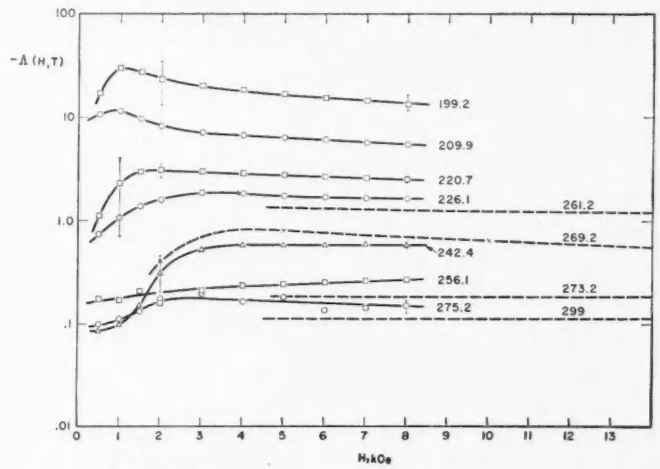

FIG. 10. $\Lambda \equiv [(A_H - A_0)/A_0]/[(\rho_H - \rho_0)/\rho_0]$. The full curves correspond to the present work. The dashed curves show part of the data of a previous note (Fischer and MacDonald 1957).

2. It is possible, in the frame of this model, to work out the numbers of both types of charge carriers and their mobilities from the observed functions $\rho(H, T)$ and $A_H(H, T)$. In fact either of the pairs $\rho(H, T)$ and $A_0 \equiv A_H(0, T)$ or $\rho_0 \equiv \rho(0, T)$ and $A_H(H, T)$ will suffice. The complete knowledge of both functions, however, allows us to check the theory more fully by way of the formulae (2.5′) and (2.8).

3. An analysis of the function $\Lambda(H, T)$ as defined by (1.7) gives some indication of the dependence of the charge-carrier mobilities on the magnetic field.

4. In order to carry out fully the analysis outlined under 2 and 3 above, the measurements must be performed with great accuracy. Our present measurements cannot claim that they are accurate enough for definite conclusions always to be drawn.

5. When the computation is carried out with the knowledge of the field dependence of only *one* of the two functions $\rho(H, T)$ and $A_H(H, T)$, more reliable results will generally be obtained if $\rho(H, T)$ is fully known, for ρ results from a direct measurement, while A_H is derived from the quotient of two measured quantities.

We should like to thank warmly Dr. J. W. Leech for helpful discussions and for checking calculations in this paper.

8. APPENDIX

We wish to consider, under reasonable simplifying assumptions, the limiting relationship of Λ_∞ to Λ_0 when some dependence of the charge mobilities on magnetic field is recognized.

We assume that the separate resistivities of each band, ρ_1 and ρ_2, and the separate Hall coefficients, A_1 and A_2, remain finite as $H \to \infty$. We assume further that

$$\rho_{1_H}/\rho_{1_0} = \rho_{2_H}/\rho_{2_0} \quad \text{and} \quad A_{1_H}/A_{1_0} = A_{2_H}/A_{2_0};$$

and in particular we write

$$\rho_{1_\infty}/\rho_{1_0} = \gamma \qquad \text{(where we assume } \gamma \geqslant 1\text{)}$$

and

$$A_{1_\infty}/A_{1_0} = \alpha \qquad \text{(where we assume } \alpha \leqslant 1\text{)}.$$

For the over-all resistivity we write

$$\rho_\infty/\rho_0 = Q > 1.$$

The condition that $Q > 1$ follows from the assumptions of our model, and is very generally observed. Possible exceptions may occur in InSb at very low temperatures (Fritzsche and Lark-Horovitz 1955; Frederikse 1957), and in some dilute alloys of a metal such as gold, also at very low temperatures (cf. e.g. MacDonald 1951, where references are given).

By some elementary algebra following equations (1.1) and (1.2) in the text one readily derives the relation

$$\Lambda_0 = \left\{\frac{\Lambda_\infty + (1-\alpha)/(Q-1)}{1+(1-\gamma)/(Q-1)}\right\}\frac{\gamma}{\alpha}. \tag{8.1}$$

It follows that

$$\Lambda_0 \geqslant \Lambda_\infty, \tag{8.2}$$

the equality sign obtaining only if $\alpha = \gamma = 1$, corresponding to the model with mobilities independent of the magnetic field. Reasonable values of α and γ which might be encountered (cf. Wilson 1953) are $\alpha \cong 0.8$ and $\gamma \cong 1.3$.

REFERENCES

BURSTEIN, E., PICUS, G. S., GEBBIE, H. A., and BLATT, F. 1956. Phys. Rev. **103**, 826.
CHAMBERS, R. G. 1952. Proc. Phys. Soc. (London), A, **65**, 903.
——— 1956. Proc. Roy. Soc. (London), A, **238**, 344.
DAUPHINEE, T. M. and MOOSER, E. 1955. Rev. Sci. Instr. **26**, 660.
DAUPHINEE, T. M. and PRESTON-THOMAS, H. 1954. Rev. Sci. Instr. **25**, 884.
DRESSELHAUS, G., KIP, A. F., KITTEL, C., and WAGONER, G. 1955. Phys. Rev. **98**, 556.
FISCHER, G. and MACDONALD, D. K. C. 1957. Phil. Mag. **2**, 1393.
FREDERIKSE, H. P. R. 1957. Private communication.
FRITZSCHE, H. and LARK-HOROVITZ, K. 1955. Phys. Rev. **99**, 400.
HERMAN, F. 1955. J. Electronics, **1**, 103.
HOWARTH, D. J., JONES, R. H., and PUTLEY, E. H. 1957. Proc. Phys. Soc. (London), B, **70**, 124.
HROSTOVSKI, H. J. and TANNENBAUM, M. 1954. Physica, **20**, 1065.
KAPITZA, P. 1929. Proc. Roy. Soc. (London), A, **123**, 292.
KEYES, R. J., ZWENDERLING, S., FONER, S., KOLM, H. H., and LAX, B. 1956. Phys. Rev. **104**, 1804 and 1805.
MACDONALD, D. K. C. 1951. Phil. Mag. **42**, 756. (Also: 1952. Phil Mag. **43**, 124.)
——— 1957. Proc. Fifth Int. Low Temp. Conference (Madison, Wis., U.S.A.); and Phil. Mag. **2**, 97 (1957).
PEARSON, G. L. and TANNENBAUM, M. 1953. Phys. Rev. **90**, 153.
WELKER, H. 1954. Physica, **20**, 893.
WILSON, A. H. 1936. The theory of metals, 1st ed. (Cambridge University Press, London).
——— 1953. The theory of metals. 2nd ed. (Cambridge University Press, London).

A THEORETICAL RATE–AMPLITUDE RELATION IN METEORIC FORWARD-SCATTERING[1]

C. O. HINES

ABSTRACT

The theory of the forward-scattering of radio waves by ionized meteor trails is applied to the development of a rate–amplitude relation. This relation expresses the anticipated occurrence rate of scattered signals which exceed a chosen amplitude level, as a function of that level. It is compared with preliminary observational data, and found to be in good agreement both qualitatively and quantitatively. Closest agreement is obtained only with an appropriate choice of two scaling factors. These provide an abstract of the observations in a form which is convenient for further study and interpretation.

INTRODUCTION

Radio signals scattered from ionized meteor trails exhibit a wide range of peak amplitudes, whose distribution can be determined directly from standard amplitude–time recordings, after appropriate analysis. The records are scaled at several amplitude levels in turn, and the number of excursions of the signal above each chosen level, during a fixed time interval, is noted and compared with the others. The 'rate–amplitude' relation thus obtained varies appreciably with the observational interval and with the radio frequency, but it always exhibits a preponderance of weak signals. The relation can be written in the form

$$N_c \propto A_c^{-a}, \tag{1}$$

where N_c is the number of signals which exceed the counting amplitude A_c, and a is a slowly varying function of A_c, lying usually in the range $1 < a < 4$.

It is the purpose of the present paper to determine the theoretical analogue of (1), on the basis of simplifying assumptions which can be applied readily to varying circumstances. These assumptions lead to the intermediate conclusion that

$$\begin{aligned} N_c &\propto A_c^{-1} \quad \text{for} \quad A_c < A_T, \\ N_c &\propto A_c^{-4} \quad \text{for} \quad A_c > A_T, \end{aligned} \tag{2}$$

where A_T is some transitional amplitude dependent on the position and orientation of individual trails. An integration over all observable positions and orientations then transforms the abrupt transition given in (2) into a smooth rate–amplitude relation comparable with (1).

The form of the derived relation is found to be in excellent agreement with preliminary observational data, and complete congruence can be established if the rates and amplitudes are scaled suitably. Variations in the observations can then be analyzed as variations of two scaling factors, to provide a useful abstract of the available information.

[1]Manuscript received December 19, 1957.
Contribution from the Radio Physics Laboratory, Defence Research Board, Ottawa, Canada. The work was performed under project PCC No. D48-95-11-01.

The specific development undertaken here is applicable only to forward-scatter experiments in which the transmitter and receiver are separated by many hundreds of kilometers. The corresponding backscatter analysis would follow the same pattern, however, while the general case of arbitrary transmitter–receiver separation could be treated in a similar but much more tedious fashion.

BASIC ASSUMPTIONS

It will be assumed that all signals observed in practice are scattered specularly—that is, that the incident and scattered rays make supplementary angles with the axis of the meteor trail in each case. This implies that the only trails of interest are those which lie tangent to one or other of a family of ellipsoids of revolution, drawn about the transmitter T and receiver R as common foci. The condition will be slightly altered, however, to simplify the problem of geometry: the 'cylindrical approximation' will be adopted, whereby the trails of interest are assumed to be those which lie tangent to one or other of a family of circular cylinders drawn about the T–R line as common axis. Predictions based upon this approximation have been compared with those based on the accurate condition in other statistical problems, and the agreement is generally good (Hines and Pugh 1956; Hines 1958). The approximation reduces the requisite labor by an order of magnitude at least, and in the present analysis it should be quite acceptable provided the transmitter–receiver separation is many hundreds of kilometers.

Two distinct classes of meteor trail, termed 'underdense' and 'overdense' respectively, are to be considered. The distinction lies initially in the degree of coupling which exists between the scattering electrons of the trail, or in the degree of free penetration of the trail by the incident wave, but it can be related to the line density of electrons along the trail.

The underdense trails, with the lower ionizations, provide signals in which the peak received power is

$$P_u = P_T K_1 q^2 G_T G_R \sin^2\alpha\, r_T^{-1} r_R^{-1} (r_T + r_R)^{-1} (1 - \cos^2\beta \sin^2\phi)^{-1} \tag{3}$$

(Eshleman and Manning 1954). Here, P_T is the transmitted power; K_1 is a function of the radio frequency alone (given below); q is the number of electrons per unit length of the trail at the point S where the specular condition is fulfilled; r_T and r_R are the distances TS and RS respectively; G_T and G_R are the corresponding antenna gains, relative to isotropic radiators; α is the angle between the incident (linearly polarized) electric vector at S and the direction SR; β is the angle between the axis of the trail and the plane TSR; and 2ϕ is the angle TSR.

The peak signal power received from overdense trails is given by a similar relation,

$$P_o = P_T K_2 q^{\frac{2}{3}} G_T G_R \sin^2\alpha\, r_T^{-1} r_R^{-1} (r_T + r_R)^{-1} (1 - \cos^2\beta \sin^2\phi)^{-1} \tag{4}$$

(Hines and Forsyth 1957), which differs only by virtue of the K factor and

the exponent of q. Although (4) is not as well founded as (3), it provides the only practical point of departure for the present analysis.*

It will be assumed that (3) applies exactly for all $q < q_T$, and that (4) applies exactly for all $q > q_T$, where q_T is a transitional value of q chosen to equalize (3) and (4):

$$q_T = (K_2/K_1)^{2/3}. \tag{5}$$

This value may be determined from the relations

$$\begin{aligned} K_1 &= \lambda^3 \mu_0^2 e^4/256\pi^4 m_e^2, \\ K_2 &= \lambda^3 \mu_0^{\frac{1}{2}} e/64\pi^{7/2}\epsilon^{\frac{1}{2}} m_e^{\frac{1}{2}} \end{aligned} \tag{6}$$

in which λ is the radio wavelength, μ_0 is the permeability of free space (in a rationalized system of units), e is the electronic charge, m_e is the electronic mass, and ϵ is the base of the natural logarithms. From these, $q_T = 0.75 \times 10^{14}$ electrons/meter. This estimate of the transitional q is somewhat less than others which are quoted frequently, and which are based on other criteria, but any single choice is artificial and therefore somewhat arbitrary. The criterion adopted here seems to be the one most suited to the present analysis, since it provides a continuous variation in peak received power. The discontinuity implicit in the assumed *rate* of variation cannot be expected in practice, of course. However, backscatter measurements made with high gain antennas during a period of shower activity, and therefore concerned primarily with trails which were localized in position and orientation, indicate that the transition is complete within a range of two-to-one in signal amplitude (cf. Kaiser 1953). The observed forward-scatter transition for sporadic meteors (random orientations, broad-beamed antennas) extends over an amplitude range of ten-to-one or more, so the foregoing approximation for the elementary transition is reasonable.

It will be assumed that the maximum line density of electrons, and the distribution of electrons along the trail, are governed by the relations

$$q_{\max} = K_3 m \cos \zeta \tag{7}$$

and

$$q = Z q_{\max}, \tag{8}$$

respectively, where K_3 is a constant, m is the mass of the parent meteoric particle, and ζ is the zenith angle of the meteor radiant. Z is a rapidly varying function of height and a very slowly varying function of trail orientation, derived by Herlofson (1947). Its dependence on orientation will be ignored here, and the form

$$Z = \frac{9}{4} \exp\left(\frac{h_0 - h}{H}\right) \cdot \left[1 - \frac{1}{3} \exp\left(\frac{h_0 - h}{H}\right)\right]^2 \tag{9}$$

*Equation (4) is equivalent to equation (18) of the paper cited. A correction to equation (17) of that paper should be noted: a bracket should be inserted at the end of the first line, and another at the start of the second line (following the multiplication sign).

employed by Eshleman (1957) will be adopted. Here, h_0 is a constant height at which maximum ionization is produced, H is the local scale height of the atmosphere, which will be taken to be 7 km., and h is the height variable.

It will be assumed that the number of meteoric particles with masses which exceed a given mass is inversely proportional to that mass (cf. Kaiser 1953). Further, it will be assumed that the radiant distribution of sporadic meteors is isotropic—that the meteoric particles are incident on the earth from all directions in equal numbers. This assumption is certainly faulty, and it precludes any possibility of predicting temporal variations in the rate–amplitude relation due to actual anisotropies, but it will serve the immediate purpose of this study.

The last two assumptions can be expressed mathematically with the aid of two polar coordinates, θ and ψ. These are used to locate radiant positions on that half of the celestial sphere which is visible from the mid-point of the forward-scatter path: θ measures the angle between the direction of the radiant point and the direction of the T–R axis, while ψ measures the angle between the vertical plane through the T–R axis and the inclined plane in which θ is measured. The isotropy condition implies that the number of meteor radiants which lie in the element $d\theta\, d\psi$ is proportional to the solid angle $\sin\theta\, d\theta\, d\psi$. When this is combined with the projection factor

$$\cos\zeta = \sin\theta\cos\psi \tag{10}$$

(neglecting earth curvature), it implies that the number of trails that pierce a horizontal element of area $dx\, dy$, with orientations in the range $d\theta\, d\psi$, is proportional to $\sin^2\theta\cos\psi\, d\theta\, d\psi\, dx\, dy$. (The angle θ now measures the angle between the axis of the trail and the T–R axis, but it has the same value as before.) Finally, when combined with the assumed mass distribution, these relations imply that

$$d^4N = K_4 m_c^{-1} \sin^2\theta\cos\psi\, d\theta\, d\psi\, dx\, dy, \tag{11}$$

where K_4 is a constant and d^4N is the number of trails which pierce the horizontal area $dx\, dy$ per unit time, with orientations in the range $d\theta\, d\psi$, produced by meteoric particles whose masses exceed some value m_c.

Of greater immediate interest is the corresponding number of trails whose ionizations at some specified height exceed some specific value, q_c. From (7), (8), and (10), this would be the number whose masses exceed

$$m_c = q_c K_3^{-1} Z^{-1} \csc\theta\sec\psi \tag{12}$$

and from (11) this number is given by

$$d^4N = K_3 K_4 Z q_c^{-1} \sin^3\theta\cos^2\psi\, d\theta\, d\psi\, dx\, dy. \tag{13}$$

Absolute estimates of rates will require the evaluation of the product K_3K_4, and this may be accomplished by integrating (13) over the limits $0 \leqslant \theta \leqslant \pi$, $-\pi/2 \leqslant \psi \leqslant \pi/2$, to get a total incidence rate on the element $dx\, dy$. The

integral should be evaluated at height h_0, where $Z = 1$, so that the maximum ionization densities will be involved:

$$(d^2N)_{h=h_0} = (2\pi/3)K_3K_4q_c^{-1}\,dx\,dy. \tag{14}$$

It has been estimated that a maximum ionization of 2×10^{14} electrons/meter corresponds to a fifth magnitude meteor (Millman and McKinley 1956), and that meteors of fifth magnitude or brighter are incident at an average rate which corresponds to 2×10^{-3} hr.$^{-1}$ km.$^{-2}$ (Watson 1941). The estimate

$$K_3K_4 \approx 2\times10^{11} \text{ electrons/meter/hr./km.}^2\text{/steradian} \tag{15}$$

may then be derived from (14).

DISTRIBUTION OF POTENTIALLY OBSERVABLE TRAILS

Potentially observable trails are taken to be those which satisfy the condition set out in the cylindrical approximation. For any given orientation, such trails are confined to a relatively small region of space, which will now be located. For this purpose, a Cartesian coordinate system may be introduced whose origin is at the mid-point of the T–R axis, whose positive x axis lies along the T–R axis in the direction $\theta = 0$, and whose positive z axis is directed vertically upwards. The positive y axis points in the direction $\theta = \pi/2 = -\psi$, in accordance with 'right-handed coordinate' conventions.

The h_0 height provides a convenient reference level, since the greatest part of the total ionization in meteor trails is confined to a narrow range of heights near it. This level may be specified by the surface $z = z_0$, where $z_0 = z_0(x, y)$ if a spherical earth is assumed and $z_0 =$ constant if a plane-earth approximation is adopted. (In the latter case, however, the approximation is improved by taking account of the depth of the mid-point of the T–R axis below the actual surface of the spherical earth, when converting an assumed h_0 into the corresponding z_0; z_0 exceeds h_0 by this depth.) For purposes of discussion, a constant z_0 will be assumed and trails will be located initially by the x and y coordinates of the point where they intersect the $z = z_0$ level.

In the cylindrical approximation, the point which corresponds to the specular point S lies in the inclined plane $y \tan \psi = z$ (cf. Hines 1955, with a change of coordinates). A trail which pierces the z_0 level at x, y then has its effective point of specularity at a level given by

$$z = y \cos\psi \sin\psi + z_0 \sin^2\psi \tag{16}$$

(see Fig. 1). With the aid of this relation, trails may be located by their z coordinate at the specular point rather than by their y coordinate at the z_0 level, and the conversion

$$dy = \csc\psi \sec\psi\, dz \tag{17}$$

may be introduced. Equation (13) then transforms into

$$d^4N = K_3K_4Zq_c^{-1} \sin^3\theta \cot\psi\, d\theta\, d\psi\, dx\, dz, \tag{18}$$

which gives the occurrence rate of trails whose orientations lie in the range $d\theta\, d\psi$, whose x coordinate at $z = z_0$ lies in the range dx, whose z coordinate

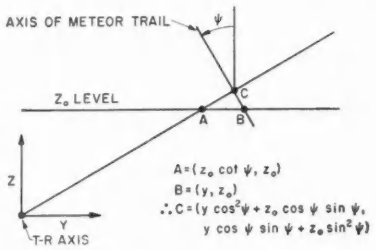

FIG. 1. Projection on the y, z plane, showing the geometry of meteor scattering when the cylindrical approximation is used to locate the specular point S and its projection C.

at the point of specularity lies in the range dz, and whose ionization density at that point exceeds q_c. Z is to be evaluated at the point of specularity, and it may be rewritten for this purpose as an explicit function of z:

$$Z = \frac{9}{4}\exp\left(\frac{z_0-z}{H}\right)\cdot\left[1-\frac{1}{3}\exp\left(\frac{z_0-z}{H}\right)\right]^2 \tag{19}$$

from (9), by setting $h_0-h = z_0-z$.

Equation (18) expresses the distribution of potentially observable trails in terms of the parameters θ, ψ, x, z, and q_c. (The last of these does not appear in differential form, since the specification that q exceeds q_c already contains an implicit integration over the distribution of ionizations.) It is now necessary to determine the fraction of these trails that will in fact be observable, and so to determine the distribution of observable trails.

DISTRIBUTION OF OBSERVABLE TRAILS

Observable trails are taken to be those which are detected by means of signals which exceed some counting level. The analysis may be developed in terms of a numerical amplitude, A, related to received power P by

$$A = (P/P^*)^{\frac{1}{2}}, \tag{20}$$

where P^* is some standard power. The counting level may then be specified by an amplitude level A_c.

When rewriting P_u and P_0 in terms of amplitude, as will now be done, two simplifications may be introduced. The angle β in (3) and (4) may be replaced by θ, since these two are equal when the cylindrical approximation is employed to locate the specular point. Again, it is permissible to evaluate both ϕ and the combination

$$g^2 = G_T G_R \sin^2\alpha\, r_T^{-1} r_R^{-1}(r_T+r_R)^{-1} \tag{21}$$

at $y \tan\psi = z = z_0$, and to ignore further variations of these quantities with y and z, since any such variations are minor compared with the dominant variation of q with z (and with y, along $y \tan\psi = z$).

With these substitutions, the peak amplitude received from an underdense trail may be expressed as

$$A_u = (P_T/P^*)^{\frac{1}{2}} K_1^{\frac{1}{2}} q g (1-\cos^2\theta \sin^2\phi)^{-\frac{1}{2}} \tag{22}$$

and that received from an overdense trail as

$$A_0 = (P_T/P^*)^{\frac{1}{2}} K_2^{\frac{1}{2}} q^{1/4} g (1-\cos^2\theta \sin^2\phi)^{-\frac{1}{2}}. \tag{23}$$

The transitional amplitude

$$A_T = (P_T/P^*)^{\frac{1}{2}} K_1^{-1/6} K_2^{2/3} g (1-\cos^2\theta \sin^2\phi)^{-\frac{1}{2}} \tag{24}$$

is obtained when $q = q_T$.

Observable trails, as already indicated, are those which provide amplitudes that exceed A_c. If $A_c < A_T$, a trail must have at the specular point a q which exceeds

$$q_u = A_c (P_T/P^*)^{-\frac{1}{2}} K_1^{-\frac{1}{2}} g^{-1} (1-\cos^2\theta \sin^2\phi)^{\frac{1}{2}} \tag{25}$$

if it is to be observable, by virtue of (22). The occurrence rate of potentially observable trails that have such q's is given by the distribution

$$d^4N_c = K_3 K_4 Z A_c^{-1} (P_T/P^*)^{\frac{1}{2}} K_1^{\frac{1}{2}} g (1-\cos^2\theta \sin^2\phi)^{-\frac{1}{2}} \sin^3\theta \cot\psi \, d\theta \, d\psi \, dx \, dz \tag{26}$$

by virtue of (18). On the other hand, if $A_c > A_T$, a trail must have a q which exceeds at the specular point

$$q_0 = A_c^4 (P_T/P^*)^{-2} K_2^{-2} g^{-4} (1-\cos^2\theta \sin^2\phi)^2 \tag{27}$$

if it is to be observable, by virtue of (23), and then the relation

$$d^4N_c = K_3 K_4 Z A_c^{-4} (P_T/P^*)^2 K_2^2 g^4 (1-\cos^2\theta \sin^2\phi)^{-2} \sin^3\theta \cot\psi \, d\theta \, d\psi \, dx \, dz \tag{28}$$

gives the corresponding distribution of observable trails.

From (26) and (28), it is apparent that the simple rate–amplitude relation described by (2) results from the assumptions which have been made, provided that attention is confined to trails characterized by θ, ψ, x, z parameters in an elementary range $d\theta \, d\psi \, dx \, dz$. The simple relation would continue to hold, even when applied to the whole array of trails, if the transitional amplitude were independent of these parameters. But such is not the case; $A_T = A_T(\theta, \psi, x)$ as given by (24). The general relation can then be obtained only by integrating (26) and (28) over ranges of θ, ψ, and x which vary with A_c. A height-integration must also be performed, although the relevant range in this case is effectively independent of A_c.

TOTAL NUMBER OF OBSERVABLE TRAILS

The height-integration may be completed first, as it is the least complicated. Z is the only factor in (26) or (28) which is still taken to be varying with height, and it may therefore be integrated separately:

$$\int_{z_1}^{\infty} Z \, dz = 9H/4, \tag{29}$$

where $z_1 = z_0 - H \ln 3$ is the lower limit of trail formation ($Z = 0$). Although $z = \infty$ is taken to be the upper limit of trail formation, the greater part of the integral is obtained from a region of about $2H$ in depth, and it is on this basis that height variations of ϕ and g may be ignored.

The θ-integration can be completed explicitly, so it will be undertaken next. For this purpose, it is convenient to introduce the quantity

$$u_T^2 \equiv \sec^2\phi\,[1-(P_T/P^*)K_1^{-1/3}K_2^{4/3}g^2A_c^{-2}], \tag{30}$$

which is a function of the pair $[\psi, x]$ through ϕ and g. Inspection will show that there exists some region of $[\psi, x]$ variation for which $u_T^2 > 1$, if only by virtue of vanishing antenna gain or distance attenuation in the g factor. This region, which will be termed Region I, would actually embrace the whole of the available range $[-\pi/2 \leqslant \psi \leqslant \pi/2, -\infty < x < \infty]$ if A_c were sufficiently large. This corresponds to the physical fact that only overdense trails can be detected above some particular counting level. Further inspection will show that, for lower A_c's, a Region II will exist in which $0 \leqslant u_T^2 \leqslant 1$, and that there may even exist a Region III in which $u_T^2 < 0$. The form of the θ-integral differs in each of these regions, and it is for this reason that the distinction is made.

The differential form (28) applies whenever $A_c > A_T$, or, by virtue of (24), whenever $\cos^2\theta$ is less than u_T^2. This is the case for all θ's, when $[\psi, x]$ lies in Region I, so in that region the θ-integration of (28) will extend over the entire range $0 \leqslant \theta \leqslant \pi$. In Region II, on the other hand, the condition obtains only for a limited range of θ's, and the integration of (28) extends only over that range. The remaining range of θ's is included by the integration of (26), which is applicable whenever $A_c < A_T$ and so whenever $\cos^2\theta > u_T^2$. Finally, in Region III, this last condition is obtained for all θ's, and the integration of (26) extends over the entire range $0 \leqslant \theta \leqslant \pi$.

The actual integration may be performed most conveniently after a change of variable to

$$u \equiv \cos\theta. \tag{31}$$

The range $0 \leqslant \theta \leqslant \pi$ then corresponds to a double traverse of the range $1 \geqslant u \geqslant 0$ for purposes of integration. The integrals take on standard forms:

$$V(\mathrm{I}) \equiv 2\int_1^0 (u^2-1)(1-u^2b^2)^{-2}du \tag{32}$$

$$= \frac{1+b^2}{2b^3}\ln\left(\frac{1+b}{1-b}\right) - \frac{1}{b^2}$$

in Region I,

$$V_0(\mathrm{II}) \equiv 2\int_{u_T}^0 (u^2-1)(1-u^2b^2)^{-2}du \tag{33}$$

$$= \frac{1+b^2}{2b^3}\ln\left(\frac{1+u_Tb}{1-u_Tb}\right) - \frac{1-b^2}{1-u_T^2b^2}\frac{u_T}{b^2},$$

$$V_u(\mathrm{II}) \equiv 2\int_1^{u_T}(u^2-1)(1-u^2b^2)^{-\frac{1}{2}}du \tag{34}$$

$$= V(\mathrm{III})-\frac{u_T(1-u_T{}^2b^2)^{\frac{1}{2}}}{b^2}-\frac{2b^2-1}{b^3}\arcsin(u_Tb)$$

in Region II, and

$$V(\mathrm{III}) \equiv 2\int_1^{0}(u^2-1)(1-u^2b^2)^{-\frac{1}{2}}du \tag{35}$$

$$= \frac{(1-b^2)^{\frac{1}{2}}}{b^2}+\frac{2b^2-1}{b^3}\arcsin b$$

in Region III. Each of the V's is a function of ψ and x through

$$b \equiv \sin\phi \tag{36}$$

and, in Region II, through u_T.

The integration over ψ and x cannot be performed explicitly, and recourse must be made to numerical computations at this point. Formally, the final integrals are

$$N_c(\mathrm{I}) = K_3K_4(9H/4)A_c{}^{-4}(P_T/P^*)^2K_2{}^2\iint_{\mathrm{I}} V(\mathrm{I})\, g^4\cot\psi\, d\psi\, dx, \tag{37}$$

$$N_c(\mathrm{II}) = K_3K_4(9H/4)A_c{}^{-4}(P_T/P^*)^2K_2{}^2\iint_{\mathrm{II}} V_0(\mathrm{II})\, g^4\cot\psi\, d\psi\, dx \tag{38}$$

$$+K_3K_4(9H/4)A_c{}^{-1}(P_T/P^*)^{\frac{1}{2}}K_1{}^{\frac{1}{2}}\iint_{\mathrm{II}} V_u(\mathrm{II})\, g\cot\psi\, d\psi\, dx,$$

$$N_c(\mathrm{III}) = K_3K_4(9H/4)A_c{}^{-1}(P_T/P^*)^{\frac{1}{2}}K_1{}^{\frac{1}{2}}\iint_{\mathrm{III}} V(\mathrm{III})\, g\cot\psi\, d\psi\, dx, \tag{39}$$

where the region of integration is indicated by I, II, or III. The total occurrence rate of observable trails is then

$$N_c = N_c(\mathrm{I})+N_c(\mathrm{II})+N_c(\mathrm{III}), \tag{40}$$

and its variation with A_c gives the theoretical rate–amplitude relation which has been sought.

COMPUTED RATE–AMPLITUDE RELATION

The computations required for the evaluation of (37)–(39) have been completed for one specific case which is realized closely by the experimental circuits operated by this laboratory. A transmitter–receiver separation of 1000 km. was assumed, and the z_0 surface was chosen to lie 100 km. above a spherical earth. The $\sin^2\alpha$ factor in g^2 was altered to a $\cos^2\gamma$ factor to take account of the selective reception of polarized fields; γ is the angle between the

polarization vector incident on the trail and the component of polarization accepted by the receiving antenna from the direction of the trail. The antennas employed experimentally are five-element yagis mounted horizontally, so it was assumed in the computations that the radiated and accepted components of polarization were horizontal. Again, the antennas are directed along the great circle path between the terminals, and mounted at a height intended to produce maximum gain over the mid-point of the path at the meteor level. The schematic antenna pattern employed in earlier work (Hines 1955) was therefore assumed in the computations, as a good approximation; a maximum free-space gain factor of 10 was increased to 40 by an assumed perfect ground reflection. The absolute values employed for H, K_1, K_2, and K_3K_4 were those which have been quoted above.

Examination of (30) and (37)–(39) will reveal that N_e is a function of A_e, λ, P_T, and P^* only in the combination $A_e\lambda^{-3/2}P_T^{-\frac{1}{2}}P^{*\frac{1}{2}}$, and this product might well be used as the independent variable in presenting the computed rate–amplitude relation. To illustrate representative values, however, it will be assumed that $\lambda = 7.5$ meters (frequency = 40 Mc./s.), $P_T = 100$ watts = the nominal radiated power in the experimental work, and $P^* = 2\times10^{-14}$ watts. The last choice permits A_e to be interpreted as a microvolt measurement across a 50-ohm receiver input resistance, since this is the standard unit used in presenting the experimental results.

The rate–amplitude relation obtained in these circumstances is presented as a continuous curve in Fig. 2. The amplitude scale alone would have to be altered in this figure if other λ's or P's were required, the rate scale alone would be altered if H or K_3K_4 were changed, while the whole relation would have to be recalculated if the path length, meteor height, polarization factor, or antenna pattern were changed radically.

Logarithmic scales are employed in Fig. 2, in order to exhibit clearly the limiting behavior at large and small A_e's. As A_e increases from transitional values, the simple relation $N_e \propto A_e^{-4}$ is approached. In fact, this relation obtains exactly when A_e exceeds some value A_P given by

$$A_P = (P_T/P^*)^{\frac{1}{2}}K_1^{-1/6}K_2^{2/3}\,[g \sec \phi]_{\max}, \tag{41}$$

where $[g \sec \phi]_{\max}$ is the maximum value attained by $g \sec \phi$ under variations of ψ and x. This amplitude, A_P, is the maximum amplitude attainable in a signal scattered from an underdense trail, when the trail has optimum orientation, position, and ionization ($x = 0 = \psi - \pi/2$ in the present case, $\theta = 0$, and $q = q_T$). When $A_e > A_P$, Region I exists alone and the integral contained in (37) is independent of A_e; hence, $N_e \propto A_e^{-4}$. The value of N_e corresponding to $A_e = A_P$ is

$$N_P = K_3K_4(9H/4)K_1^{2/3}K_2^{-2/3}[g \sec \phi]_{\max}^{-4}\, V(\mathrm{I})\, g^4 \cot \psi \, d\psi \, dx, \tag{42}$$

which, incidentally, is independent of λ and P_T. The point P, at which $A_e = A_P$ and $N_e = N_P$, is indicated in Fig. 2. In the circumstances assumed there, $A_P = 7.9$ μv. and $N_P = 0.022$ hr.$^{-1}$.

As A_e decreases, the simple form $N_e \propto A_e^{-1}$ is approached asymptotically

but never attained exactly. The asymptotes to the rate–amplitude curve in a logarithmic plot are shown by broken lines in Fig. 2. They have slopes of -1 and -4, and they intersect at a point Q which lies near the full curve in the region of greatest curvature.

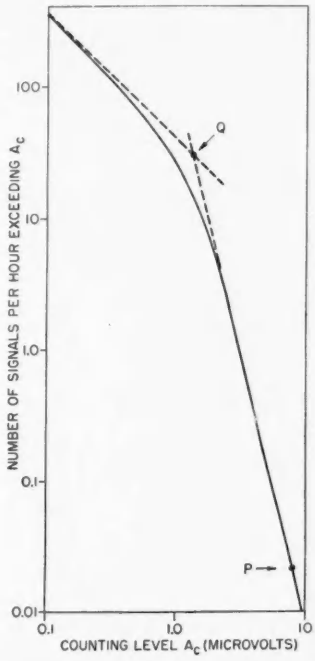

FIG. 2. Theoretical rate–amplitude relation, computed for the specific parameters quoted in the text.

As an abstract of an observed rate–amplitude variation, it appears that the position of the Q point would provide the most satisfactory single item of information. Not only does it lie in the vicinity of the major transition, but it is the only unique point that could be expected to emerge from an observational plot. Its coordinates are $A_Q = 1.3$ μv., $N_Q = 31$ hr.$^{-1}$, in the circumstances implicit in Fig. 2, although this value for A_Q would be altered by the factor $(\lambda/7.5)^{3/2}$ for observations at wavelength λ (meters).

COMPARISON OF THEORY AND EXPERIMENT

Several experimental VHF forward-scatter circuits have been operated by this laboratory over the past year or two, under the direction of Dr. E. L. Vogan. Dr. Vogan has kindly provided some preliminary rate–amplitude data obtained from his program, for comparison with the theory at this stage.

The data were obtained during the period Aug. 24–30, 1955, over the path

from Greenwood, N.S., to Ottawa, Ont., a distance of about 860 km. For purposes of analysis, each day was divided into four 6-hour intervals, and the data obtained from corresponding intervals on successive days were combined. The observed occurrence rate was corrected in the manner described by Vogan and Campbell (1957), to take account of the possible masking of one meteor signal by another. Three frequencies were employed: 49.98, 39.22, and 32.22 Mc./s. (λ = 6.0, 7.6, and 9.3 m., respectively).

The experimental data are displayed by vertical bars in Fig. 3. The length of each bar indicates the uncertainty in the measurement due to statistical fluctuations in the occurrence of meteors, and to an uncertainty in the correction factor.

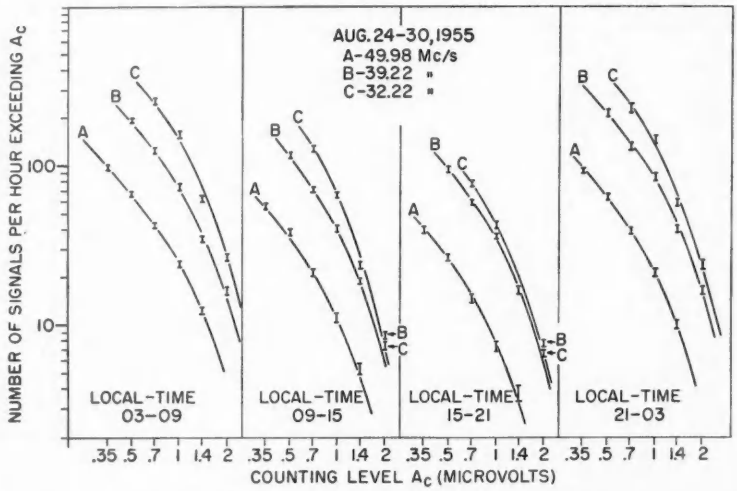

FIG. 3. Observed rates at various amplitudes, shown by vertical bars, with segments of the theoretical rate–amplitude relation shown in the positions of best fit.

A comparison of the scales in Fig. 3 with those in Fig. 2 makes evident immediately the general agreement between experiment and theory, insofar as the location of the main transition region is concerned. Segments of the theoretical curve have been superimposed on the experimental plots in Fig. 3, in the positions of best fit; the theoretical form of the variation is obviously confirmed.

Once the position of best fit of the curve has been established, the quantitative comparison of theory and experiment is most simply carried out by noting the location of the Q point of Fig. 2 in the coordinates of Fig. 3, and by comparing this location with that predicted theoretically. This is done in Table I.

It is interesting to speculate on the cause of the variations which occur in the columns of this table. The basic point must be made, however, that the

TABLE I

Period of observation (hours E.S.T.)	49.98 Mc./s.		39.22 Mc./s.		32.22 Mc./s.	
	A_Q (μv.)	N_Q (hr.$^{-1}$)	A_Q (μv.)	N_Q (hr.$^{-1}$)	A_Q (μv.)	N_Q (hr.$^{-1}$)
03–09	1.2	32	1.4	80	1.3	170
09–15	1.0	23	1.1	64	1.0	150
15–21	1.0	18	1.2	52	1.1	68
21–03	1.1	37	1.3	96	1.2	190
Predicted	0.93	31	1.3	31	1.8	31

theoretical predictions result from an assumed isotropic incidence pattern of meteors, whereas the actual incidence pattern is known to be anisotropic. Anisotropies could be included in the theory by introducing an appropriate weighting factor, $W(\theta, \psi)$, and they would lead to an altered rate–amplitude relation. This relation would vary with time, as the incidence pattern itself is varied. The P point would shift somewhat, and the Q point would shift even more. Accordingly, it would be premature to undertake any detailed examination of the variations of A_Q and N_Q until the anisotropies have been taken into account.

However, if Fig. 2 and Table I are accepted at face value, the following points may be made: Variations in the observed A_Q at a given frequency must result from variations in $[g \sec \phi]_{\max}$, from (41). Such variations might result from the diurnal changes which are known to occur in the heights of formation of trails. The differences between the mean observed A_Q's and the corresponding predicted A_Q's could result from errors in the assumed antenna gains or radiated powers. Variations in the observed N_Q, at a given frequency, almost certainly result primarily from diurnal variations in the absolute incidence rate. The frequency-variation of the observed N_Q's is not so readily explained, however. Within the limits set by the basic assumptions, it can result only from a variation in the antenna patterns employed, as is evident from (42). This is a plausible explanation, particularly since the antenna gains enter (42) in the rapidly-varying form $G_T^2 G_R^2$, but it may not be wholly satisfactory. As already indicated, the discrepancy cannot be assessed adequately until the anisotropic incidence patterns are incorporated in the theory.

FURTHER APPLICATIONS OF THE BASIC THEORY

Even at this stage, two further applications of the basic theory warrant consideration. They concern, respectively, the detection rate of overdense trails, and the spatial distribution of all observable trails.

The foregoing analysis was concerned with the detection rate of all trails, both overdense and underdense, but the detection rate of overdense trails alone can be computed by similar means. Obviously, whenever $A_c > A_T$ the contribution $d^4N_c^*$ to the observable overdense rate will equal the contribution d^4N_c to the total observable rate, since no underdense trails contribute to the latter: $d^4N_c^* = d^4N_c$ as given by (28). When $A_c < A_T$, however, the differen-

tial d^4N_c given in (26) represents both overdense and underdense contributions. It must be replaced by

$$d^4N_c^* = K_3K_4ZK_1^{2/3}K_2^{-2/3}\sin^3\theta\cot\psi\,d\theta\,d\psi\,dx\,dz, \tag{43}$$

which results from (18) when q_c is replaced by q_T. This is the differential which must be integrated over the range $u^2 > u_T^2$ in Regions II and III, to obtain a replacement for the second term in (38) and for the whole of (39).

The duration of an overdense signal is proportional to the value of q at the specular point. As q decreases towards q_T, the duration decreases to a fraction of a second and the signal form is not markedly different from the actual form of an underdense signal. For observational purposes, an overdense signal may not be recognized as such unless the pertinent q exceeds q_T by an appreciable factor. To permit ready comparison with observation, then, the theory may be applied to determine the detection rate of signals produced by a q equal to nq_T, say, where $n \geqslant 1$. In this case, the differential (28) would apply for $A_c > n^{1/4}A_T$, while the differential (43), reduced by the factor n, would apply when $A_c < n^{1/4}A_T$.

The detection rates of trails with $q > nq_T$ have been calculated for $n = 1$, 4, and 16, under the conditions described in the preceding section. These rates have been expressed as percentages of the total detection rate, and they are illustrated in this form in Fig. 4. A portion of the rate–amplitude curve has been superimposed, for direct comparison of the amplitudes at which the

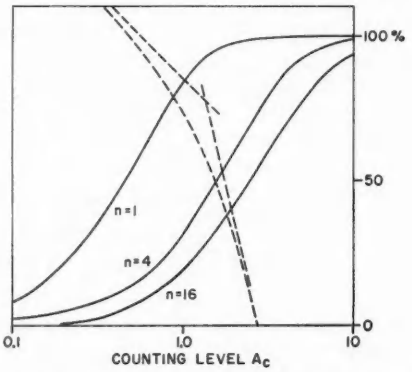

FIG. 4. Percentages of observable trails having $q > nq_T$ at the point of specularity, for $n = 1$, 4, and 16, shown as functions of the counting amplitude, with a portion of the rate–amplitude relation indicated by a broken curve for comparison.

different variations occur. The overdense fraction of observable trails has not been determined experimentally with any precision, but rough counts (probably comparable to $n = 4$ or 5) have indicated something of the order 20% to 40% in the region of most rapid transition. Such results are evidently consistent with the theoretical prediction.

The second application to be considered here concerns the spatial distri-

bution of observable trails. This problem has been treated extensively in the past (Eshleman and Manning 1954; Pugh 1956; Hines and Pugh 1956) for isotropic incidence, but always with the assumption that all trails could be treated as if underdense. That restriction can now be removed.

The analysis requires only a recasting of (37)–(40). In equations (37)–(39), ψ should be treated as a function of y, through the relation $y \tan \psi = z_0$ which locates observable trails. If these equations are added as in (40), before integration, then the form

$$N_e = \mathcal{N}(x, y)\, dx\, dy \tag{44}$$

will be obtained; $\mathcal{N}(x, y)$ gives the required distribution function.

This function varies with A_e in a complicated manner, making it impossible to give a single contour chart of even the relative distribution $\mathcal{N}(x, y)/\mathcal{N}_{\max}$. The same applies to the variation with antenna pattern. The relative distribution has been plotted in Fig. 5, under the conditions previously assumed, for three cases of interest. These arise when A_e is very large, intermediate,

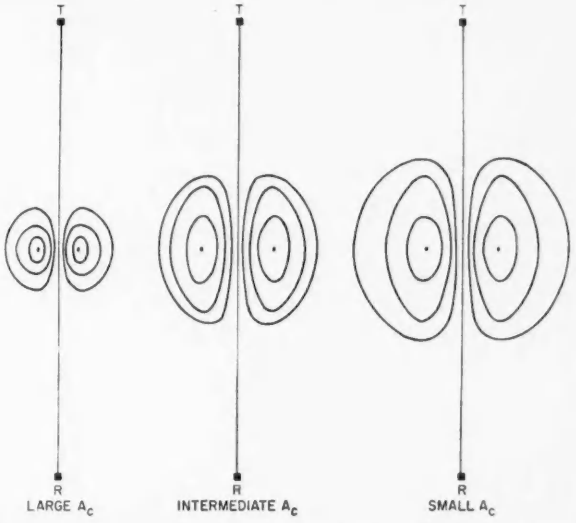

FIG. 5. Plan views of the transmission path, showing the spatial distribution of observable trails for three counting amplitudes. The charts indicate relative numbers only, with maxima at the point centers and successive contours at 75%, 50%, and 25% of these maxima.

and very small, respectively. More specifically, the first applies exactly for $A_e > A_P$, the last applies asymptotically as A_e is decreased below the main transition region, while the intermediate case applies during the main transition (at $A_e = 1$, in terms of the amplitude scale employed in Fig. 2). The results for A_e very small are equivalent to those that would be obtained from the earlier analysis (Hines and Pugh 1956) in combination with the present antenna pattern.

CONCLUSION

The theoretical rate–amplitude relation which has been derived here is in good agreement with observational data, both in the form of the variation and in the range of absolute values involved. It can be applied profitably to such data, to provide an abstract of the observations for further study and interpretation.

A quantitative comparison with some preliminary data has revealed a variation of numbers with frequency which would not have been anticipated. The discrepancy may arise from inadequate approximations to the actual antenna patterns, or it may result from erroneous basic assumptions. It merits further study.

Insofar as there is general agreement between theory and experiment, the relation (4) for the peak signal scattered by an overdense trail appears to be confirmed statistically and its value in the present type of analysis is established. This value is illustrated further by the development of new contour charts, which give the spatial distribution of observable trails in systems of low sensitivity.

REFERENCES

ESHLEMAN, V. R. 1957. J. Atmospheric and Terrest. Phys. **10**, 57.
ESHLEMAN, V. R. and MANNING, L. A. 1954. Proc. Inst. Radio Engrs. **42**, 530.
HERLOFSON, N. 1947. Repts. Progr. in Phys. **11**, 444.
HINES, C. O. 1955. Can. J. Phys. **33**, 493.
——— 1958. Can. J. Phys. **36**, 117.
HINES, C. O. and FORSYTH, P. A. 1957. Can. J. Phys. **35**, 1033.
HINES, C. O. and PUGH, R. E. 1956. Can. J. Phys. **34**, 1005.
KAISER, T. R. 1953. Advances in Phys. **2**, 495.
MILLMAN, P. M. and MCKINLEY, D. W. R. 1956. Can. J. Phys. **34**, 50.
PUGH, R. E. 1956. Can. J. Phys. **34**, 997.
VOGAN, E. L. and CAMPBELL, L. L. 1957. Can. J. Phys. **35**, 1176.
WATSON, F. G. 1941. Between the planets (The Blakiston Co., Philadelphia).

RADIOACTIVE ISOTOPES OF RHENIUM AND OSMIUM FORMED BY THE BOMBARDMENT OF RHENIUM WITH PROTONS[1]

J. S. Foster, J. W. Hilborn,[2] and L. Yaffe

ABSTRACT

Targets of normal rhenium, and of rhenium enriched in each stable isotope, were bombarded by protons in the energy range 10 to 80 Mev. These produced osmium and rhenium isotopes of masses 185, 183, 182, 181, and 180. After chemical separations, the gamma rays and conversion electrons were examined for half-lives, and to determine certain conversion coefficients. Independent isomers of Os^{183} with 10 and 15.4 hour half-lives were found. Gamma rays with energies 168.1, 850, and 1097 kev. were assigned to the 10 hour isomer, and gamma rays with energies 114.6, 168.7, and 382.4 kev. were assigned to the 15.4 hour isomer. In addition, the half-lives of Os^{185}, Os^{182}, and Re^{183} were observed to be 93.4 days, 21.9 hours, and 67.6 days respectively. Activities with half-lives of 19 hours, 23 minutes, 18 minutes, and 2 minutes were tentatively assigned to Re^{181}, Os^{181}, Re^{180}, and Os^{180} respectively.

INTRODUCTION

This investigation has removed some of the uncertainties in the mass assignments, half-lives, and decay schemes for several neutron-deficient nuclides of rhenium and osmium.

Active osmium isotopes were produced by (p, xn) reactions in targets of natural rhenium and of rhenium enriched in each of the stable isotopes. These were bombarded at suitable energies in the McGill cyclotron.

EXPERIMENTAL METHODS

(*1*) *Instruments*

The analyses and measurements have been made with a gamma-ray spectrometer and a Slatis–Siegbahn beta-ray spectrometer.

(*a*) *Gamma-Ray Spectrometer*

A $1\frac{1}{2}$ in. by 1 in. cylindrical NaI(Tl) crystal and Dumont 6292 photomultiplier were used with the necessary electronic equipment to make an automatic-scanning, automatic-recording, single-channel pulse-height spectrometer. The gate was generally kept at 2% of full scale and the resolution of the Cs^{137} 661 kev. gamma ray was 8%. Well-known gamma rays were used for the energy calibration and the energy was found to be proportional to pulse height. The 511 kev. annihilation radiation from Na^{22} was used as a reference to correct for possible channel-width variations. A convenient variety of scanning rates was available. The maximum energies measured were in the neighborhood of 1 Mev.

[1]Manuscript received in original form December 13, 1957, and in revised form February 7, 1958.

A joint contribution from the Radiation Laboratory, Department of Physics, and Radiochemistry Laboratory, Department of Chemistry, McGill University, Montreal, Quebec.

[2]Present address: Atomic Energy of Canada Limited, Chalk River, Ontario.

(*b*) *Beta-Ray Spectrometer* (*Slatis and Siegbahn 1949*)

This type of spectrometer has the distinct advantage of being effectively screened from external magnetic fields by its heavy cylindrical casing of Armco iron. Thus no compensation was necessary for the earth's field, or for the field of the cyclotron magnet.

The magnetic field within the spectrometer was generated by a symmetrical system of internal coils excited by a suitable range of currents. Thus electrons of given energy from a point source near one end of the axis may be caused to spiral around to a central ring focus, and to continue on to a small detector near the other end of the axis. The anthracene detector was 32 in. from the source and was screened from direct gamma rays by 1 foot of lead. This crystal was a polished button 0.200 in. in diameter and 0.030 in. thick. Light pulses from the crystal were carried through the heavy iron pole piece by a tapered lucite rod $8\frac{1}{2}$ in. long and 2 in. in diameter at the photomultiplier tube.

Sources were mounted on a 5 μg./cm.^{2} VYNS film (Pate and Yaffe 1955) which was spread over a $\frac{1}{4}$ in. hole in a thin lucite disk. Sources were deposited either as a solution or as a slurry, the final diameter being $\frac{1}{8}$ in. or less.

The instrument had an automatic scanning mechanism which continuously varied the magnet current. At the same time, the counting rate was measured with a counting-rate meter, and the resulting spectrum continuously recorded on a strip chart. Calibration was carried out with the well-known Cs^{137} and Th-*F* lines. Observations on other known lines from 500 to 10,000 gauss-cm. indicated a probable error in momentum of $\pm 0.2\%$, provided thin sources were used.

While the resolution (1.8%) was satisfactory, the transmission (0.3%) indicated that the shape of the magnetic field could be improved. Subsequent modifications increased the transmission to 1.4% with corresponding resolution 2.1% (Epp 1955).

(*2*) *Cyclotron Target Materials*

The rhenium bombarded was (*a*) normal rhenium metal (Re^{185}—37.07%, Re^{187}—62.93%) "spec-pure" grade obtained from Johnson, Matthey and Mallory, (*b*) rhenium metal enriched* in Re^{185} containing 85.38% Re^{185} and 14.62% Re^{187}, and (*c*) rhenium metal* enriched in Re^{187} containing 98.22% Re^{187} and 1.78% Re^{185}.

(*3*) *Target Mounting*

About 100 mg. rhenium metal was placed in a thin-walled tube (2S aluminum of wall thickness 0.0015 in.). The tube fitted conveniently into a C-shaped target holder which was bolted to the end of the water-cooled cyclotron probe.

(*4*) *Chemical Separation*

After the irradiation, the aluminum tube was split longitudinally and the

*We wish to express our thanks to the Stable Isotopes Research and Production Division of Oak Ridge National Laboratory, Oak Ridge, Tenn., for providing the enriched rhenium metal.

irradiated material transferred to a distilling flask which contained 1 mg. of osmium carrier as osmic acid. The sample was dissolved in nitric acid and—with slight heating in a current of air—osmium tetroxide was distilled into ice-cold 6 *N* sodium hydroxide. Osmium sulphide was then precipitated using hydrogen sulphide. The precipitate was washed and the slurry used as the source material.

This procedure was found to produce osmium free from rhenium and other contaminating activities. However, a careful check showed that only about 75% of the osmium was removed in this manner. For some unknown reason, the remainder did not oxidize readily to the octavalent state nor exchange with the osmium carrier.

To produce "line" sources for the 180° beta-ray spectrograph (see later), the separated osmium sulphide was dissolved in a minimum of concentrated hydrochloric acid plus hydrogen peroxide, and the resulting solution rendered just alkaline with sodium hydroxide. A 1 inch length of 0.008 in. aluminum wire, which had been thoroughly cleaned with carbon tetrachloride, was fastened to the end of the spectrograph holder and suspended for 1 hour in the osmium solution. Under these conditions osmium metal deposited electrochemically on the wire.

EXPERIMENTAL RESULTS AND DISCUSSION

(*a*) Os^{185}

The table of isotopes (Hollander, Perlman, and Seaborg 1953) lists Os^{185} with a "B" designation, i.e., element certain, mass assignment probable. This nuclide is characterized by 646 kev., 872 kev., and 879 kev. gamma rays as the main transitions after *K* capture, and has a reported half-life of 93.6 days (Johns, Nablo, and King 1957).

Targets of normal rhenium, and enriched Re^{185}, were separately bombarded with 10 Mev. protons and the gamma-ray transitions of the separated osmium examined with the gamma-ray spectrometer. The ratios of the observed gamma-ray intensities corresponded with the isotopic abundance of Re^{185} in the targets. Since the activity was shown chemically to be due to an osmium isotope, and the proton energy was 10 Mev., the reaction must be (p, n). The activity was thus identified as Os^{185}.

The assignment was further verified by bombardments of normal and enriched Re^{187} at 20 and 25 Mev. The ratios of the gamma-ray intensities now corresponded to the isotopic abundance of Re^{187}. At these proton energies the more probable nuclear reactions were $(p, 2n)$ and $(p, 3n)$. The former, however, would have produced stable Os^{184} from Re^{185} and stable Os^{186} from Re^{187}. The latter would have produced relatively short-lived Os^{183} from Re^{185} (see later) and Os^{185} from Re^{187}. It was concluded that the observed gamma rays at 645 kev. and 880 kev. should be assigned to Os^{185}.

The half-life was measured by observing the decay of the 645 kev. peak over a period of 300 days. In order to compensate for instrumental drifts the 511 kev. peak from the annihilation radiation of Na^{22} was used as a reference. The half-life of Os^{185} was found to be 93.4 ± 1.8 days by a least squares analysis,

based on a half-life of 2.6 years for Na^{22}, which confirms the value of Johns, Nablo, and King.

The K-conversion coefficient of the 645 kev. gamma ray was measured using the beta-ray spectrometer. Figure 1 (upper part) shows the K and L conversion peaks of the 645 kev. gamma ray at 573 kev. and 632 kev. The K-conversion line of the 660 kev. Cs^{137} gamma ray was then scanned in the same fashion (Fig. 1, lower part). A comparison of the same two sources was then made using the gamma-ray spectrometer to determine the intensity ratio

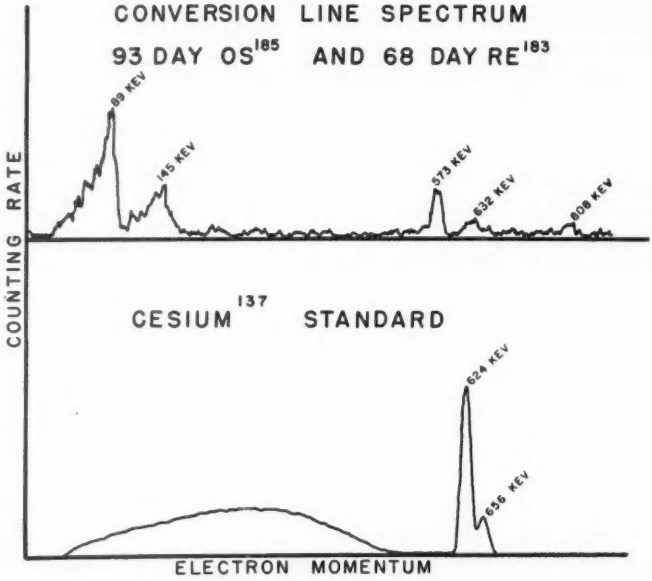

FIG. 1. Conversion line spectrum from osmium fraction of normal rhenium target exposed to 25 Mev. protons. The spectrometer scan was made 1 week after chemical separation to allow short-lived products to decay. Hence the source contained Os^{185}, and Re^{183}, the decay product of 10 hour and 15 hour Os^{183}. The lower spectrum is from a Cs^{137} standard used in measuring the conversion coefficient of the 650 kev. gamma ray from Os^{185}.

of the respective gamma-ray peaks. Assuming the K-conversion coefficient of the Cs^{137} line to be 0.087 (Wagonner 1951; Azuma 1954) the K-conversion coefficient of the 650 kev. Os^{185} gamma ray was determined to be 0.0084 ± 0.0015. This indicates an $E2$ transition (Rose 1955). The K/L ratio from the beta-ray spectrometer records was between 4 and 5, and this is consistent with the above classification. Johns, Nablo, and King (1957) came to similar conclusions.

*(b) Os^{183}**

As a product of the bombardment of rhenium with 25 Mev. protons, Jones-

*These data were presented at the Chemical Institute of Canada Symposium on Radiochemistry, September 7–10, 1955, and published in the preprints in preliminary form.

Stover (1950) reported a 12 hour osmium activity decaying by *K*-capture. The present study showed that targets of rhenium similarly bombarded yielded gamma-ray activities with two distinct half-lives. One set of gamma-ray transitions decayed with a half-life of 10 hours, the other with a half-life of 15.4 hours. Bombardments with enriched isotopes showed that both activities resulted from reactions on Re^{185} rather than Re^{187}. The nuclides were chemically identified as osmium.

These were assigned to Os^{183} since the $(p, 3n)$ reaction is the most probable at a proton energy of 25 Mev. (Bell and Skarsgard 1956). A $(p, 2n)$ reaction would produce stable Os^{184}. This assignment was later confirmed by Epp (1955), who determined the shape of the yield curves and compared them with the curves of Bell and Skarsgard. Figure 2 is a reproduction of Epp's curve for the 15 hour activity. His curve for the 10 hour activity is similar. These isomers fit into the "islands of isomerism" formed by known long-lived isomers as systematized by Goldhaber and Hill (1952).

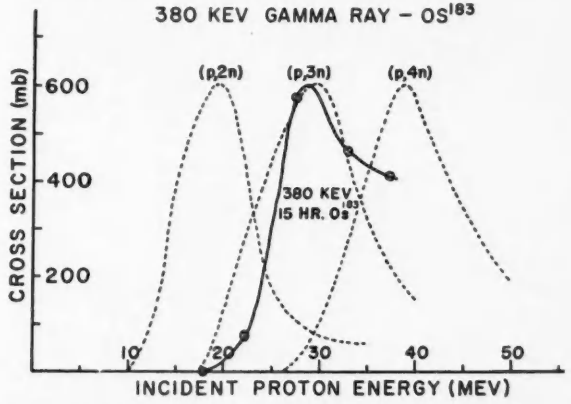

FIG. 2. Excitation function for the 380 kev. gamma ray of 15 hour Os^{183} produced from Re^{185}. The dotted curves are excitation functions for a bismuth target, normalized to the peak of the rhenium curve.

Figure 3 shows a 1 hour scan from the sodium iodide gamma spectrometer. The 73 kev. peak is due to the *K* X-ray of rhenium, greatly attenuated by a cadmium absorber. The three most prominent peaks at 120, 162, and 380 kev. all decayed with a 15.4 ± 0.3 hour half-life. The three weaker lines at 486, 846, and 1110 kev. all decayed with a 10 ± 1 hour half-life. The 15.4 hour value was the average of two 100 hour observations of the 380 kev. gamma ray. The 10 hour value was the average of two 70 hour observations of the 1100 kev. gamma ray. Figure 4 shows a beta-ray spectrometer trace of the conversion lines of these gamma rays. The relatively thick source contributed to the poor resolution.

Normal rhenium metal powder was then bombarded for 3 hours at 30 Mev. This source was exposed in the spectrograph for periods of up to 80 hours.

It would be expected to contain Os^{182}, Os^{185}, and the Re^{182} and Re^{183} decay products, as well as Os^{183}.

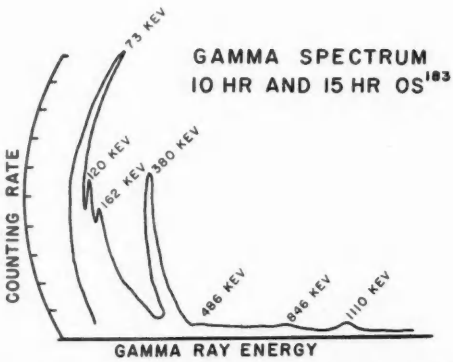

FIG. 3. Gamma spectrum from osmium fraction of Re^{185} enriched target exposed to 25 Mev. protons. The lines at 120, 162, and 380 kev. all decay with a 15.4 ± 0.3 hour half-life; the weaker lines at 486, 846, and 1110 kev. all decay with a 10 ± 1 hour half-life.

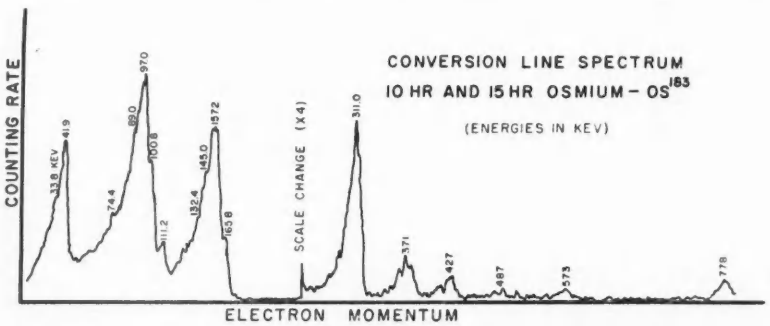

FIG. 4. Conversion line spectrum from osmium fraction of normal rhenium target exposed to 25 Mev. protons. The lines are identified in Table I. Note, however, that the weak lines at 89 and 145 kev. belong to Re^{183}, and the line at 573 kev. belongs to Os^{185}. Two additional 10 hour lines not included in Fig. 3 were observed at 1025 and 1080 kev.

The internal conversion spectrum was studied in detail (Epp 1955) using a 180° beta-ray spectrograph with 0.2% resolution. The spectrograph was accurately calibrated using a thorium (B+C+C″) source. The spectrograph was adjusted to record a useful energy range from 20 kev. to 320 kev. It required a strong line source.

In all, 34 lines of varying intensity were observed between 42.9 and 310.7 kev. Of these, 14 lines have been assigned to five gamma rays of Os^{183} as indicated in Table I. Lines appearing at the following energies are as yet unassigned: 54.7, 58.5, 60.7, 64.4, 66.6, 75.4, 79.3, 81.6, 87.3, 88.5, 89.8, 92.6, 108.5, 125.8, 138.7, 142.5, 150.3, 160.2, 168.6, and 170.2 kev. The error in

TABLE I

ASSIGNMENTS FROM CONVERSION LINE SPECTRA OF Os^{183} (CONVERTED IN Re^{183})

Conversion line energy, kev.					ΔE, binding energy	Gamma-ray energy,† calc., kev.	Gamma spectrometer energy, kev.	Half-life, hours	Intensity ratio
Spectrograph	Spectrometer	Intensity*	Assignment	ΔE, obs.					
42.9	41.9	b	K	$K-L_I = 59.2$	59.2	114.6±0.1	120	15	$K/L \sim 3$
102.1		a	L_I					15	
102.6	100.8	d	L_{II}					15	$L_I/L_{II} \sim 10$
103.9		d	L_{III}	$K-M_I = 68.8$	68.8			15	$L_I/L_{III} \sim 20$
111.7	111.2	b	M_I					15	$L/M \sim 6$
114.0		c	N_I	$K-N_I = 71.1$	71.1			15	
73.8	74.4	b	K	$K-L_I = 59.2$	59.2	145.5±0.2		10 or 15	$K/L \sim 5$ L_I/L_{II} large
133.0	132.4	c	L_I					10 or 15	L_I/L_{III} large
96.4	97.0 composite	a	K	$K-L_I = 59.2$	59.2	168.1±0.2		10	$K/L \sim 5$
155.6	157.2 composite	b	L_I					10	L_I/L_{II} large
165.1	165.8	d	M_I	$K-M_I = 68.7$	68.8			10	L_I/L_{III} large $L/M \sim 4$
97.0	97.0	c	K			168.7	162	15	$K/L \sim 1$–2
158.1	157.2 composite	b	L_{III}	$K-L_{III} = 61.1$	61.2			15	L_I/L_{III} small L_{II}/L_{III} small
310.7	311.0	c	K	$K-L = 60$		382.4±0.4	380	15.4±0.3	$K/L \sim 4$
	371.0		L						
	427		K	$K-L = 60$	59.2	499	486	10 or 15	
	487		L						
	778		K			850	846	10	
	1025		K	$K-L = 55$	59.2	1097	1110	10±1	
	1080		L						

*a—very strong, b—strong, c—medium, d—faint.
†Hill, Church, and Mihelich 1952.

measuring energy using the 180° spectrograph was ±0.2%. Gamma-ray energies were calculated by adding the binding energy for rhenium, 71.7 kev. (Hill, Church, and Mihelich 1952), to the energy of the conversion electrons.

In addition five more lines were observed with the Slatis–Siegbahn spectrometer at energies greater than 311 kev. and assigned to three additional gamma rays of Os^{183}. Gamma-ray energies were calculated as above. The agreement between the two columns headed ΔE confirmed the assignment of the various conversion lines to the electron shells shown in the table.

Precise half-life measurements were made with the gamma-ray spectrometer only. The half-lives of conversion lines were determined accurately enough to assign them to either the 10 or the 15 hour activity. In the spectrograph the "half-plate" technique was a valuable aid in making such an assignment. Half of the plate was exposed for 15 hours while the other half was shielded. The second half was then exposed for a time long compared with the half-life while the first half was shielded. The 15 hour electron lines were equally dense on the two halves of the plate, while the 10 hour lines were somewhat more dense on the first half. Intensity ratios between the conversion lines were estimated from the photographic plate and are only approximate.

The 114.6, 145.5, and 168.1 kev. gamma rays have measured properties consistent with $M1$ radiation.

(*c*) *Os^{182}*

Beta-ray spectrometer measurements of normal rhenium, which had been bombarded at 60 Mev., resulted in a complex line spectrum. One pair of lines, a K–L pair at 437 and 495 kev., was very clearly resolved and gave a good half-life measurement. A chemical separation showed that they are osmium lines and hence converted in rhenium. The corresponding gamma-ray energy was found to be 509 kev.

Observation of the 437 kev. peak for 135 hours gave a half-life of 21.9±0.1 hours when analyzed by the method of least squares. This is very likely the 24 hour activity assigned by Jones-Stover (1950) to Os^{182}. Evidence for a 12.7 hour rhenium daughter (Dybvig and Pool 1950; Wilkinson and Hicks 1950) was indicated by conversion lines at 87.8 kev. and 1.11 Mev., both of which grew to a maximum in approximately 22 hours. It can be shown that for a 21.9 hour parent and 12.7 hour daughter the maximum should occur at 23.7 hours. The subsequent decay could not be followed long enough for a good half-life measurement. However, observation of the daughter activity over a period of 110 hours indicated that it was controlled by the parent half-life of 20 to 24 hours, which is consistent with the expected value, 21.9 hours.

(*d*) *Re^{183}*

Wilkinson and Hicks (1950) observed a rhenium activity with a half-life of approximately 240 days resulting both from alpha-particle bombardment of tantalum and from proton bombardment of tungsten. Turner and Morgan (1951) believed that what the former had observed was really a mixture of Re^{183} and 250 day Re^{189} which yielded a half-life longer than their own estimate of 120–140 days. Lindner (1951), on the other hand, suggested that the 250

day radiation observed by Turner and Morgan was not associated with Re^{189} and that the half-life of Re^{189} was either 150 days or greater than 5 years. Jones-Stover (1950) mentioned 120 days as the half-life, but did not specify whether this was a measurement or a restatement of some previous value. A complete investigation of the decay scheme was very recently published by Thulin *et al.* (1956). They cite a value of 70 ± 10 days for the half-life, obtained by Strominger.

A rhenium target was bombarded at 25 Mev. and the osmium separated chemically after irradiation. The separated osmium should have contained mainly Os^{183} and Os^{185}. The 10 and 15 hour Os^{183} activities were allowed to decay for several weeks so that the sample contained the long-lived Re^{183} daughter and Os^{185}. Figure 5 shows the characteristic lines of the gamma-ray activities obtained and the upper part of Fig. 1 shows the corresponding electron conversion lines.

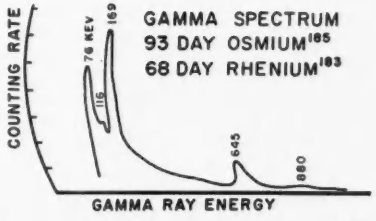

FIG. 5. Gamma spectrum from osmium fraction of normal rhenium target exposed to 25 Mev. protons. The spectrometer scan was made 1 week after chemical separation to allow short-lived products to decay. Hence the source contained Os^{185}, and Re^{183}, the decay product of 10 hour and 15 hour Os^{183}.

In Fig. 5 the lines at 645 and 880 kev. arise from Os^{185}. There is an X-ray peak at about 76 kev., and peaks at 116 and 169 kev. which are those of Re^{183}. The half-life of the 169 kev. peak was measured with the gamma-ray spectrometer over a period of 300 days. The half-life was found, by least squares, to be 67.6 ± 2.5 days. This value agrees well with that recently found by Strominger as reported by Thulin *et al.* (1956).

(*e*) *Re^{181} and Os^{181}*

When this work was begun no data on these nuclides had been reported. Recently Gallagher, Sweeney, and Rasmussen (1957) reported a 20-hour electron-capturing nuclide which they assigned to Re^{181}. This nuclide emits a gamma ray of energy 365.5 kev. and was produced by the reaction $Ta^{181}(\alpha, 4n)Re^{181}$.

In our work we have produced a 19 hour nuclide emitting a gamma ray of 367 kev. energy by the bombardment of Re^{185} with 60 and 80 Mev. protons and by the bombardment of tungsten with 25 and 35 Mev. protons. The most probable reactions indicate the production of Re^{181} although Re^{180} cannot be excluded. A rapid osmium separation showed the decay of a 23 minute nuclide with conversion lines at 93 and 101 kev. which we have assigned to Os^{181}. Growth of the 294 kev. and 352 kev. conversion lines of the 19 hour Re^{181}

daughter was observed with the maximum occurring at the calculated time (approximately 150 minutes after separation).

(*f*) *Re^{180} and Os^{180}*

Bombardment of rhenium with 80 Mev. protons yielded an 18 minute rhenium activity with conversion lines at 154 and 209 kev. A rapid chemical separation, and comparison of separated and unseparated fractions, showed that this must have grown in from an osmium isotope with half-life less than 2 minutes.

The same two conversion lines were observed following a bombardment of tungsten with 35 Mev. protons, but were not observed following a bombardment at 25 Mev. The evidence indicates Re^{180} as the most likely assignment for the 18 minute activity.

Recently Haldar and Wiig (1957) suggested a 20 hour positron emitter as Re^{180}. It appears that further experiments are required to assign masses 180 and 181 with certainty.

REFERENCES

AZUMA, T. 1954. J. Phys. Soc. Japan, **9**, 1.
BELL, R. E. and SKARSGARD, H. 1956. Can. J. Phys. **34**, 745.
DYBVIG, T. and POOL, M. L. 1950. Phys. Rev. **80**, 126.
EPP, E. 1955. Ph.D. Thesis, Radiation Laboratory, McGill University, Montreal, Que.
GALLAGHER, C. J., Jr., SWEENEY, M., and RASMUSSEN, J. O. 1957. Phys. Rev. **108**, 108.
GOLDHABER, M. and HILL, R. D. 1952. Revs. Modern Phys. **24**, 179.
HALDAR, B. C. and WIIG, E. O. 1957. Phys. Rev. **105**, 1285.
HILL, R. D., CHURCH, E. L., and MIHELICH, J. W. 1952. Rev. Sci. Instr. **23**, 523.
HOLLANDER, J. M., PERLMAN, I., and SEABORG, G. T. 1953. Revs. Modern Phys. **25**, 469
JOHNS, M. W., NABLO, S. V., and KING, W. J. 1957. Can. J. Phys. **35**, 1159.
JONES-STOVER, B. 1950. Phys. Rev. **80**, 99.
LINDNER, M. 1951. Phys. Rev. **84**, 240.
PATE, B. D. and YAFFE, L. 1955. Can. J. Chem. **33**, 15.
ROSE, M. E. 1955. Beta and gamma spectroscopy, *edited by* K. Siegbahn (North-Holland Publishing Co., Amsterdam).
SLATIS, H. and SIEGBAHN, K. 1949. Arkiv Fysik, **1**, 399.
THULIN, S., RASMUSSEN, J. O., GALLAGHER, C. J., Jr., SMITH, W. G., and HOLLANDER, J. M. 1956. Phys. Rev. **104**, 471.
TURNER, S. E. and MORGAN, L. O. 1951. Phys. Rev. **81**, 881.
WAGONNER, M. A. 1951. Phys. Rev. **82**, 906.
WILKINSON, G. and HICKS, H. G. 1950. Phys. Rev. **77**, 314 (1950).

A NEW BAND SYSTEM OF THE P_2 MOLECULE ANALOGOUS TO THE LYMAN–BIRGE–HOPFIELD BANDS OF N_2[1]

A. E. Douglas and K. Suryanarayana Rao[2]

ABSTRACT

Five bands of a new band system of P_2 have been photographed at high dispersion and analyzed. The upper state of the system is a $^1\Pi_g$ state and lies lower than any previously known excited singlet state. The lower state of the new system is the ground state of P_2 and the analysis of the new bands has given improved constants for this state. The new system appears to be the analogue of the Lyman–Birge–Hopfield bands of N_2. The electron configuration of the low excited states of P_2 and of related molecules is discussed.

INTRODUCTION

The absorption and emission spectrum of the diatomic phosphorus molecule has been studied quite extensively but up to the present only three band systems involving four states have been discovered. Two of the band systems have been investigated at low dispersion by Dressler (1955) and little is known of the upper states of these systems. The third system of P_2 is an extensive one which has been investigated both in absorption and in emission. In emission, this system gives many strong bands covering the whole spectral range from about 3500 Å to the vacuum ultraviolet. Rotational analysis of many of these bands has been carried out by Herzberg (1932), Ashley (1933), Herzberg, Herzberg, and Milne (1940), and Marais (1946). The band system arises from a $^1\Sigma_u^+$—$^1\Sigma_g^+$ transition in which the lower state is the ground state of the molecule. Since all the strongest emission bands involve only relatively high vibrational levels of the ground state and since the absorption spectrum is difficult to obtain, the lowest vibrational level of the ground state that has been investigated is that with $v'' = 5$. Up till the present work, the $^1\Sigma_u^+$ upper state of this system was the lowest excited electronic state that had been found either in emission or in absorption and it has been assumed that this $^1\Sigma_u^+$ state is the lowest excited singlet state of P_2.

The present work concerns a newly discovered band system of P_2 which arises from a $^1\Pi$—$^1\Sigma$ transition. The lower state of the new band system is the ground state of P_2 and the $^1\Pi$ state is a previously unknown state which lies lower than the $^1\Sigma_u^+$ state. The constants of both states have been determined and since this band system makes it possible, for the first time, to analyze a band involving the $v'' = 0$ level of the ground state, the constants for this state have been somewhat improved.

EXPERIMENTAL

The spectrum was excited in a pyrex discharge tube about 12 mm. in

[1]Manuscript received February 20, 1958.
Contribution from the Division of Pure Physics, National Research Council, Ottawa, Canada.
Issued as N.R.C. No. 4703.
[2]National Research Laboratories Postdoctorate Fellow.

TABLE I

WAVE NUMBERS OF THE LINES OF THE P_2 BANDS

	1–0 λ_{head} = 2852.23 Å			0–0 λ_{head} = 2902.99 Å			0–1 λ_{head} = 2969.84 Å			0–2 λ_{head} = 3039.29 Å			0–3 λ_{head} = 3112.43 Å		
J	$P(J)$	$Q(J)$	$R(J)$	$P(J)$	$Q(J)$	$R(J)$	$P(J)$	$Q(J)$	$R(J)$	$P(J)$	$Q(J)$	$R(J)$	$P(J)$	$Q(J)$	$R(J)$
1					34434.23			33658.98			32889.53				
3				34432.24	33.91		33657.08*	58.64*			89.27				
5		35046.33		30.82	33.45		55.49*	58.24			88.81			32125.17	
7	35041.75*	45.54		29.10*	32.70		53.72	57.53	33661.84	32884.25	88.16			24.54*	
9	39.66*	44.51		26.79	31.72*		51.70	56.61	62.07*	82.34	87.26*	32892.82*		23.72	
11	37.27*	43.25		24.50	30.52*	34437.24	49.46	55.49*	62.07*	80.18	86.21	92.82*		22.72	
13	34.68*	41.75*		21.96	29.10*	36.78*	46.99	54.12	61.84	77.79*	84.94	92.59		21.48*	
15	31.83	39.98	35048.26	19.22	27.45	36.23*	44.34	52.57	61.33	75.25	83.46	92.24	32111.85	20.12	
17	28.75	38.00		16.23	25.57	35.43*	41.48*	50.79	60.65	72.44	81.77*	91.65	09.20	18.54	
19	25.42	35.76	46.65	13.04	23.48*	34.42	38.38	48.79	59.74	69.46	79.88	90.85	06.35	16.74	
21	21.85	33.29	45.26	09.51*	21.13	33.18	35.05	46.57	58.64*	66.26	77.79*	89.84	03.28	14.79	32126.85
23	18.03	30.58	43.61	05.98*	18.55	31.72*	31.52	44.14	57.29	62.88	75.49	88.65	00.02	12.62	25.77
25	13.98	27.62	41.75*	02.07	15.77	30.01	27.77	41.48*	55.74	59.26	72.99	87.26*	32096.56	10.25*	24.54*
27	09.89*	24.41	39.66*	34397.94	12.74	28.09	23.82	38.62*	53.98	55.48	70.28	85.62	92.91	07.72	23.05
29	05.14	20.97	37.27*	93.60	09.51*	25.92	19.63	35.51*	51.98	51.47	67.37	83.79		04.97	21.48*
31	00.43	17.28	34.68*	89.02	05.98*	23.48*	15.24	32.23	49.77	47.26	64.25	81.77*	85.05	02.05	19.57
33	34995.41	13.36		84.21	02.31	20.93	10.63	28.72	47.33	42.84	60.92	79.56	80.84	32098.91	17.52
35	89.97*	09.19		79.13	34398.35	18.06	05.80	24.97	44.66	38.22	57.39	77.10	76.42	95.58	15.30
37		04.78		73.92	94.18	14.98	00.76	21.02	41.81	33.39	53.66	74.46	71.80	92.08	12.87
39		00.10		68.43	89.79	11.67	33595.46	16.85	38.62*	28.35	49.71	71.61	66.95	88.36	10.25*
41		34995.20		62.71	85.16	08.12	90.00	12.46	35.51*	23.12	45.56	68.54		84.47	
43		89.97*		56.76	80.29	04.36	84.31	07.85	31.96	17.66	41.22	65.27		80.36	
45				50.59	75.20	00.35	78.39	03.03	28.15		36.64	61.78		76.05	
47					69.88	34396.11	72.26	33597.98	24.19		31.88			71.58	
49					64.34	91.66	65.91	92.72	20.07		26.90				
51					58.54		59.34	87.21	15.61		21.72				
53					52.51		52.51	81.52			16.32				
								75.59							
								69.44							
								63.07							
								56.46							
								49.66							

* Overlapped lines.

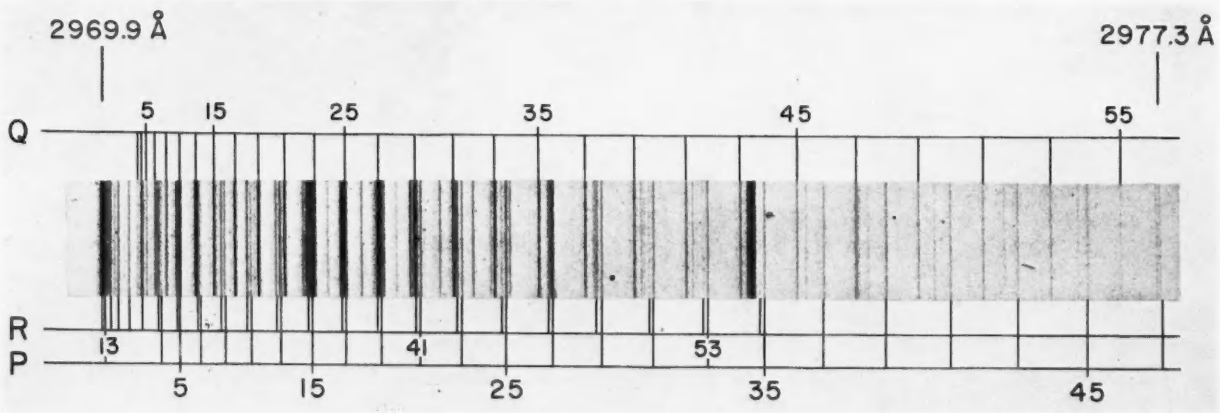

FIG. 1. The 0–1 band of the $^1\Pi_g$—$^1\Sigma_g^+$ system of P_2. The lines which are not marked are lines of a band of the $^1\Sigma_u^+$—$^1\Sigma_g^+$ system.

diameter through which helium containing a trace of phosphorus vapor was pumped. In the first experiments the discharge was excited in an electrodeless discharge by a 2000 Mc./sec. oscillator but later experiments showed that the same spectrum could be excited equally well by the usual type of positive column discharge between electrodes which were supplied by a 4000-volt 60-cycle transformer. It is essential to allow only a very small quantity of phosphorus vapor to enter the tube; otherwise the bands of the $^1\Sigma_u^+$—$^1\Sigma_g^+$ system which occur in the same region become much stronger than the new bands. The bands were photographed with a 10 meter concave grating at a dispersion of 0.32 Å/mm.

Five bands belonging to the new system have been found. The band heads are at 2852, 2903, 2970, 3039, and 3112 Å, with the 2970 Å band being the strongest. It is difficult to obtain stronger spectra, which would probably show more bands, since the whole region is covered by a large number of bands of the $^1\Sigma$—$^1\Sigma$ system and it is only the stronger bands of the new system which show above these.

RESULTS

The wave numbers of the lines of the bands are given in Table I. The five bands are the 1–0, 0–0, 0–1, 0–2, and 0–3 bands. The 0–1 band is shown in Fig. 1. Since each of the bands has one state in common with at least one other band, the analysis of the bands presented no difficulty. The analysis shows that the bands are $^1\Pi$—$^1\Sigma$ bands of the P_2 molecule with the lower state being the ground state of the molecule. Successive lines in each branch should show a 3:1 intensity ratio since the nuclear spin of phosphorus is one-half. In Table I only the strong lines are listed and in fact only a very few of the weaker set of lines can be seen at all. In the 0–1 band, which is the strongest of the group, the positions of the strongest of the weak set of lines are overlapped by lines of the 7–23 band of the $^1\Sigma_u^+$—$^1\Sigma_g^+$ system. Thus the new bands are too weak to show that a 3:1 intensity alternation exists but the analysis does show quite definitely that all the observed lines must be given odd J numbers.

The origins and B values of the bands are given in Table II. B_0' was found from the mean values of the combination differences $\Delta_1F'(J)$ of the 0–0, 0–1, 0–2, and 0–3 bands. The Λ doubling of the $^1\Pi$ state is very small and of

TABLE II

BAND ORIGINS AND B VALUES OF THE OBSERVED BANDS

Band	ν_0	B'	B''
1–0	35047.24	0.27267	0.30285
0–0	34434.30	0.27436	0.30285
0–1	33659.06	0.27436	0.30138
0–2	32889.59	0.27436	0.29988
0–3	32125.89	0.27436	0.29837

the order of the experimental error. A rough estimate is that the Λ doubling constant $q = 0.00003$ cm^{-1}. The B'' values for the 0–0, 0–1, 0–2, and 0–3

TABLE III

CONSTANTS OF THE ELECTRONIC STATES OF P_2

State	T_e	ω_e	$\omega_e x_e$	$\omega_e y_e$	B_e	α	r_e	Observed transition: Designation	Observed transition: ν_{00}	References
J		[e]						$J \rightarrow X$	66282	Dressler (1955)
F		[d]						$F \rightarrow X$	59409	Dressler (1955)
$B\,^1\Sigma_u^+$	46942.9	475.24[c]	2.633[c]	+0.0217[c]	0.2416[6]	0.00165	2.122	$B \leftrightarrow X$		[f]
$A\,^1\Pi_g$	34515.34	618.88	2.97[b]		0.27520	0.00169	1.9883	$A \rightarrow X$	34434.30	Present work
$X\,^1\Sigma_g^+$	0	780.89	2.820	−0.00511	0.30359	0.001477[a]	1.8931	$B \leftrightarrow X$		
								$A \rightarrow X$		[f]

[a] $B_v = 0.30359 - 0.001477\ (v+\frac{1}{2}) - 3.2\times10^{-6}(v+\frac{1}{2})^2$.

[b] $\omega_e x_e$ has been calculated from α and is probably quite inaccurate.

[c] From band head measurements.

[d] $\Delta G(\frac{1}{2}) = 626\ \text{cm}^{-1}$.

[e] $\Delta G(\frac{1}{2}) = 683\ \text{cm}^{-1}$.

[f] These constants are obtained from the several papers referred to in the text.

bands were found from B_0' and the values of $(B'-B'')$ determined from the P and R branches of the bands. For the 1–0 band, which is rather weak, the upper state B value was determined from B_0' and the $(B_1'-B_0')$ value determined from the differences between the Q branch lines in the 0–0 and the 1–0 band. The constants determined here have been combined with those derived by Herzberg (1932), Ashley (1933), Herzberg, Herzberg, and Milne (1940), and Marais (1946) to give the constants of P_2 listed in Table III.

DISCUSSION

The fact that the new bands are indeed a band system of P_2 is readily established. The values of B_0'', α'', and $\Delta G''$ $(\frac{1}{2})$ found from the new system are 0.30285, 0.00148, and 775.24 cm^{-1}, which may be compared with the values 0.30256, 0.00142, and 774.82 cm^{-1} given by Herzberg (1950) for the ground state of P_2. When one considers that all of the values given by Herzberg have been obtained by extrapolating from higher vibrational levels of the ground state, the agreement is remarkably good. Also the nature of the light source and the fact that only lines with odd J values are observed confirms the conclusion that the bands are due to P_2.

Since the lower state of the new system is the ground state of P_2, it must be a $^1\Sigma_g^+$ state (see Herzberg 1950, p. 343). The bands of the new system are $^1\Pi$—$^1\Sigma$ bands and therefore the upper state of the new system must be a $^1\Pi$ state. From the observed bands it is not possible to determine whether the upper state is $^1\Pi_g$ or $^1\Pi_u$. While it is true that a $^1\Pi_g$—$^1\Sigma_g$ transition is forbidden for electric-dipole radiation it may still occur through magnetic-dipole and electric-quadrupole radiation.

The new band system arises from the lowest of the known excited states of P_2 and occurs in a spectral region which is very convenient to observe. In spite of this, bands of the new system have not been observed in the absorption experiments of Jakowlewa (1931) or Herzberg, Herzberg, and Milne (1940). It therefore appears certain that the bands arise from a transition with a low transition probability. From an emission source, it is difficult to draw any definite conclusions regarding the transition probability but it is worth noting that diluting an active gas with a large amount of an inert gas as has been done here is often a very effective way of causing the emission of "forbidden" transitions. The experimental facts are therefore quite consistent with the assumption that the bands result from a $^1\Pi_g$—$^1\Sigma_g$ transition.

The low-lying electron configurations of P_2 and the resulting singlet states are

$$KKLL(\sigma_g3s)^2\ (\sigma_u3s)^2\ (\pi_u3p)^4\ (\sigma_g3p)^2 \qquad {}^1\Sigma_g^+$$
$$KKLL(\sigma_g3s)^2\ (\sigma_u3s)^2\ (\pi_u3p)^4\ (\sigma_g3p)\ (\pi_g3p) \qquad {}^1\Pi_g$$
$$KKLL(\sigma_g3s)^2\ (\sigma_u3s)^2\ (\pi_u3p)^3\ (\sigma_g3p)^2\ (\pi_g3p) \qquad {}^1\Sigma_u^+\ \ {}^1\Sigma_u^-\ \ {}^1\Delta_u$$

Here it can be seen that the only low-lying $^1\Pi$ state is a $^1\Pi_g$ state. Thus it seems most probable that the observed bands arise from a $^1\Pi_g$—$^1\Sigma_g$ transition.

The bands observed here appear to be analogous to the Lyman–Birge–Hopfield bands of N_2, which Herzberg (1946) showed most probably in-

volved a $^1\Pi_g$—$^1\Sigma_g$ transition. This assumption has recently been proved experimentally by Wilkinson and Mulliken (1957), who observed the O and S branches. Probably the only reason the band system described here was not discovered many years ago is the fact that it is quite difficult to obtain a long absorption path of diatomic phosphorus. Also the weakness of the emission bands prevented the observation of these bands in the past and at present prevents the observation of O and S branches which, in the manner of Wilkinson and Mulliken, would, if observed, give definite proof of the nature of the upper state.

It is interesting to note that the existence of the $^1\Pi$ state at an energy of about 34,000 cm^{-1} might have been predicted from the known spectra of the isoelectronic molecules AlCl and SiS which have their first excited singlet states at 38,254 and 32,450 cm^{-1} respectively. These two molecules may be expected to have electronic structures similar to P_2 but their $^1\Pi$—$^1\Sigma$ bands are not forbidden since the *g* or *u* symmetry is no longer present in the heteronuclear molecules. Thus the new band system arising from the $^1\Pi_g$ state of P_2 at 34,500 cm^{-1} seems to fit very well into this isoelectronic group.

Since prior to this work the lowest excited state of P_2 which was known was the $^1\Sigma_u$ state, it had been assumed that the $^1\Sigma_u$ state was lower than the $^1\Pi_g$. Thus insofar as the simple molecular orbital picture is valid it was assumed that the ground state of P_2 should be written $KKLL(\sigma_g 3s)^2\ (\sigma_u 3s)^2\ (\sigma_g 3p)^2\ (\pi_u 3p)^4$ and was not closely analogous to the ground state of N_2 for which the configuration is $KK(\sigma_g 2s)^2\ (\sigma_u 2s)^2\ (\pi_u 2p)^4\ (\sigma_g 2p)^2$. The present work shows that the $^1\Sigma^+$ state of the $\ldots\ (\sigma_g 3p)^2\ (\pi_u 3p)^3\ (\pi_g 3p)$ configuration is higher than the $^1\Pi_g$ state of the $\ldots\ (\sigma_g 3p)\ (\pi_u 3p)^4\ (\pi_g 3p)$ configuration. It appears more reasonable therefore to write the ground state of P_2 as $\ldots\ (\pi_u 3p)^4\ (\sigma_g 3p)^2$. The ground-state configurations of N_2 and P_2 are therefore exact analogues. If this is so, one may reasonably believe that the ground states of P_2^+ and Si_2 are $^2\Sigma_g$ and $^1\Sigma_g$ rather than $^2\Pi_u$ and $^3\Sigma_g$ as has been assumed (Herzberg 1950; Douglas 1955; and Narasimham 1957). The present experimental data on P_2^+ and Si_2 are not sufficient to determine the symmetry of the ground state.

ACKNOWLEDGMENT

We wish to thank Dr. G. Herzberg for his helpful discussions and interest in this work.

REFERENCES

Ashley, M. 1933. Phys. Rev. **44**, 919.
Douglas, A. E. 1955. Can. J. Phys. **33**, 801.
Dressler, K. 1955. Helv. Phys. Acta, **28**, 563.
Herzberg, G. 1932. Ann. Physik, **15**, 677.
——— 1946. Phys. Rev. **69**, 362.
——— 1950. Spectra of diatomic molecules (D. Van Nostrand Company, Inc., New York).
Herzberg, G., Herzberg, L., and Milne, G. 1940. Can. J. Research, A, **18**, 139.
Jakowlewa, A. V. 1931. Z. Physik, **69**, 548.
Marais, E. J. 1946. Phys. Rev. **70**, 499.
Narasimham, N. A. 1957. Can. J. Phys. **35**, 1242.
Wilkinson, P. G. and Mulliken, R. S. 1957. Astrophys. J. **126**, 10.

SPIN–ORBIT INTERACTION IN NUCLEI[1]

B. P. NIGAM[2] AND M. K. SUNDARESAN[3]

ABSTRACT

Brueckner's theory of nuclear structure has been used to estimate the spin–orbit interaction of a single nucleon interacting with the core arising from the tensor force of the two-body interaction. Using Yamaguchi's separable two-body interaction, the doublet splitting for Ca^{41} and O^{17} has been calculated (i) in the first Born approximation and (ii) with an exact solution of the reaction matrix in which the exclusion principle has been taken into account. It is found that the values of the splittings calculated exactly are smaller than the experimental values.

INTRODUCTION

Calculations of the spin–orbit interaction of a single nucleon interacting with a core of nucleons have been carried out previously. Two main approaches to this problem can be distinguished. One of these is to renounce any possibility of describing the nucleon–nucleon interaction by means of a potential and to obtain the spin–orbit coupling part of the two-nucleon reaction matrix (involved in the definition of the single-particle potential) directly through recourse to experimental data and to use this to estimate the spin–orbit interaction in nuclei. A thorough investigation using this approach is due to Bell and Skyrme (1956), who show that the observed doublet splittings in O^{17} and N^{15} can be obtained from the experimental two-body scattering data up to about 100 Mev. The other approach is to retain the description of the nucleon–nucleon interaction in terms of a potential and to estimate the contribution to the splitting arising from the tensor force in the potential or from any spin–orbit coupling term that may be present in the nucleon–nucleon interaction itself. This latter approach has been the basis of the work of Hughes and Lecouteur (1950), Keilson (1951), Elliott and Lane (1954), Blin-Stoyle (1955), and Kisslinger (1956). When a spin–orbit interaction is included in the nucleon–nucleon interaction itself, the first approximation in which the reaction matrix of the two-particle system is replaced by the potential itself is finite and the splitting can be obtained relatively easily. The second- and higher-order corrections to the reaction matrix are assumed small because of the inhibition of their effects by the exclusion principle. However, in the case of the tensor force, the first approximation to the reaction matrix leads to a vanishing result for the splitting because a sum over the spins of the core particles is involved. Hence one has to evaluate its contribution in the second order, including the effects of the exclusion principle for the nucleons

[1]Manuscript received December 9, 1957.
Contribution from the Division of Pure Physics, National Research Council, Ottawa, Canada.
Issued as N.R.C. No. 4704.
[2]National Research Laboratories Postdoctorate Fellow; on leave from Delhi University, Delhi, India.
[3]National Research Laboratories Postdoctorate Fellow.

in the core, which is a lot more difficult to calculate accurately. Kisslinger has evaluated the contribution to the spin–orbit interaction arising from a two-body tensor force with exponential radial dependence. However, he has not included the effects of the exclusion principle, as according to him this should not cause much error because the main contribution to this interaction should come from nucleons with momenta near the Fermi maximum. He obtained results which are of the order of magnitude of the observed splittings but somewhat smaller. Jancovici (1957) has carried out similar calculations and finds however that the calculated second-order contributions are considerably smaller than the experimental values. Thus there is considerable uncertainty about the actual magnitude of the contribution to doublet splitting arising from a two-body tensor force owing to difficulties of correctly evaluating the reaction matrix.

It is the object of this paper to estimate as accurately as possible the spin–orbit interaction arising from the tensor force of Yamaguchi's separable two-body interaction within the framework of Brueckner's theory of nuclear structure (Brueckner 1955). The advantage of the separable potential is that the equation for the reaction matrix can be easily solved exactly including the effects of the exclusion principle and also without it. A comparison can be made of the relative contributions from the first-order approximation (which in this case leads to non-vanishing results for the splitting) and from the higher-order terms of the reaction matrix. Further, the effect of the exclusion principle can be easily seen. In the first part of the paper we evaluate the contribution to the splitting of the level of a nucleon at the top of the Fermi distribution from the first-order approximation to the reaction matrix. Since there is no repulsive core in this potential, the first approximation of replacing the reaction matrix by the potential matrix itself should be good (Bethe 1956). This is checked in the latter part of the paper by using the exact solution to the reaction matrix including effects of the exclusion principle, and the results are compared with the first-order results. The theory has been applied to the $l = 1$ and $l = 3$ levels of Ca^{41} and $l = 2$ level of O^{17}. It is assumed that the central part of the two-nucleon potential leads (in the effective-mass approximation) to an effective mass $M^*/M = 0.6$. This value is used in the calculations below.

FIRST-ORDER BORN APPROXIMATION

We use the Yamaguchi separable potential given by

$$(\mathbf{k}|V|\mathbf{k}') = -\frac{\lambda}{M} g(\mathbf{k})g(\mathbf{k}'), \tag{1}$$

where $\mathbf{k}$ and $\mathbf{k}'$ are the momenta of the nucleons in the center-of-mass system and

$$\begin{aligned} g(\mathbf{k}) &= C(k)+\frac{1}{\sqrt{8}}S(\mathbf{k})\,T(k), \\ S(\mathbf{k}) &= 3\frac{(\boldsymbol{\sigma}_1 \cdot \mathbf{k})(\boldsymbol{\sigma}_2 \cdot \mathbf{k})}{k^2}-(\boldsymbol{\sigma}_1 \cdot \boldsymbol{\sigma}_2), \\ C(k) &= (k^2+\beta^2)^{-1} \quad \text{and} \quad T(k) = -tk^2(k^2+\gamma^2)^{-2}. \end{aligned} \tag{2}$$

β, γ, and t are constants which are determined from a fit to the low-energy neutron–proton scattering data and the properties of the deuteron. The interaction strength parameter λ is calculated from the relation

$$\frac{1}{a} = -\frac{\beta^4}{2\pi^2\lambda}+\frac{\beta}{2}+\frac{t^2\beta^4}{16\gamma^3}, \tag{3}$$

where a is the scattering length.

Since only the tensor part of the interaction can be expected to give rise to a spin–orbit interaction, the interaction energy responsible for the displacement of a level becomes in momentum space (Kisslinger 1956)

$$\begin{aligned}\Delta E &= (\Psi_0, V\Psi_0)\\ &= \sum_c \int \psi_0^*(\mathbf{k}_1)\psi_c^*(\mathbf{k}_2)\, I_1(\mathbf{k},\mathbf{K};\mathbf{k}',\mathbf{K}')\psi_0(\mathbf{k}_1')\psi_c(\mathbf{k}_2')d^3k_1\, d^3k_2\, d^3k_1'\, d^3k_2',\end{aligned} \tag{4}$$

where ψ_0 and ψ_c are the wave functions of the extra core nucleon and the core nucleon respectively, and

$$I_1(\mathbf{k},\mathbf{K};\mathbf{k}',\mathbf{K}') = -\frac{9i}{4}\frac{\lambda}{M}\frac{T(k)\,T(k')}{k^2k'^2}(\mathbf{k}\,.\,\mathbf{k}')(\boldsymbol{\sigma}_1,[\mathbf{k}\times\mathbf{k}'])\delta(\mathbf{K}-\mathbf{K}'), \tag{5}$$

where a summation over the spins of the core particles 2 has been carried out. This interaction arises only if the two nucleons considered are in the triplet state. Later we shall include a statistical factor $\frac{3}{4}$ to take care of the singlet states. Here $\mathbf{K} = \mathbf{k}_1+\mathbf{k}_2$, $\mathbf{k} = \frac{1}{2}(\mathbf{k}_1-\mathbf{k}_2)$, and $\mathbf{k}' = \frac{1}{2}(\mathbf{k}_1'-\mathbf{k}_2')$. We now integrate over $\mathbf{k}_2'$, introducing the Fourier transforms of the core functions $\psi_c^*(\mathbf{k}_2)$ and $\psi_c(\mathbf{k}_2')$. We also introduce the variables $\mathbf{R} = \frac{1}{2}(\mathbf{r}_1+\mathbf{r}_2)$, $\mathbf{r} = \mathbf{r}_1-\mathbf{r}_2$, and following Kisslinger (1956) approximate† $\sum_c\psi_c^*(\mathbf{r}_1)\psi_c(\mathbf{r}_2)$ by $\rho(R)e^{-\alpha r^2}$, where $\alpha = 4.61/R_0^2$, $R_0 = 1.18\times10^{-13}\,A^{1/3}$ cm. Then we obtain

$$\begin{aligned}\Delta E = \frac{9it^2}{2}\frac{\lambda}{M}\int \psi_0^*(\mathbf{k}_1)\rho(R)\exp[i(\mathbf{k}_1'-\mathbf{k}_1,\mathbf{R})]\\ \times I_2(\mathbf{k}_1,\mathbf{k}_1')\,\psi_0(\mathbf{k}_1')\,d^3k_1\,d^3k_1'\,d^3R,\end{aligned} \tag{6}$$

where

$$\begin{aligned}I_2(\mathbf{k}_1,\mathbf{k}_1') = \int d^3r\,d^3k\exp(-\alpha r^2+i\mathbf{k}_1\,.\,\mathbf{r})\exp(-2i\mathbf{k}\,.\,\mathbf{r})\\ \times\left\{\exp[-\tfrac{1}{2}i(\mathbf{p}\,.\,\mathbf{r})]\frac{(\mathbf{k},\mathbf{k}+\mathbf{p})(\boldsymbol{\sigma}_1,[\mathbf{k}\times\mathbf{p}])}{(k^2+\gamma^2)^2[(\mathbf{k}+\mathbf{p})^2+\gamma^2]^2}\right\}\end{aligned} \tag{7}$$

with $\mathbf{p} = \mathbf{k}_1'-\mathbf{k}_1$. From equation (6) we see that the contribution to ΔE will be small for large values of $\mathbf{p} = \mathbf{k}_1'-\mathbf{k}_1$ owing to rapid oscillations of the wave functions. Thus we expand the quantity inside the curly bracket of equation (7) in powers of p about $p = 0$ and retain only the leading term $(\boldsymbol{\sigma}_1,[\mathbf{k}\times\mathbf{p}])k^2/(k^2+\gamma^2)^4$, which involves only the first derivative of $\psi_0^*(\mathbf{R})\psi_0(\mathbf{R})$; the higher powers of p involve higher derivatives of this quantity. Then the

†This approximation has been discussed in detail by Kisslinger (1956) in the appendix of his paper and depends mainly on the fact that correlations between nucleons in a Fermi gas are limited to distances which satisfy $\mathbf{k}_F|\mathbf{r}_1-\mathbf{r}_2| \ll 1$.

integration over the angular parts of $\mathbf{k}$ and $\mathbf{r}$ gives, after the variables $x = k/k_F$, $y = k_1 r$ have been introduced,

$$I_2(\mathbf{k}_1, \mathbf{k}_1') = -\frac{([\boldsymbol{\sigma}_1 \times \mathbf{p}], \mathbf{k}_1)}{k_1^3} I(k_1) \tag{8}$$

with

$$I(k_1) = 8\pi^2 \int_0^1 dx\, \gamma^3 F(x) \int_0^\infty dy\, 2y^2 \exp\left(-\frac{\alpha}{k_1^2} y^2\right) \frac{d}{dy}\left(\frac{\sin y}{y}\right) \frac{d}{d(2xy)}\left(\frac{\sin 2xy}{2xy}\right)$$

and

$$F(x) = \gamma^{-3}\left(\frac{k_1}{\gamma} x\right)^5 \left[1 + \left(\frac{k_1}{\gamma}\right)^2 x^2\right]^{-4}.$$

The x and y integrations were carried out numerically using Simpson's one-third rule.

Now we are interested in the splitting of the level of the extra core nucleon and hence we consider a nucleon at the top of the Fermi distribution. Then $\psi_0(\mathbf{k}_1)$ and $\psi_0(\mathbf{k}_1')$ can be written as

$$\psi_0(\mathbf{k}_1) = \delta(k_1 - k_F)\, Y_l^0(\hat{k}_1); \qquad \psi_0(\mathbf{k}_1') = \delta(k_1' - k_F)\, Y_l^0(\hat{k}_1'), \tag{9}$$

where $Y_l^0(\hat{\mathbf{k}}_1)$ and $Y_l^0(\hat{\mathbf{k}}_1')$ are the usual spherical harmonics involving the angular parts of $\mathbf{k}_1$ and $\mathbf{k}_1'$ specified by the unit vectors $\hat{k}_1$ and $\hat{k}_1'$ respectively. Substituting these wave functions in (6) and making use of the approximate expression (8) for $I_2(\mathbf{k}_1, \mathbf{k}_1')$, we can easily integrate over $\mathbf{k}_1$ and $\mathbf{k}_1'$ and we get, after a slight rearrangement of constant factors,

$$\Delta E = \frac{9}{2} \frac{t^2}{M k_F^3} \left(\frac{\lambda}{\gamma^3}\right) I(k_F) \begin{bmatrix} \frac{1}{2}l \\ -\frac{1}{2}(l+1) \end{bmatrix} \int_0^\infty j_l^2(k_F R)\, \frac{1}{R} \frac{d\rho}{dR} R^2 dR, \tag{10}$$

where the upper line holds for $j = l + \frac{1}{2}$ and the lower line for $j = l - \frac{1}{2}$. The value of λ/γ^3 can be obtained from equation (3) by using the values of β, γ, and t given by Yamaguchi and the triplet neutron–proton scattering length. We get

$$\lambda/\gamma^3 = 1.274/2\pi^2. \tag{11}$$

The value of $I(k_F)$ for Ca^{41} found by numerical integration was

$$I(k_F) = 0.614.$$

Using these values in equation (10), the expression for doublet splitting becomes

$$\Delta(\Delta E) = \frac{3}{4}(5.561 \times 10^{-54}\,\text{cm.}^4)\, \frac{2l+1}{2} \frac{\int_0^{R_0} j_l^2(k_F R)\, R \frac{d\rho}{dR} dR}{\int_0^{R_0} j_l^2(k_F R)\, R^2 dR}, \tag{12}$$

where the factor $\frac{3}{4}$ is included in equation (12) to take account of singlet state collisions. For O^{17}, the numerical factor in equation (12) turns out to be $\frac{3}{4}(3.781 \times 10^{-54})$ cm.^{4} To evaluate the actual magnitude of splittings, we

have to make some assumptions about the density distribution in the nucleus. For this we take

$$\begin{aligned} \rho(R) &= \rho && \text{for } 0 \leqslant R \leqslant R_0 - a\lambda\!\!\!^{-}_{\pi}, \\ &= \frac{\rho}{a\lambda\!\!\!^{-}_{\pi}} R_0\left(1-\frac{R}{R_0}\right) && \text{for } R_0 - a\lambda\!\!\!^{-}_{\pi} \leqslant R \leqslant R_0, \\ &= 0 && \text{for } R > R_0, \end{aligned} \tag{13}$$

where $\lambda\!\!\!^{-}_{\pi}$ is the Compton wavelength of the pion divided by 2π. We have to impose the condition $\int \rho(R) d^3R = A$, from which we can fix the value of ρ. We calculate splittings for two values of a in equation (14), namely, for $a = 1$ and $a = 1.5$. These values are given in the third and fourth columns of Table I.

EXACT SOLUTION

The reaction matrix T satisfies the integral equation

$$(\mathbf{k}'|T|\mathbf{k}) = (\mathbf{k}'|V|\mathbf{k}) + P\int_{k_F} d^3p \, \frac{(\mathbf{k}'|V|\mathbf{p})(\mathbf{p}|T|\mathbf{k})}{(k^2-p^2)/M^*}, \tag{14}$$

where k_F has been written as the lower limit of the integral to take account of the exclusion principle. Here M^* is the effective mass, which we shall take in the following to be $0.6\,M$. Since $(\mathbf{k}'|V|\mathbf{k})$ is separable, the solution of equation (14) is (in triplet states)

$$(\mathbf{k}'|T|\mathbf{k}) = -\frac{\lambda}{M} \frac{g(\mathbf{k}')g(\mathbf{k})}{1+\lambda(M^*/M)J(k)}, \tag{15}$$

where

$$J(k) = P\int d^3p \, \frac{C^2(p)+T^2(p)}{k^2-p^2} \tag{16}$$

and P signifies that the principal value of this integral is taken. The evaluation of $J(k)$ is straightforward and gives

$$\begin{aligned} \frac{\gamma^3}{4\pi} J(k) = \gamma_2{}^3 &\left\{ \frac{\pi}{4} \frac{\beta_1{}^2x^2-1}{(\beta_1{}^2x^2+1)^2} + f_1(x,\beta_1) \right\} \\ &+ t^2 \left\{ \frac{\pi}{2} \frac{1}{\gamma_1{}^2x^2} \left(x_1{}^4 - \frac{x_1{}^3}{2} - \frac{x_1{}^2}{8} - \frac{x_1}{16} \right) + f_2(x, x_1, \gamma_1) \right\}, \end{aligned} \tag{17}$$

where

$$\begin{aligned} f_1(x,\beta_1) = -\frac{1}{2(\beta_1{}^2x^2+1)^2} &\left\{ \beta_1 x \ln\left|\frac{x+1}{x-1}\right| + (\beta_1{}^2x^2-1)\tan^{-1}\beta_1 \right\} \\ &+ \frac{\beta_1}{2(1+\beta_1{}^2)} \frac{1}{(\beta_1{}^2x^2+1)}, \end{aligned}$$

and

$$f_2(x, x_1, \gamma_1) = -\frac{(\gamma_1 x)^5}{2(1+\gamma_1{}^2x^2)^4} \ln\left|\frac{x+1}{x-1}\right| + \frac{1}{\gamma_1{}^2x^2}(Ax_1{}^4 + Bx_1{}^3 + Cx_1{}^2 + Dx_1),$$

$$A = -\tan^{-1}\gamma_1, \qquad B = \frac{1}{2}\left(\frac{\gamma_1}{1+\gamma_1^2}+\tan^{-1}\gamma_1\right),$$

$$C = \frac{1}{4}\left(-\frac{\gamma_1}{(1+\gamma_1^2)^2}+B\right), \qquad D = \frac{\gamma_1}{6(1+\gamma_1^2)^3}-\frac{7}{24}\frac{\gamma_1}{(1+\gamma_1^2)^2}+\frac{B}{8},$$

$$x = \frac{k}{k_F}, \qquad \beta_1 = \frac{k_F}{\beta}, \qquad \gamma_1 = \frac{k_F}{\gamma}, \qquad \gamma_2 = \frac{\gamma}{\beta},$$

and

$$x_1 = \frac{\gamma_1^2 x^2}{1+\gamma_1^2 x^2}. \tag{18}$$

The calculation of the doublet splitting proceeds in exactly the same manner as in the first order, except that now we use the T matrix, equation (15), instead of the potential matrix V. The only change this introduces is that in equation (7) for $I_2(\mathbf{k}_1, \mathbf{k}_1')$, an extra factor, $[1+\lambda(M^*/M)J(k)]^{-1}$, appears under the sign of integration. After carrying out the integrations over the angular parts of $\mathbf{k}$ and $\mathbf{r}$, we obtain (introducing $y = k_1 r$ and $x = k/k_F$)

$$I_2(\mathbf{k}_1, \mathbf{k}_1') = -\frac{([\boldsymbol{\sigma}_1\times\mathbf{p}], \mathbf{k}_1)}{k_1^3} I'(k_1), \tag{19}$$

where

$$I'(k_1) = 8\pi^2 \int_0^1 dx\, \gamma^3 F'(x) \int_0^\infty dy\, 2y^2 \exp\left(-\frac{\alpha}{k_1^2}y^2\right) \frac{d}{dy}\left(\frac{\sin y}{y}\right)\frac{d}{d(2xy)}\left(\frac{\sin 2xy}{2xy}\right),$$

$$F'(x) = \gamma^{-3}\left(\frac{k_1}{\gamma}x\right)^5\left[1+\left(\frac{k_1}{\gamma}\right)^2 x^2\right]^{-4}\left[1+\lambda\frac{M^*}{M}J(x)\right]^{-1}. \tag{20}$$

The double integral in equation (19) was evaluated numerically, using Simpson's rule. The factor $[1+\lambda(M^*/M)J(k)]^{-1}$ needs careful consideration. For $x = 1$, i.e. $k = k_F$, it is zero, but very close to $x = 1$, on either side of this value, it has a singularity and the principal value of the integral is calculated at the point below k_F. The contribution due to the singularity is estimated to be about nine per cent of the total value of the double integral. We obtain

$$I_2(\mathbf{k}_1, \mathbf{k}_1') = -\frac{([\boldsymbol{\sigma}_1\times\mathbf{p}], \mathbf{k}_1)}{k_F^3}[1.080] \qquad (\text{for } Ca^{41}), \tag{21}$$

$$= -\frac{([\boldsymbol{\sigma}_1\times\mathbf{p}], \mathbf{k}_1)}{k_F^3}[0.837] \qquad (\text{for } O^{17}), \tag{22}$$

for a nucleon at the top of the Fermi distribution. Thus we have that for Ca^{41}, using the wave functions given in equation (9), the expression corresponding to equation (10) is

$$\Delta E = \frac{9t^2}{2Mk_F^3}\left(\frac{\lambda}{\gamma^3}\right)[1.080]\begin{bmatrix} \frac{1}{2}l \\ -\frac{1}{2}(l+1)\end{bmatrix}\int_0^\infty j_l^2(k_F R)\, R\frac{d\rho}{dR}\, dR, \tag{23a}$$

$$= 9.798\times10^{-54}\text{cm.}^4\begin{bmatrix} \frac{1}{2}l \\ -\frac{1}{2}(l+1)\end{bmatrix}\int_0^\infty j_l^2(k_F R)\, R\frac{d\rho}{dR}\, dR, \tag{23b}$$

and for O^{17}, the factor in the square bracket of equation (23*a*) is [0.837], so that the corresponding numerical factor in equation (23*b*) is 7.595×10^{-54} cm.^{4}.

If we neglect the effects of the exclusion principle, that is put $k_F = 0$ in equation (14), the value for the square bracket in equation (23*a*) for Ca^{41} is [1.011].

CONCLUSIONS

The above calculations were performed mainly with a view to seeing the effect of the different approximations made by different people in obtaining the spin–orbit interaction. We see that the results for the double integral over **r** and **k** can be compared in different cases. We discuss the case for Ca^{41}; similar considerations hold for O^{17}. When the effects of the exclusion principle are taken into account and the exact solution of the reaction matrix is used we find that the result for the splitting is larger than the first-order result by 57% of the first order. Of this, we find that a contribution somewhat less than 10% is due to the singularity alone, arising from the vanishing of $1+\lambda(M^*/M)J(k)$ in the denominator. We find further that when the exclusion principle is not taken into account, no singularity occurs and the result for the splitting is only slightly different from that in the case with the exclusion principle. This result may be interpreted as meaning that the exclusion principle makes only a little difference in the calculations because we are interested in nucleons at about the top of the Fermi distribution. We have evaluated the double integrals numerically by using Simpson's rule checked by a graphical method and we feel that the calculations warrant the general conclusions drawn above.

Using the density distribution given in equation (13) with a linear fall to zero in a region $a\lambda_\pi$ of the nuclear radius (with $a = 1.0$ and 1.5) we obtain a table of values for the splitting energies (Table I), where the calculations of this section lead to the figures in the fifth and sixth columns.

TABLE I

SPIN–ORBIT SPLITTING IN MEV.

		Calculated			
		First order		Exact	
	Observed	$a = 1.0$	$a = 1.5$	$a = 1.0$	$a = 1.5$
Ca^{41} ($l = 1$)	0.5	0.03	0.09	0.05	0.14
Ca^{41} ($l = 3$)	>2	0.29	0.24	0.51	0.42
O^{17} ($l = 2$)	5.0	0.22	0.17	0.45	0.35

We see that the results of our calculations indicate smaller values for the spin–orbit splittings than are indicated experimentally. To account for the difference, one may perhaps have to invoke the presence of spin–orbit coupling in the two-body interaction itself.

ACKNOWLEDGMENTS

The authors are grateful to the National Research Council for the award

of Postdoctoral Research Fellowships which enabled them to carry out this work. They would also like to express their appreciation to Dr. T. Y. Wu for his kind interest in this work.

REFERENCES

BELL, J. S. and SKYRME, T. H. R. 1956. Phil. Mag., Ser. 8, **1**, 1055.
BETHE, H. A. 1956. Phys. Rev. **103**, 1353.
BLIN-STOYLE, R. J. 1955. Phil. Mag. **46**, 973.
BRUECKNER, K. A. 1955. Phys. Rev. **97**, 1353.
ELLIOTT, J. P. and LANE, A. M. 1954. Phys. Rev. **96**, 1160.
HUGHES, J. and LECOUTEUR, K. J. 1950. Proc. Phys. Soc., A, **63**, 1219.
JANCOVICI, B. 1957. Phys. Rev. **107**, 631.
KEILSON, J. 1951. Phys. Rev. **82**, 759.
KISSLINGER, L. 1956. Phys. Rev. **104**, 1077.
YAMAGUCHI, Y. 1954. Phys. Rev. **95**, 1635.

A STUDY OF NUCLEON FORCES WITH REPULSIVE CORES

IV. CALCULATIONS OF THE SHAPE-DEPENDENT PARAMETERS IN NEUTRON–PROTON SCATTERING[1]

R. L. PRESTON[2] AND M. A. PRESTON

ABSTRACT

The magnitudes of the coefficients P and Q in the phase-shift expansion $k \cot \delta = -1/a+\frac{1}{2}r_0k^2-r_0^3Pk^4+r_0^5Qk^6+\ldots$ have been investigated in the case of repulsive-core NP interactions. For square, Gaussian, exponential, and Yukawa shapes, which fit experimental values of the scattering length and the effective range, the shape-dependent parameter P has been computed as a function of r_c in both singlet and triplet states. Also, for square and Yukawa shapes, which fit the scattering length and effective range, Q has been computed in the singlet state.

A. INTRODUCTION

It is well known that the S-wave neutron–proton scattering phase shift δ can be expanded as

$$k \cot \delta = -1/a+\tfrac{1}{2}r_0k^2-Pr_0^3k^4+Qr_0^5k^6+\ldots. \tag{A.1}$$

A complete discussion of the derivation of this formula, together with references to the original papers, may now be found in an article by Hulthén and Sugawara (1957) in the *Encyclopedia of Physics*. Some of the results of the present work have also been quoted there. For a discussion of the low-energy properties of a two-nucleon interaction, it is desirable to know with some accuracy the value of the effective range r_0. Values of the effective range deduced from experimental scattering cross sections, the binding energy of the deuteron, and photodisintegration cross sections depend upon the values assumed for the higher-order terms in the phase-shift expansion and, in particular, on those assumed for P and Q. The values of P for potentials of various shapes without repulsive cores have been calculated by Blatt and Jackson (1949). Because of our interest in repulsive-core potentials, we have investigated the effect of the introduction of a repulsive core on the magnitude of P and Q. The potential shapes used are not "cut off" at the core radius, r_c, as is the case in previous reports (Shapiro and Preston 1956), but are displaced from the origin. Thus, in considering the Yukawa potential, we are considering a potential which has an attractive infinity just at r_c, where the infinite repulsive potential starts. Since the potentials deduced from meson theories would be expected to cut off with a finite, though possibly large, value at the core, the potentials considered here may be said to cover the range of reasonable shapes.

[1]Manuscript received February 12, 1958.
Contribution from the Physics Department, Hamilton College, McMaster University, Hamilton, Ontario. Partially supported by a grant from the National Research Council. The paper is based on a thesis submitted by R. L. Preston in 1954 for the degree of M.Sc.
[2]Now at the University of Indiana, Bloomington, Indiana.

P_s has been calculated at various values of r_c for square, Gaussian, exponential, and Yukawa shapes, which give a singlet scattering length and an effective range $a_s = -23.68\times10^{-13}$ cm. and $r_{0s} = 2.6\times10^{-13}$ cm. P_t has been calculated for the four shapes in agreement with a triplet scattering length and an effective range $a_t = 5.28\times10^{-13}$ cm. and $r_{0t} = 1.56\times10^{-13}$ cm.

B. METHOD OF CALCULATION AND RESULTS

The parameters r_0, P, and Q associated with a potential

$$\text{(B.1)} \qquad \begin{aligned} V &= -V_0 f[(r-r_c)/r_b], & r &> r_c, \\ V &= \infty, & r &< r_c, \end{aligned}$$

are functions of the parameters r_0', P', and Q' associated with the potential

$$\text{(B.2)} \qquad V' = -V_0 f(r/r_b), \qquad r > 0.$$

V is the same potential as V' except that it is displaced from the origin a distance r_c. Since the radial wave function $u(r)$ vanishes at $r = r_c$, the effect of displacing the potential is to displace the associated wave function u through the same distance, i.e.

$$\text{(B.3)} \qquad u(r-r_c) = u'(r).$$

Since asymptotically $u(r) \sim \sin(kr+\delta)$, we see that

$$\text{(B.4)} \qquad \delta' = \delta - kr_c.$$

Expressions for the unprimed parameters in terms of the primed, and the primed in terms of the unprimed, then follow by equating coefficients of equal powers of k^2 in the expansions of the two identities

$$\text{(B.5}a\text{)} \qquad k\cot\delta = k\cot(\delta'+kr_c),$$

$$\text{(B.5}b\text{)} \qquad k\cot\delta' = k\cot(\delta-kr_c).$$

(*a*) *Evaluation of P*

For the shapes considered $P'(\alpha' r_0')$ is given by Blatt and Jackson (1949). α is the reciprocal scattering length, $1/a$. Hence, by giving α and r_0 suitable values and using the first two terms in identity (B.5*b*) to calculate $\alpha' r_0'$ at desired values of r_c, P was evaluated by equating the coefficients of k^4 in identity (B.5*a*) for the four shapes in both singlet and triplet states. The values are tabulated in Table I and the results for the four shapes are shown in Figs. 1 and 2.

As an independent check, P_s has also been calculated directly for a particular square well and a particular exponential well. If $u(r)$ is expanded about zero energy,

$$\text{(B.6)} \qquad u = u_0(r)+k^2u_1(r)+\ldots,$$

and if its asymptotic form v is also expanded,

$$\text{(B.7)} \qquad v = v_0(r)+k^2v_1(r)+\ldots,$$

TABLE I

SINGLET AND TRIPLET SHAPE-DEPENDENT PARAMETER P AS A FUNCTION OF CORE RADIUS FOR THOSE "DISPLACED" POTENTIALS OF THE SHAPES LISTED, WHICH GIVE r_0 AND a VALUES AS QUOTED IN SECTION A

Core radius, 10^{-13} cm.	Square	Gaussian	Exponential	Yukawa
Singlet parameter P_s				
0.0000	−.03068	−.01764	.009813	.05445
0.2000	−.03438	−.02664	−.01035	.01654
0.43691	−.03721	−.03362	−.02609	−.01274
0.82743	−.03923	−.03876	−.03745	−.03601
1.0000	−.03950	−.03940	−.03921	−.03887
1.2345	−.03951	−.03951	−.03951	−.03951
Triplet parameter P_t				
0	−.039	−.018	.0275	.1355
0.1	−.0419	−.028	.0037	.0785
0.2	−.0443	−.0351	−.0144	.0326
0.3	−.0462	−.0404	−.0273	.0004
0.4	−.04781	−.0443	−.0366	−.0208
0.6	−.05007	−.0492	−.0473	−.0438
0.7	−.05107	−.05073	−.05007	−.0488
0.8	−.05205	−.05197	−.05184	−.05154
0.9	−.04958	−.04958	−.04958	−.04958

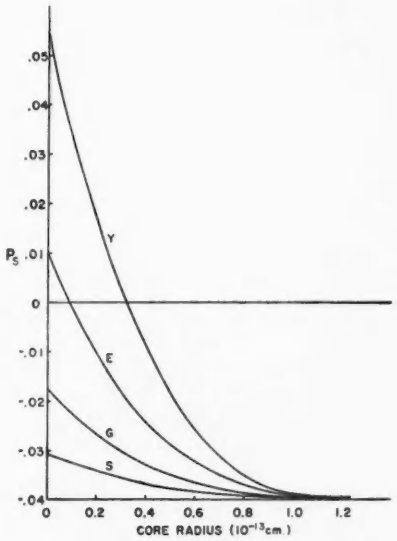

FIG. 1. The singlet parameter P_s plotted against core radius r_c for several potential shapes.

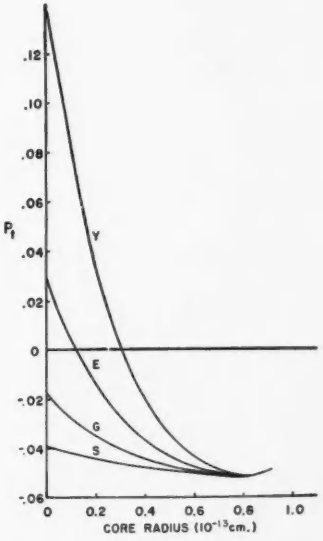

FIG. 2. The triplet parameter P_t plotted against core radius r_c for several potential shapes.

then exact expressions for P and Q (Jackson and Blatt 1950) are

$$r_0^3 P = \int_0^\infty (u_0 u_1 - v_0 v_1) dr, \tag{B.8}$$

$$r_0^5 Q = \int_0^\infty (v_1^2 - u_1^2) dr. \tag{B.9}$$

Here u_0 and u_1 vanish at the origin and satisfy

$$-\frac{\hbar^2}{M}\frac{d^2u_0}{dr^2} + Vu_0 = 0, \tag{B.10}$$

$$-\frac{\hbar^2}{M}\frac{d^2u_1}{dr^2} + Vu_1 = \frac{\hbar^2}{M}u_0, \tag{B.11}$$

and

$$v_0 = 1 - \frac{r}{a}, \tag{B.12}$$

$$v_1 = \frac{1}{2}r(r_0 - r) + \frac{1}{6}\frac{r^3}{a}. \tag{B.13}$$

For the square well, P was calculated by means of exact integration. Numerical integrations of (B.11) using Milne's formulas as in Shapiro and Preston (1956) were carried out to obtain P for the exponential shape. For these two cases the particular well parameters and the values of P obtained are listed in Table II and are seen to be in agreement with the corresponding values in Table I.

TABLE II

SINGLET PARAMETERS P_s AND Q_s FOR TWO PARTICULAR POTENTIALS

Shape	V_0, Mev.	r_b, 10^{-13} cm.	r_c, 10^{-13} cm.	P_s	Q_s
Square	149.35	1.64	0.8274	−.0392	.00364
Exponential	295.2	0.4400	0.4575	−.02571	.00187

(b) Evaluation of Q

When coefficients of k^6 in (B.5*a*) were equated, Q was obtained in terms of the primed parameters. However, in this case it was necessary to calculate $Q'(\alpha' r_0')$ for the desired shapes. For the square and Yukawa shapes in the singlet state an approximation for $Q'(\alpha' r_0')$ was obtained by evaluating the first two terms of a Taylor series expansion of Q'

$$Q'(\alpha' r_0') = Q'(0) + \left.\frac{\partial Q'}{\partial(\alpha' r_0')}\right|_{\alpha=0} (\alpha' r_0'). \tag{B.14}$$

For the two cases the approximations obtained are:

$$\text{Square:} \quad Q_s' = 0.001713 + 0.0020(\alpha' r_0'), \tag{B.15}$$

$$\text{Yukawa:} \quad Q_s' = 0.0113 + 0.113(\alpha' r_0'). \tag{B.16}$$

For the square well Q was also evaluated by exact integrations at five values of r_c. To obtain the Q' expansion (B.16) for the Yukawa shape, it was necessary to carry out numerical integrations of differential equations for v_0-u_0, v_1-u_1, $\partial u/\partial\alpha$, $\partial u_1/\partial\alpha$, at $\alpha = 0$. The variation of α is produced by altering V, thus producing different u_0 and u_1. The values of Q_s obtained for the square well and for the Yukawa are tabulated in Table III.

TABLE III

SINGLET PARAMETER Q_s FOR SQUARE AND YUKAWA SHAPES FOR POTENTIALS WHICH GIVE a_s AND r_{0s} VALUES QUOTED IN SECTION A

r_c, 10^{-13} cm.	Q_s, square well: (a) From integration	Q_s, square well: (b) From use of Q_s'	Q_s, Yukawa
0		$.0014_9$	$-.0012$
0.04516	.00176	$.0016_5$	
0.1		$.0019_6$	$-.0014$
0.2		$.0024_2$	$-.0014$
0.3		$.0027_6$	$-.0009$
0.4369	.00315	$.0031_1$	.0001
0.5		$.0032_3$	.0006
0.6		$.0035_4$	.0016
0.63195	.00348	$.0036_4$	
0.8274	.00364	$.0036_8$	.0029
1			.0035
1.2200	.00374		
1.2345		$.0037_5$	.0037

Q_s was also calculated for a particular exponential, and the calculated value is listed with the potential in Table II. The results for Q_s are compared in Fig. 3.

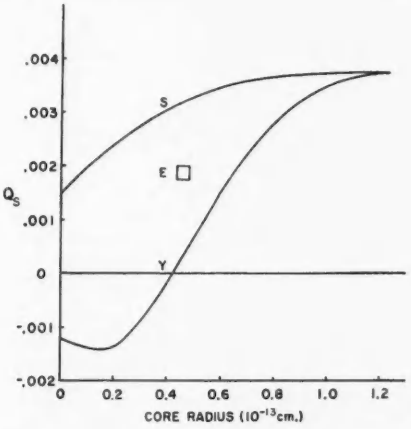

FIG. 3. The singlet parameter Q_s as a function of core radius for square and Yukawa attractive potentials, with one point for an exponential shape.

In order that r_0' remain positive, it is necessary that r_c be less than a certain limiting value, which for the singlet state is 1.234×10^{-13} cm. We

have not considered values of r_c greater than this. It will be observed that, as r_c increases to its limiting value, both P and Q tend to a limit independent of the shape of the attractive potential.

REFERENCES

BLATT, J. M. and JACKSON, J. D. 1949. Phys. Rev. **76**, 18.
HULTHÉN, L. and SUGAWARA, M. 1957. The two-nucleon problem, *in* Encyclopedia of Physics, Vol. 39, *edited by* S. Flügge (Springer-Verlag, Berlin).
JACKSON, J. D. and BLATT, J. M. 1950. Revs. Modern Phys. **22**, 77.
SHAPIRO, J. and PRESTON, M. A. 1956. Can. J. Phys. **34**, 451.

THE FREEZING POINTS OF HIGH PURITY METALS AS PRECISION TEMPERATURE STANDARDS

III. THERMAL ANALYSES ON EIGHT GRADES OF ZINC WITH PURITIES GREATER THAN 99.99+%[1]

E. H. McLaren

ABSTRACT

Extensive thermal analyses have been carried out on eight grades of high purity zinc with the suppliers' analyzed impurity contents in the range <0.5 to <70 p.p.m. The liquidus points have been intercompared with a precision of about 0.0002° C. and the alloy melting ranges have been examined following different rates of freezing. A melting range parameter may provide a more sensitive index of the purity than the liquidus temperature since the shape of the melting curve is strongly influenced by segregation of impurities due to coring on freezing. Two grades of Russian high purity zinc have liquidus points and melting ranges so close to those of New Jersey S.P. zinc that it is difficult to discriminate among them using precision resistance thermometry. This shows that a reported discrepancy of about 0.1° C. in the freezing points of zinc between the Russian and Canadian laboratories is not due to different impurity contents of the zincs that were used.

INTRODUCTION

Precision thermal analyses on eight samples of high purity zinc procured from four countries (U.S., U.S.S.R., U.K., and Canada) have been carried out for two reasons: to investigate a difference of about 0.1° C. in the freezing temperatures of zinc reported by the D.I. Mendeleev Institute of Metrology, Leningrad (1955), and by McLaren (1955); and to demonstrate the usefulness of precision resistance thermometry in the detection of soluble impurities in high purity metals.

The Russian and Canadian values of the freezing points of high purity zinc were 419.59±0.03° C. (Int.) and 419.50±0.01° C. (Int.) respectively. The Canadian value was based on the freezing point of the Super Pure grade zinc prepared by the New Jersey Zinc Company, Palmerton, Pa., U.S.A., and was the average of the 'freezing point temperatures' given by eight standard thermometers, seven with National Bureau of Standards (Washington) calibrations and the other with a National Physical Laboratory (Teddington) calibration. It seems probable that this discrepancy was due to difficulties in the realization of the Boiling Point of Sulphur on the International Temperature Scale. However, an interchange of high purity zincs was arranged with the Russian laboratory so that an intercomparison of freezing temperatures could determine conclusively whether or not the reported large difference was due to impurity contents of the Russian and American zincs. Samples of high purity zinc from British and Canadian sources were included in the comparison at this laboratory.

[1]Manuscript received December 23, 1957.
Contribution from the Division of Applied Physics, National Research Council, Ottawa, Canada.
Issued as N.R.C. No. 4709.

McLaren (1957*a*, *b*) has shown that precision thermal analysis is capable of revealing alloy structures on the thermal curves of zinc, cadmium, and tin of purities greater than 99.99+%. The investigation of eight grades of high purity zinc provides a broader basis for assessing the usefulness of resistance thermometry in the selection of high purity metals and affords a direct comparison between the thermal effects of impurities and the chemical analyses of the eight alloys.

Material

Table I lists the origin, grade, and form of the zinc metal as received and Table II shows the chemical analyses supplied by the sources. Where possible, estimates were made of the slopes of the liquidus and solidus at the zinc-rich end of the phase diagrams for the impurities listed in Table II in order to calculate the changes in the liquidus and solidus temperatures from the freezing temperature of the pure element and the melting ranges that would be expected for the eight samples; these estimates are shown in Tables III and IV.

TABLE I

IDENTIFICATION OF THE ZINC SAMPLES

Sample	Origin	Grade	Form
R.1	D.I. Mendeleev Institute of Metrology, Leningrad, U.S.S.R.	Highest Purity	Rod, 8 mm. diam.
R.2		High Purity	Rod, 8 mm. diam.
S.4	New Jersey Zinc Company, Palmerton, Pa., U.S.A.	Super Pure*	Crystalline aggregate
5.7		Chemically Pure*	Rod, 8 mm. diam.
C.1	The Consolidated Mining and Smelting Company, Trail, B.C., Canada	High Purity No. 678	Cast slab
C.2		Tadanac	Cast slab
B.1	Imperial Smelting Corporation Limited, London, U.K.	Spectrographically Pure†	Rod, 7 mm. diam.
B.2		Crown Special	Ball, 2 in. diam.

*See Cyr (1927), Truesdale and Edmunds (1939).
†See Twyman (1951).

TABLE II

IMPURITY CONTENTS OF THE ZINC SAMPLES SUPPLIED BY THE SOURCES

Sample	Wt. (p.p.m.)						Total (p.p.m.)
	Fe	Cd	Cu	Pb	Sn	As	
R.1			Better than R.2				<0.5
R.2	<0.2	<0.1	0.01	<0.2	<0.02		<0.5
S.4	—	<0.5	—	<2	—		<2
5.7	4	0.5	0.5	1	0.5	0.04	6
C.1	2	0.1	0.5	<2	—		<4
C.2	10	10	10	20	—		50
B.1	—	—	—	<1	—		<1
B.2	<30	20	<10	<10	—		<70

TABLE III

SLOPE OF THE SOLIDUS AND LIQUIDUS AT THE ZINC-RICH END OF THE PHASE DIAGRAMS FOR PARTICULAR IMPURITIES

Impurity	Wt.% eutectic	Solid solubility limit (wt.%)	°C., ΔT(Zn-eutectic)	°C./wt.%, slope liquidus	°C./wt.%, slope solidus	References
Fe	0.0122	0.0015	+0.05	−4.1	−33	Edmunds (1944) Truesdale *et al.* (1936) Anderson (1953)
Cd	82.5	2.0	+154	−1.9	−77	Metals Handbook (1948)
Cu*	1.8	2.7	−4.5	+2.5	+1.7	" " "
Pb	0.9	—	+1.7	−1.9	—	" " "
Sn	91	—	+220	−2.4	—	" " "

*Peritectic at 2.7% Cu, liquidus at 1.8% Cu.

TABLE IV

ESTIMATED CHANGE IN THE SOLIDUS AND LIQUIDUS TEMPERATURES FROM THOSE OF THE PURE ELEMENT, AND THE ASSOCIATED RANGE OF MELTING TEMPERATURES FOR THE SAMPLES LISTED IN TABLE II

Sample	Lowering of liquidus (° C.)	Lowering of solidus* (° C.)	Estimated melting range (° C.)
R.1	<0.00014	<0.0014	<0.0013
R.2	<0.00014	<0.0014	<0.0013
S.4	<0.00048	<0.0039	<0.0034
5.7	0.0019	0.0170	0.015
C.1	<0.0011	0.0073	<0.0062
C.2	0.0073	0.11	0.10
B.1	<0.00019	—	—
B.2	<0.016	<0.25	<0.23

*In these estimates it is assumed that the solid solubility of Pb and Sn in Zn is zero (see Rodda (1938) and Peirce (1923)) and that the temperature at which the bulk of these impurities dissolves into liquid alloy is primarily determined by the solidus temperature of the solid solution containing the soluble impurities in these very dilute alloys.

EXPERIMENTAL

The apparatus and techniques used in the thermal analysis have been described previously (McLaren 1957*a*, *b*). For the present work dry nitrogen atmospheres were used over the melts. Very fast freezes were made by extracting the pyrex tubes holding the crucibles of molten zinc right out of the zinc furnace and allowing solidification to take place either in room air or in another furnace nominally held at 250° C.

The analysis was divided into two parts; first, a survey of all samples was carried out to obtain freezing and melting curves under a variety of thermal conditions using a shortened measurement technique, and secondly a careful intercomparison of the plateau freezing temperatures was made using the complete precision techniques outlined by McLaren (1957*a*, *b*).

Thermal Survey

Resistance thermometry for this survey was based on NR balances at 2 ma. current, single daily measurements at the triple point of water, and approximate pressure corrections over the melts. The relative errors along a particular curve due to this shortened technique are less than 0.0001° C. but the relative

difference from curve to curve could possibly be as high as 0.0005° C. For survey work of this type where interest lies primarily on the form of the thermal curves the 2NR technique allows many measurements to be made since there are no undue dead times as the resistance thermometer comes to equilibrium at different currents. For the very fast freezes the measuring technique was further shortened to 2N balances, enabling several measurements to be made in a minute. Times for resistance balances were recorded to the nearest second.

Considerable attention has been given to the rounding at the beginning and end of arrests; Hume-Rothery *et al.* (1952) indicate that arrests may be sharpened by decreasing the thermal lag of the temperature detector and by using slow heating rates. The Meyers resistance thermometer used in this work has such a rapid response time that thermal lags due to this detector immersed in the 1-kg. samples are negligible, except possibly during very fast freezes. The rounding at the end of the melting curves may be due to convection currents in the crucible when the bulk of the sample is liquid and only a small fraction of the charge is still solid; this rounding in the few minutes prior to the liquidus break is similar from sample to sample. The best criterion that good thermal conditions exist for the transformations is the close agreement between the temperature of the liquidus break on the melting curve and the plateau temperature (i.e. liquidus point, see McLaren (1957)) for the same sample on either normal or induced slow freezes.

Freezing and remelting curves were obtained for several series of transformations which were designed to inhibit or enhance segregation of chemical impurities (coring) by control of cooling rates on the freeze and to detect these effects by examination of the remelting contour.* For each series of transformations the furnaces were adjusted to give similar thermal treatment to all samples; melting curves were taken immediately after completion of freezes to minimize annealing effects in the ingots. Table V gives a summary of transformation conditions for the thermal curves included in this paper. Series 2(*b*) and 3 were run twice; essentially the same information was obtained both times.

TABLE V

SUMMARY OF TRANSFORMATION CONDITIONS FOR THE THERMAL CURVES

Series	Designation	Duration (minutes)	Sample	Figure
1. Freeze	Fast normal	35–40	All	2
2(*a*). Freeze	Very fast normal	3	R.1	1
2(*b*). Freeze	Very fast normal	5–6	All	3
3. Melt	Slow after freezes of Fig. 3	70–100	All	4
4. Freeze	Fast induced	100	All	5
	Slow induced	C.1—150		
	Slow induced	C.2—180		
5. Melt	Slow after freezes of Fig. 5	70–100	All	6

*Melting contour is used here to mean the profile of the direct time–temperature melting curve.

Results

Fig. 1 shows representative freezing curves in sample R.1. On fast induced and fast normal freezes, curves I and II respectively, the zinc solidifies uniformly in closed cylindrical shells, providing an excellent environment and shield for the resistance thermometer. Curves III and IV were obtained at very fast

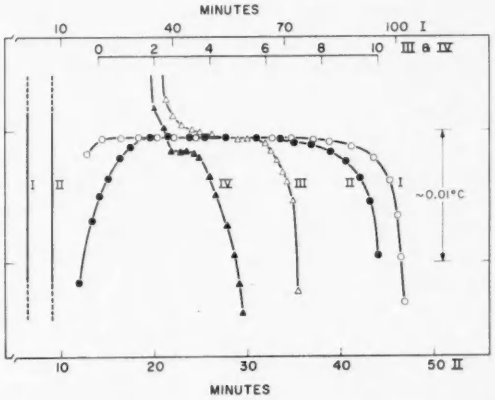

FIG. 1. Representative freezing curves on sample R.1: I, fast induced; II, fast normal; III and IV, very fast normal.

freezing rates where the rapidity and lack of uniformity in freezing would be expected to provide extremely unfavorable conditions for resistance thermometry; hence it is surprising that the arrests noted on these curves are within 0.002° C. of the plateau freezing temperatures that are obtained on slow induced freezes using the complete precision technique. Undoubtedly the very large amount of latent heat associated with 1 kg. of zinc, combined with the high purity of this sample, enables these fairly reliable temperature measurements to be made even when the ingot solidifies in 3 minutes.

Fast normal freezing curves on all the samples, obtained by monitoring temperatures in the samples as they solidified in the furnaces after the power supplies were turned off, are shown in Fig. 2. From this figure it is evident that the samples can be usefully divided into three groups on the basis of maximum temperatures attained during recalescence; group I includes R.1, R.2, and S.4; group II, C.1, B.1, and 5.7; and group III, C.2 and B.2. This figure shows freezing occurring over a range of temperatures and distinctive differences are noticed among the samples; but as liquidus arrests are screened out by supercooling (about 0.04° C. for these samples) it is difficult to obtain useful information on the relative ranges of alloy transformation temperatures from these curves. However, the extreme sensitivity and simplicity of using the resistance thermometer to sort out high purity metals is demonstrated by these curves.

The ideal range of alloy transformation temperatures is the difference in

the temperatures at which melting or freezing begins and ends in a completely homogenized alloy; or alternatively the difference in the temperatures of the solidus and liquidus for the alloy on the equilibrium diagram. In practice very great obstacles exist in realizing ideal melting ranges because it is difficult, if not impossible, to attain complete homogenization of a sample; this is a consequence of the differences in the solubilities of the impurities in the solid and liquid alloys and of the low rate of diffusion of the solute in the solid. Earlier

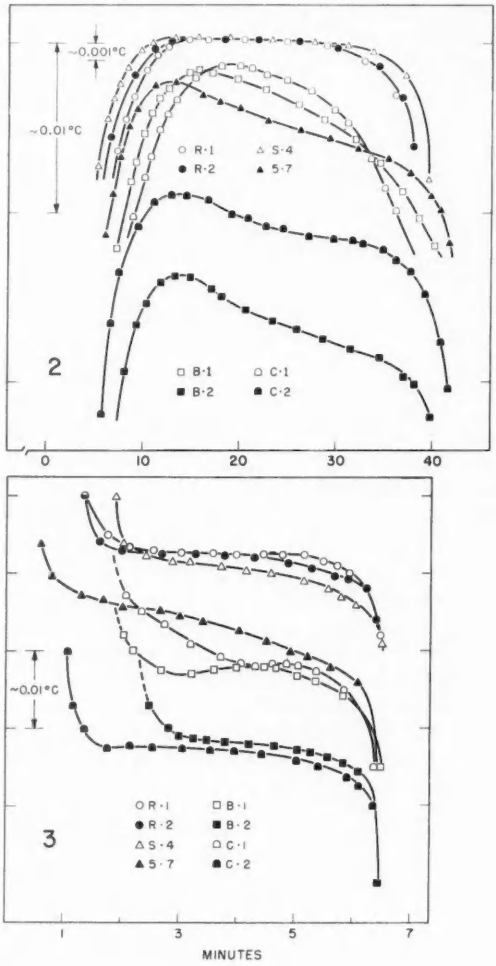

FIG. 2. Fast normal freezes on all samples; plotting begins during recalescence.
FIG. 3. Very fast freezes on all samples.

work on New Jersey zincs has shown that the best alloy ranges (i.e. approximating textbook thermal curves on simple binary alloys) are obtained from melting curves determined immediately after very fast freezes. The rapid freezing gives rise to smaller grains and the impurities must be more evenly distributed throughout the ingot than after slow freezing, which gives very large highly cored grains. The impurity concentrations near the grain boundaries in these cored grains are many times greater than the equilibrium concentrations for the ingot. These non-equilibrium concentrations of dissolved impurities cause differences between the true solidus temperatures of the alloys and the temperatures at which melting begins, but at the same time provide a mechanism for detecting the impurities and their segregation in high purity metals.

In order to distribute the impurities throughout the ingot as evenly as possible, in preparation for melting range determinations, the very fast freezes of Fig. 3 were obtained. Surprisingly these curves deserve attention in their own right because they show that even under these severe conditions the resistance thermometer is capable of distinguishing between samples of different quality. Fig. 4 shows the melting curves that were obtained immediately after these freezes; the alloy ranges varied from about 0.001° C. for the purest to a few hundredths of a degree for the least pure samples.

In order to accentuate segregation of the dissolved impurities the induced freezes shown in Fig. 5 were made and melting curves following these freezes are given in Fig. 6.

A comparison of Figs. 4 and 6 shows that although group I metals have similar alloy melting ranges following the two types of freezing, distinct differences are noted for the samples of group II and III. In Fig. 6 segregation structures have been developed on the melting curves of samples C.1 and B.1 and now very substantial fractions of all the group II metals melt well inside a range of 0.01° C. For group III samples two observations are made: the C.2 curve does not have the step near the liquidus break that appears in Fig. 4 and the general melting contours for both C.2 and B.2 lie on steeper slopes than those obtained in Fig. 4. Melting takes place over greater ranges and only the temperatures of the liquidus breaks remain unchanged.

A more detailed analysis of these melting curves allows comparative measurements to be made of the melting ranges of these samples. Measurements of three melting parameters were made: conventional melting ranges from direct melting curves, and the widths at half-maximum and at the 1% level from inverse curves.

Curve I of Fig. 7 reproduces on a larger scale the melting curve of S.4 shown in Fig. 4 and shows how the melting ranges of the alloys were estimated from the direct melting curves.

Curve II of Fig. 7 shows the inverse melting curve of I. This was derived from the times for successive equal temperature intervals and from the total melting time; the percentage of the total melting time in a given temperature interval is plotted against the average temperature of the interval. For the slow heating rates used in these experiments the furnace block temperature

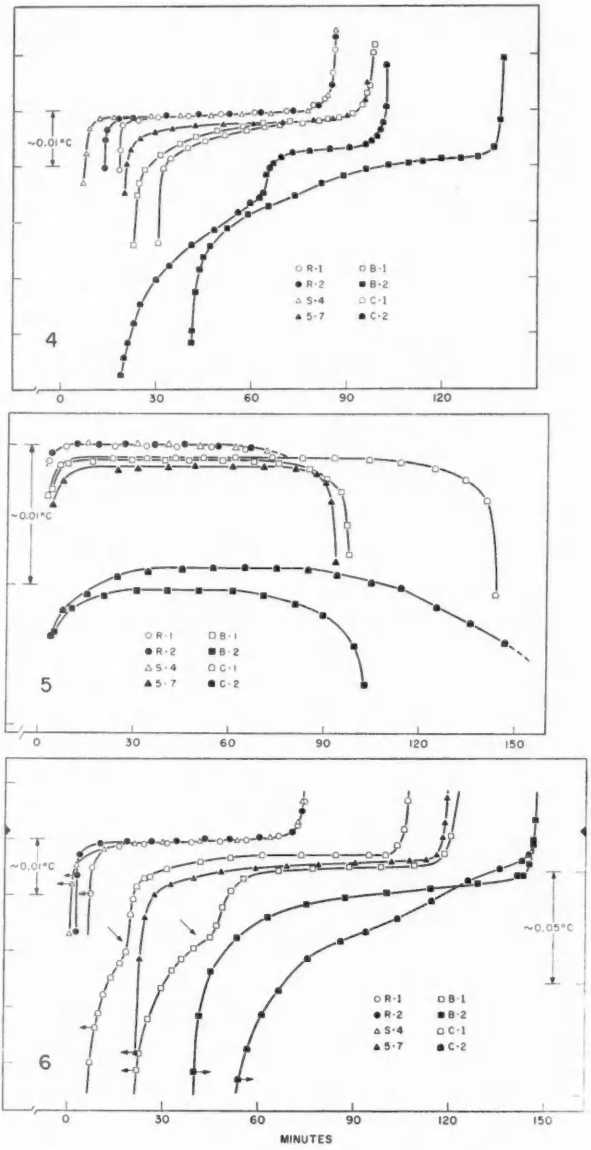

FIG. 4. Melting curves after the very fast freezes of Fig. 3.
FIG. 5. Induced freezes on all samples.
FIG. 6. Melting curves after the induced freezes of Fig. 5.

remains nearly constant during the transformation; therefore the percentage time in a given temperature interval is a fair approximation of the percentage of the sample that is melted during the interval. The inverse curve does not give as detailed information as the direct curve but it has the advantage of enabling the essential melting range information to be plotted in a smaller space. On curve II of Fig. 7 an estimate of the width at half-maximum '*W*'

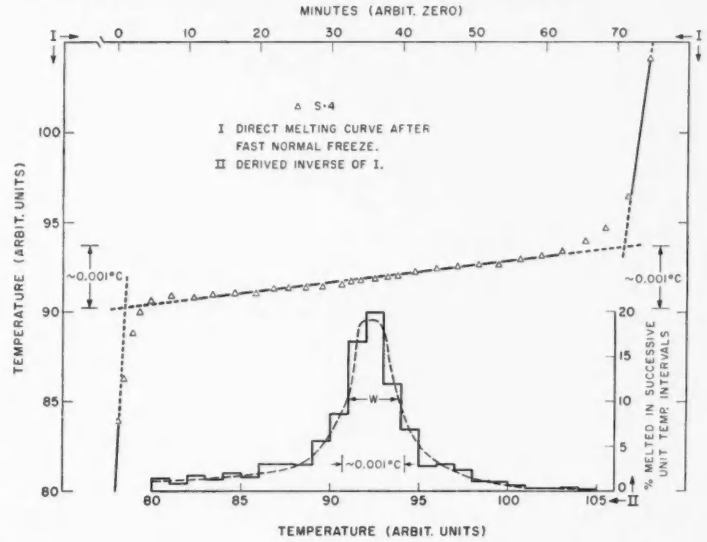

FIG. 7. I, melting curve on sample S.4 after very fast freeze on Fig. 3; II, derived inverse of I.

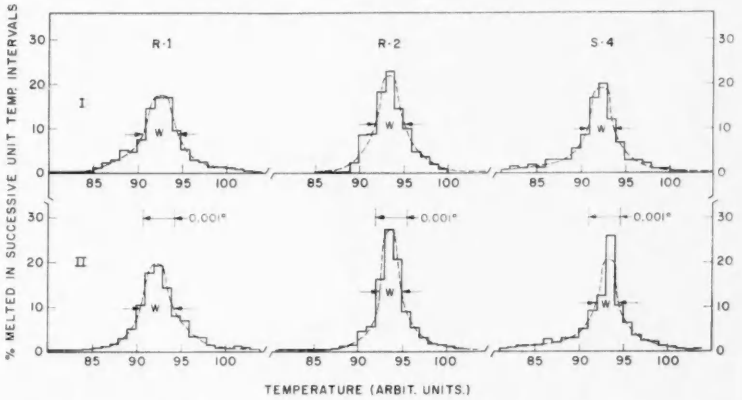

FIG. 8. Inverse melting curves of samples R.1, R.2, and S.4: I, after very fast freezes; and II, after induced freezes.

is shown; both W and the conventional melting range shown in I are approximately 0.001° C.

Figs. 8 and 9 show examples of linear and logarithmic inverse plots from which estimates of the widths at half-maximum and the widths at the 1% level of the melting ranges of all the samples were made; Table VI summarizes the measurements of the three melting parameters.

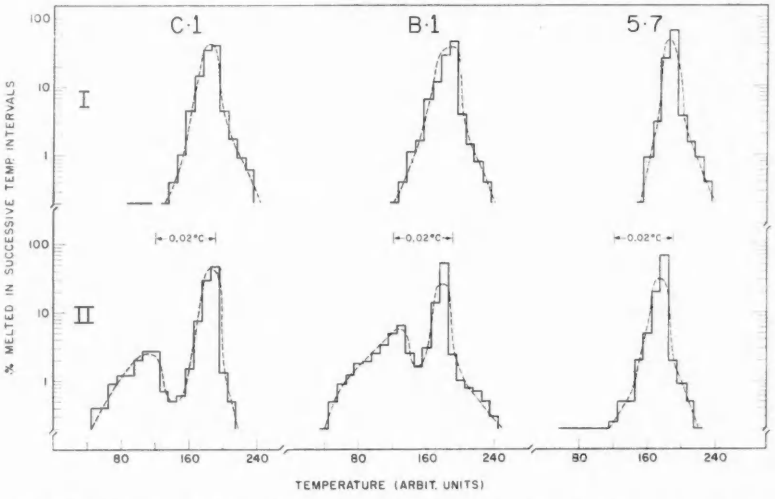

FIG. 9. Inverse melting curves of samples C.1, B.1, and 5.7: I, after very fast freezes; and II, after induced freezes.

TABLE VI

ALLOY MELTING RANGES AFTER VERY FAST FREEZES (I) AND INDUCED FREEZES (II)

Sample	From direct curves (° C.)		From inverse curves (° C.) Width at ½ max.		From inverse curves (° C.) Width at 1% level		Estimated range from Table IV (° C.)	Total impurity content (p.p.m.)
	I	II	I	II	I	II		
R.1	0.001	0.001	0.0011	0.0011	0.0045	0.0041	<0.0013	<0.5
R.2	0.001	0.001	0.0010	0.0007	0.0029	0.0032	<0.0013	<0.5
S.4	0.001	0.001	0.0008	0.0008	0.0053	0.0050	<0.0034	<2
5.7	0.005	0.007	0.0014	0.0014	0.015	0.015	0.015	6
C.1	0.01	0.03, 0.005*	0.0033	0.0009	0.019	0.036	<0.0062	<4
C.2	0.02–0.03	0.10	0.031	0.045	0.09	0.15	0.10	50
B.1	0.01	0.03, 0.005*	0.0027	0.0013	0.020	0.039	—	<1
B.2	0.01–0.02	0.04	0.003	0.004	0.020	0.019	<0.23	<70

*Melting range of the high purity cores in these samples after induced freezing.

Plateau Temperatures

The second part of the investigation involved a careful comparison of the plateau freezing temperatures developed on slow induced freezes of S.4 with the plateau temperatures on similar freezes on the seven other alloys. Two

furnaces were employed in order that sample S.4 and the sample under comparison could be allowed to undergo slow induced freezes simultaneously, enabling the measurements of the plateau temperatures to be made inside 1 hour on both samples. The measuring sequence was as follows:

a.m. Br., Bz., T.P., Zinc (S.4), Zinc (X), Br., Bz., T.P.
p.m. Zinc (X), Zinc (S.4), Br., Bz., T.P.
Br.—Bridge Ratio; Bz.—Bridge Zero; T.P.—Triple Point of Water.

Measurements were made with the mid-point of the sensing coil of a single Meyers thermometer immersed about 15 cm. in the zinc samples. A single triple-point cell was used throughout the study: one ice mantle was prepared and maintained during the work on R.1 and R.2 and another mantle was used for the comparisons on the other five samples.

Fig. 10 gives results of comparing the plateau temperatures of R.1 and R.2 with those obtained for S.4 and involves 40 slow induced freezes. Fig. 11 gives similar results on the comparisons of C.1, B.1, and 5.7 with S.4, where five determinations on each sample were made. Only two precision runs were made on each of C.2 and B.2 because the precise location of their liquidus points does not appear important in temperature-standard considerations. The intercomparisons are summarized in Table VII; and in addition the final column in the table shows the estimated lowerings of the liquidus temperatures from the pure element derived from the chemical analyses of the samples and the known phase diagrams.

TABLE VII

INTERCOMPARISON OF PLATEAU TEMPERATURES

Mean date	Sample	No. of freezes	Ratio R_{Zn}/R_{TP} Mean	$10^8\times$ Std. Dev.	Reproducibility (equivalent 10^{-4}° C.) Std. Dev.	Spread	Plateau temp. rel. to S.4 (° C.)	Liquidus depression (° C.) from Table IV
18.7.57	S.4, R.1	20	2.56806227	±60	±1.7	6.7		
	R.1	10	6194	±48	±1.4	4.5	-0.0001_8	<0.00014
	S.4	10	6259	±55	±1.6	5.7	0.0	<0.00048
25.7.57	S.4, R.2	20	2.56806359	±65	±1.9	5.5		
	R.2	10	6374	±60	±1.7	4.4	$+0.0000_9$	<0.00011
	S.4	10	6343	±70	±2.0	5.5		
21.7.57	S.4, R.1, R.2	10	2.56806293	±90	±2.6	9.0		
				$10^8\times$ Mean Dev.	Mean Dev.			
10.8.57	S.4	5	2.56806120	± 32	±0.9	3.7		
	C.1	5	5998	± 43	±1.2	4.6	-0.0003_5	<0.0011
14.8.57	S.4	5	2.56806155	± 45	±1.6	6.0		
	B.1	5	5966	± 19	±0.7	2.4	-0.0005_4	<0.00019
18.8.57	S.4	5	2.56806150	± 46	±1.6	4.3		
	5.7	5	5582	± 19	±0.7	2.4	−0.0016	0.0019
22.8.57	S.4	2	2.56806158	± 58	±1.7	3.3		
	C.2	2	3262	±122	±3.4	7.0	−0.0083	0.0073
24.8.57	S.4*	2	2.56806142	± 44	±1.3	2.5		
	B.2	2	3578	± 44	±1.3	2.5	−0.0102	<0.016

*The average R_{Zn}/R_{TP} for S.4 for the 39 slow induced freezes was 2.56806224 with a standard deviation equivalent to $\pm 0.0002_9$° C. and a spread of 0.0011° C.; these numbers reflect the stability of the whole measuring system including thermometer, triple-point cell, and bridge.

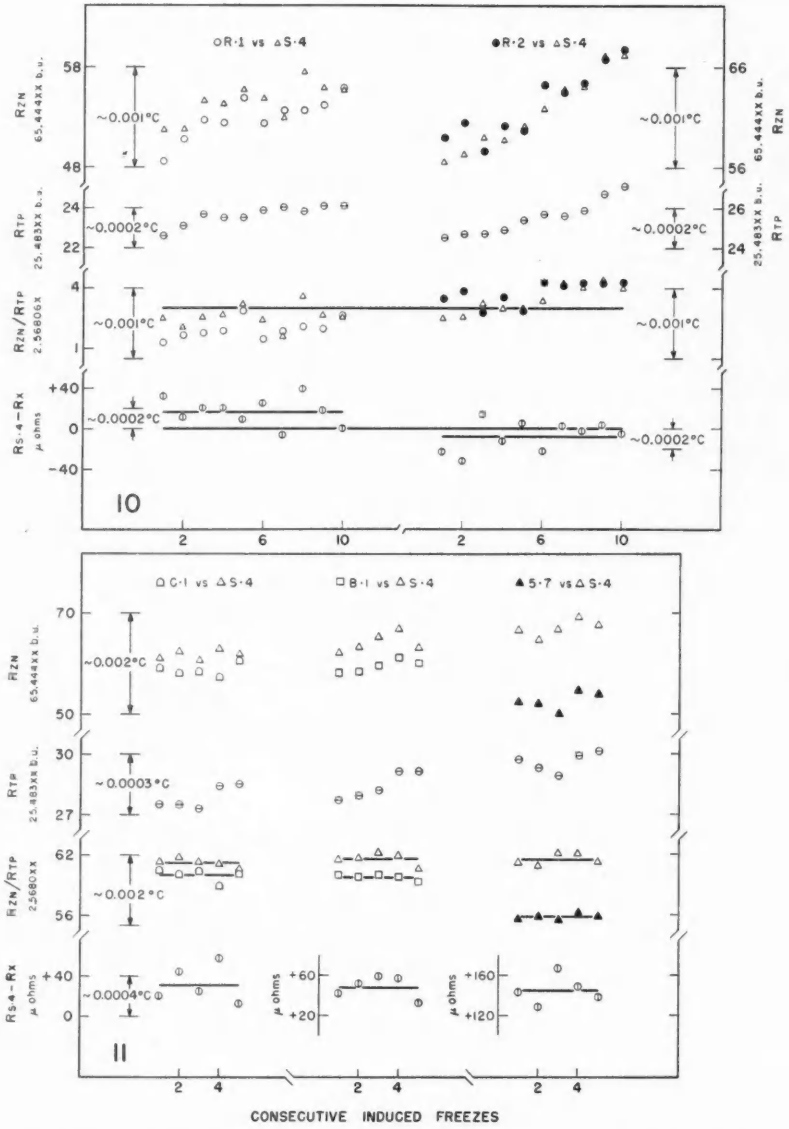

FIG. 10. Intercomparison of plateau temperatures of samples R.1 and R.2 with S.4: R_{TP} and R_{Zn}, zero-current fully corrected resistances of the thermometer at the triple point of water and zinc points respectively.

FIG. 11. Intercomparison of plateau temperatures of samples C.1, B.1, and 5.7 with S.4.

DISCUSSION

The plateau freezing temperatures developed on induced freezes of high purity zinc now appear unquestionably to be the liquidus points of the alloys.

The three melting parameters in conjunction with varied freezing techniques provide a means of gauging impurity effects from melting curves. Thus samples C.1 and B.1 under all phases of the thermal analyses are strikingly similar and one could suggest that they have nearly the same impurity contents. The segregation of a specific impurity may account for the minor arrests on the melting curves of these alloys following induced freezing and for the steps on the melting curves of C.2 after very fast freezes. It is hoped that refinements in experimental techniques will allow more detailed measurements to be made on the melting contours on a series of special alloys and so allow us to obtain information on the presence of specific impurities. Parallel metallographic inspection would undoubtedly provide valuable correlations with both thermal and chemical analysis.

As expected, the samples with the highest liquidus points have the smallest melting ranges (effects of copper impurity contents are overweighed by the other impurities); in this regard the width at the 1% level appears to be a more sensitive criterion of purity than the liquidus point of the alloy.

On the basis of both plateau temperature and alloy melting range the Russian zincs are certainly as pure as the New Jersey Super Pure Zinc and the source of the difference in the reported zinc freezing points referred to earlier must lie in other aspects of precision resistance thermometry. The sample S.4 was first used in January, 1956, and has been used occasionally for thermometer calibrations since that time, being removed from the furnace after each calibration; the Russian samples were loaded in July, 1957. The agreement in the plateau temperatures of these samples is further evidence of the high stability of the liquidus point of high purity zinc as a precision temperature standard.

The advantage of thermal analysis for the detection of soluble impurities in high purity zinc is that reasonably accurate relative numbers may be identified with liquidus points and alloy melting ranges from sample to sample. It is not necessary to depend on estimates of upper limits of these physical quantities derived from uncertain impurity analyses and even more doubtful knowledge of the phase diagrams at the zinc-rich end. The 1-kg. ingots required for precision resistance thermometry allow the liquidus-point determination to be made on fairly representative samples, which help to eliminate sampling errors frequently found in quantitative spectrochemical analysis.

The disadvantage of precision thermal analysis is that particular impurities cannot be immediately identified.

CONCLUSIONS

No measurable difference was found between the liquidus points of two samples of high purity zinc from the D.I. Mendeleev Institute of Metrology, U.S.S.R., and the liquidus point of New Jersey S.P. zinc previously examined in this laboratory.

New information on the usefulness of precision thermal analysis for metallurgical inspection of high purity metals has been presented.

ACKNOWLEDGMENTS

The author is grateful to Mr. E. G. Murdock for his very capable assistance throughout these investigations and to Dr. H. Preston-Thomas for a careful reading of the paper. He wishes to thank the Temperature Standards Section of the Mendeleev Institute of Metrology, Leningrad, for sending samples R.1 and R.2; the Consolidated Mining and Smelting Company, Trail, B.C., and Mr. G. H. Turner in particular, for samples C.1 and C.2; the Imperial Smelting Corp. Ltd., London, for supplying sample B.2 without charge; and Mr. E. A. Anderson of the New Jersey Zinc Co., Palmerton, Pa., U.S.A., for assistance at an earlier period.

REFERENCES

ANDERSON, E. A. 1953. New Jersey Zinc Co., Palmerton, Pa., U.S.A., private communication.
CYR, H. M. 1927. Trans. Am. Electrochem. Soc. **52**, 349.
EDMUNDS, G. 1944. Trans. Am. Inst. Mining Met. Engrs. **156**, 263.
HUME-ROTHERY, W., CHRISTIAN, J. W., and PEARSON, W. B. 1952. Metallurgical equilibrium diagrams (The Institute of Physics, London), Chap. 10.
MCLAREN, E. H. 1955. Comité International des Poids et Mesures, Procès-Verbaux des Séances de 1954, **24**, T163.
——— 1957*a*. Can. J. Phys. **35**, 78.
——— 1957*b*. Can. J. Phys. **35**, 1086.
MENDELEEV INSTITUTE OF METROLOGY, LENINGRAD, U.S.S.R. 1955. Comité International des Poids et Mesures, Procès-Verbaux des Séances de 1954, **24**, T122.
METALS HANDBOOK. 1948. (The American Society for Metals, Cleveland, Ohio.)
PEIRCE, W. M. 1923. Trans. Am. Inst. Mining Met. Engrs. **68**, 767.
RODDA, J. L. 1938. Mining and Met. **19**, 367.
TRUESDALE, E. C., WILCOX, R. L., and RODDA, J. L. 1936. Trans. Am. Inst. Mining Met. Engrs. **122**, 192.
TRUESDALE, E. C. and EDMUNDS, G. 1939. Trans. Am. Inst. Mining Met. Engrs. **133**, 267.
TWYMAN, F. 1951. Metal spectroscopy (Charles Griffin and Company Limited, London), p. 473.

ON THE FRICTION OF INFLATED RUBBER TIRES ON ICE[1]

C. D. NIVEN

ABSTRACT

The friction on ice of some small inflated rubber tires was measured on a turntable in a cold room. When rolling-friction force was plotted against load, the relation was either linear or slightly curved away from the load axis; such curvature implies that Thirion's Law does not hold for rolling friction. On the other hand when sliding-friction force was plotted against load the curvature was toward the load axis as would be expected if Thirion's Law applied. The coefficient of friction can go as low as 0.01 or even lower for a hard-pumped tire when the temperature is near 0° C., but at −1° C. rolling friction on dry ice is quite appreciable. The results refer only to measurements at very slow speed.

INTRODUCTION

A considerable amount of work (Gough *et al.* 1956; Hadekel 1952; Hample 1955; Milwitzky *et al.* 1955; Pike 1949; Taborex 1957) has been done on the friction and performance of rubber tires on surfaces other than ice. Förster (1956), working in Germany, has included in the various road conditions he tested the "glazed ice" condition. Laboratory work has been undertaken on small flat samples of rubber on smooth surfaces; the formula $1/\mu = a+bp$, where a and b are constants and p is pressure, has been proposed by Thirion (1946) to describe rubber friction; this law has been verified over a 10,000-fold load range by Denny (1953). Conant, Dum, and Cox (1949) have used flat rubber samples on ice and have concluded that the base polymer and the type and amount of carbon black were important; Pfalzner (1950) on the other hand has stressed the hardness of the rubber.

Little or no laboratory work has been published, however, up to this date, on inflated rubber tire samples on ice. This problem is quite exceptional from the theoretical standpoint because it involves perhaps the two most exceptional of all common substances in the field of solid friction—with the added complication that the soft substance has a gaseous substratum. The work described below is an approach to this unique friction problem and has been undertaken with a view to getting a better understanding of the ice friction mechanism rather than to improving rubber formulations. Many of the observations in the cold room confirm the statements and beliefs of winter drivers. One of these statements which is of special interest claims that "heavy vehicles grip an icy road better than light ones until they start sliding and then they slide worse". The measurements point to the reason why drivers have been led to this conclusion.

METHODS AND RESULTS

The turntable described in a previous communication (Niven 1954) was

[1]Manuscript received November 19, 1957.
Contribution from the Division of Applied Physics, National Research Council, Ottawa, Canada.
Issued as N.R.C. No. 4716.

used for the work. The straight loading arm had, however, to be changed to an arm with an arch above the track (see Fig. 1) in order to accommodate wheels up to 8 in. in diameter. Furthermore, variation in wheel diameter necessitated means to raise and lower the universal at the center of the turntable, where the arm was attached.

In the measurement of the limiting rolling friction the table was gently moved by hand, while a torque was applied to the test wheel resting on the smooth surface of ice. The torque which just caused the wheel to slip gave a measure of the rolling-friction force, provided that the radius of the wheel was known; it was necessary then to ascertain the deflection of the tire. Some measurements were also made on the sliding friction with the test wheel locked.

The variation in cold-room temperature was about $\pm 0.5°$ C. Since the main interest centers around temperatures at or just below 0° C., very little work was done at temperatures much below $-3°$ C. For measurements near the freezing point, experience showed that it was wise to keep the cold-room temperature below 0° C. in order to avoid the danger of melting the surface and of thereby increasing the friction. This temperature has been shown on the graphs in Figs. 4 and 5 as $-1°$ to 0° C. In Fig. 6, however, the temperature is shown as 0° C. because it was much nearer to the melting point of ice, on one occasion moisture on the track actually being noted.

The samples used for the work consisted of three model aeroplane tires 6 in., 4 in., and 2 in. in diameter and of two small standard tires 8 in. in diameter referred to below as A and B. A was several years old; B was new from the factory. The model tires were tubeless and were not reinforced with canvas; the small standard tires had an inner tube and a canvas-reinforced cover and could be inflated to 30 p.s.i. The model tires could not be inflated to hard pressures and their valve design provided no means for measuring air pressure. When fully inflated they were only as hard as a very softly pumped bicycle tire and could easily be pressed in with the finger and thumb. The deflection and contact areas under load, shown in Figs. 2 and 3, give an idea of their condition under test. Their widths were *ca.* $2\frac{19}{32}$ in., $1\frac{18}{32}$ in., and $\frac{28}{32}$ in. respectively. The tread was carefully buffed off. When this was done on the 4 in. tire, there appeared to be a ridge on the inside so that it was slightly different from the other two samples. The rubber in the model tires was a compound made up from natural rubber. The hardness of the inflated tire measured, on a Shore Durometer Type A, 26 for the 6 in. and 4 in. models and 33 for the 2 in. model. These figures take into account the cushioning effect of inflation.

The two standard tires had a width of about $2\frac{1}{2}$ in. They are known in the trade as 2.50–4 Industrial-type tires (in the trade tires are described by the size of the cross section rather than by the diameter). The tread, which incidentally was not buffed off, consisted of four thick ridges about $\frac{1}{4}$ in. wide, spaced about $\frac{1}{8}$ in. apart; it was composed, in the case of the A tire, of "hot GRS butadiene–styrene synthetic with a black reinforcement of channel black and high modulus furnace black", and, in the case of the B sample, of "synthetic rubber of the styrene–butadiene type and a black of one of the

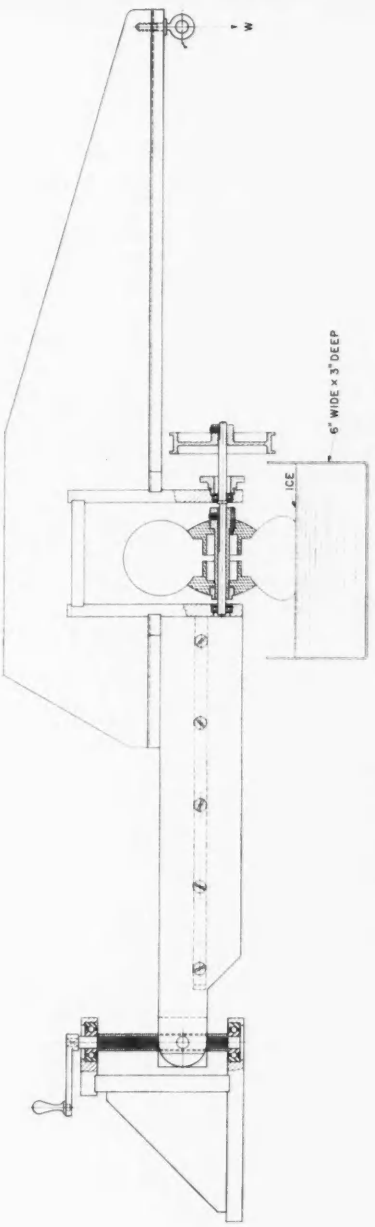

FIG. 1. Loading arm showing arch and adjustable universal joint.

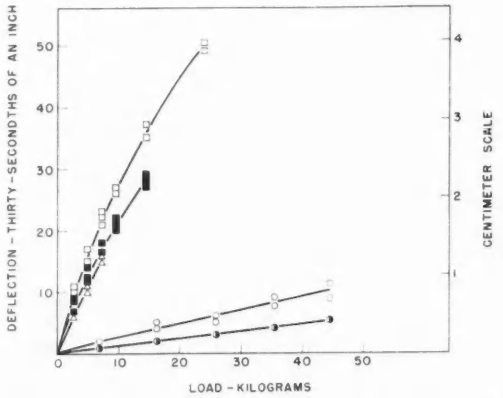

FIG. 2. Deflection vs. load. □ 6 in. model, ■ 4 in. model, △ 2 in. model, ○ 8 in. synthetic A at zero inflation pressure, ◑ 8 in. synthetics A and B at 30 p.s.i. inflation pressure.

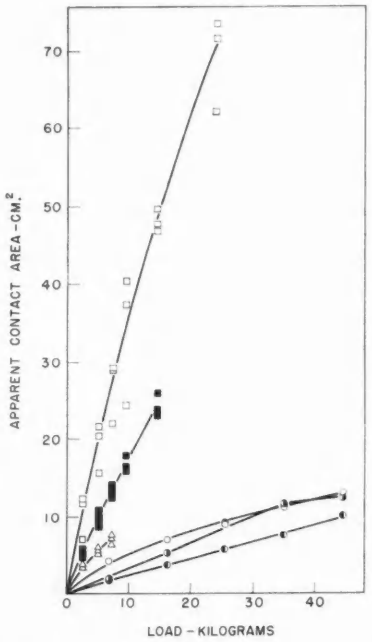

FIG. 3. Apparent contact area vs. load. □ 6 in. model, ■ 4 in. model, △ 2 in. model, ○ 8 in. synthetic A zero inflation pressure, ◐ 8 in. synthetic A 30 p.s.i. inflation pressure, ◑ 8 in. synthetic B 30 p.s.i. inflation pressure.

new furnace types". Sample A had a very strong wall and was compressed little even under a load of 44 kg. with zero inflation pressure; sample B was not nearly so strong. The hardness of sample A was 69 and of B 62 on the Shore Durometer. The cushioning effect of inflation did not arise, as these reinforced samples were so strong.

Apparent contact areas were approximately determined by pressing the tire against a rubber-stamp ink-pad and then letting it rest on a piece of white paper under load.

Obviously a great many variables were present—temperature, loading, diameter of tire, kind of tire, quality of rubber, ice conditions. Over and above these variables there were two kinds of friction to deal with, depending on whether the wheel was rolling or sliding. It was soon found that the friction of a rolling wheel was much more easily defined in words than measured in practice, because under certain conditions when the torque was applied there was a slow creep, as though the wheel were turning in a very viscous fluid. The experimenter has to decide what torque really corresponds to the limiting friction value. The writer took the torque corresponding to a very slow creep. Under other conditions, when the wheel was subjected to torque, it might suddenly "let go", just at the limiting value, and this value would then depend on how gently the turntable was rocked. The writer took the value corresponding to a very gentle movement.

After the wheel had slipped by application of too large a torque and repetition of the measurement was being made at lower torque, far lower loads on the weight pan would cause slipping than those which had failed to cause slipping only a few moments earlier. It was found, however, that by rocking the turntable without application of torque for a little while—say 20 seconds—the wheel would again take its original grip on the ice. The higher torque value was assumed to be the more correct one.

In the measurement of sliding friction of a material like rubber, which has usually a very appreciable friction, high turntable speeds cannot be used for dry ice tests—at any rate if the sample runs in the same track all the time—because water accumulates on the track and the results have little meaning. The sliding-friction values reported below refer, accordingly, to very slow or "just-stopping" speeds. It is important to emphasize this so that the reader will not apply the values reported to the practical problem of braking at speeds of 30 to 100 m.p.h.

The low-pressure tires could be deflected with load until they were almost "running on the rim". Such deflections were not feasible for the standard tires with the equipment available; they were designed to carry about 130 kg.

When friction force was plotted against load, the points for a series of measurements at different loads lay as a rule surprisingly close to a smooth curve or straight line in spite of the troubles in assessing limiting torque, but there was some lack of repetition due to the ice. That this was to blame there was no doubt, because two series of points would give similar curves, but all the points of one series would be either lower or higher than all the points of another

series. Instances of this can be seen in Fig. 6. The trouble lay not in the method of measuring the friction but in the conditions at the interface.

The ice surfaces were prepared by machining with a wide-edged steel tool without employing any special buffing technique afterwards. No attempt was made to separate the data on freshly machined ice from those on ice which had stood overnight because this would not have cleared up the trouble. Buffing the surface by having the 6 in. model tire slide on the revolving turntable at high speed, until the surface became as smooth as glass, could actually cause an *increase* in friction (except near 0° C. when the buffed surface had if anything the lower value). Presumably buffing permitted closer contact and increased adhesion. Decrease in friction could sometimes be related to the possible presence of ice crystals—so to speak the "turnings"—which had not been thoroughly enough removed after machining.

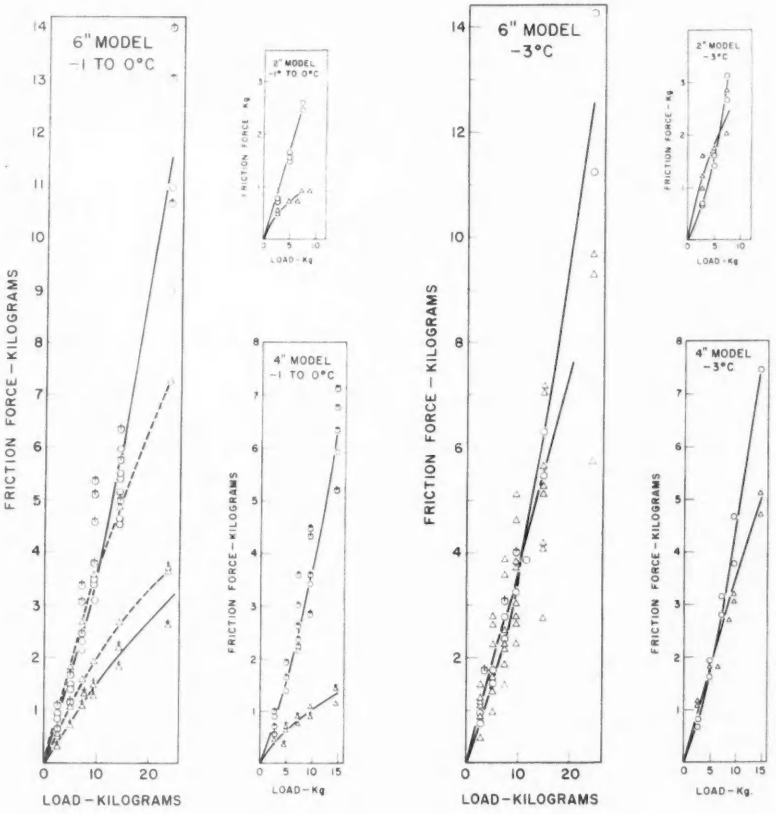

FIG. 4. Friction force vs. load curves for model tires. A circle signifies rolling friction, a triangle sliding friction, and a cross on top of a symbol water on the ice.

A true assessment of ice friction values cannot be reached by using one type of specially prepared surface. One must accept the fact that various interface conditions are possibilities. Research might conceivably succeed in attaching coefficients to specified conditions but the fact must be faced, nonetheless, that under practical conditions variation in friction coefficient occurs for

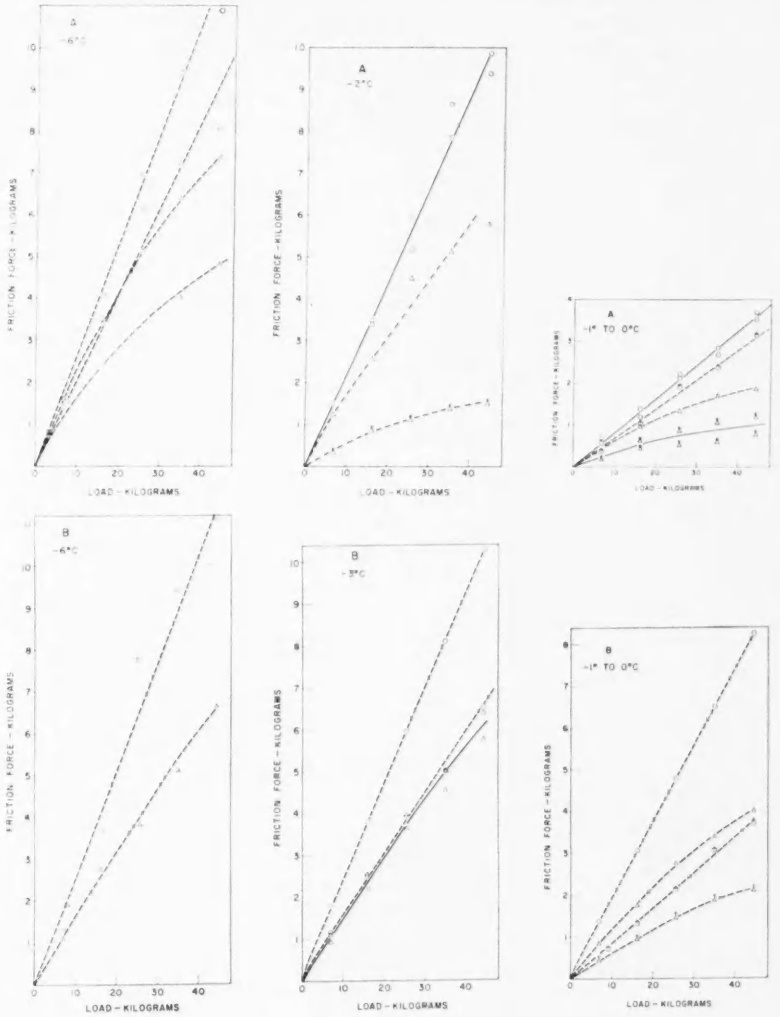

FIG. 5. Friction force vs. load curves for 8 in. (diameter) synthetic standard tires. A circle signifies rolling friction, a triangle sliding friction, and a cross on top of a symbol water on the ice.

apparently very little reason. Fortunately these variations in interface conditions do not generally affect the type of friction-force-versus-load curve obtained at a particular temperature.

Results on the model tires are shown in Fig. 4 and on the standard tires in Fig. 5. Fig. 6 shows some special curves relating to the A tire at zero inflation pressure at a temperature very near the melting point of ice, which will be discussed below.

In Figs. 4, 5, and 6 a circle signifies rolling friction, a triangle sliding friction, and a cross on top of a symbol water on the ice. Broken lines have been used in connecting points of one particular series of readings; when two or more series of readings have been combined in drawing a curve a full or unbroken line has been used. Since the load scale is one tenth of the friction force scale, coefficients can be read on the 10 kg. ordinate by merely placing a straight edge on the graph and by changing a decimal point.

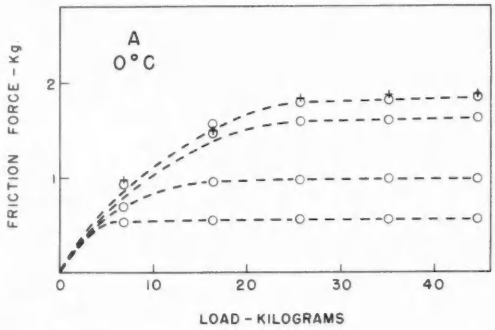

FIG. 6. Friction force vs. load curves for 8 in. (diameter) synthetic standard tire showing strong curvature of rolling-friction curves toward load axis at 0° C. and approximate constancy of friction force at high loads. Circle, dry ice; cross on top of circle, wet ice.

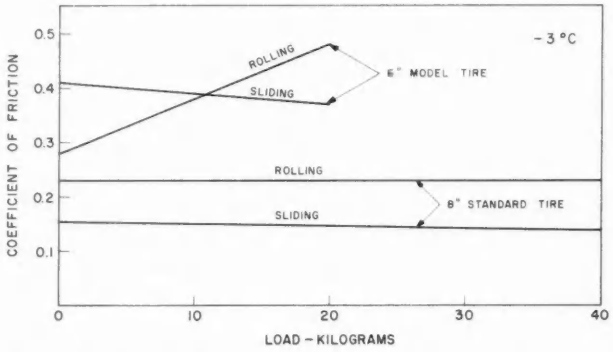

FIG. 7. Coefficients of friction at −3° C. for 6 in. model tire and 8 in. (diameter) synthetic B standard tire.

In order to assist the reader in visualizing the type of value to expect for the friction coefficient of a rubber tire on ice which is well frozen but not extremely cold, Fig. 7 has been constructed from appropriate data in Figs. 4 and 5. The four lines in Fig. 7 indicate respectively rolling and sliding friction coefficients at −3° C. for the 6 in. (diameter) soft-pumped model tire and the 8 in. (diameter) hard-pumped synthetic B standard tire; the coefficients apply to very slow speeds as stated already.

Table I gives some further details on the values of friction coefficients—also taken from the graphs. Some of these values have been read to the second significant figure but variations in ice conditions do not really warrant this accuracy. All values are approximate and the object of tabulating them is to demonstrate the wide variety of friction coefficients, each of which is a perfectly good value for a particular tire at a particular temperature on a particular ice surface.

TABLE I

Tire	Ice temperature, ° C.	Load, kg.	Friction coefficients: Rolling	Friction coefficients: Sliding (very slow speed)	Remarks
2 in. model	0 to −1	0.8	0.35	0.12	
	−3	0.8	0.45	0.31	
4 in. model	0 to −1	1.0	0.37	0.11	
	−3	0.8	0.4	0.36	
6 in. model	0 to −1	0.8	0.35	0.14 to 0.37	Including wet ice
		2.5	0.5	0.12 to 0.3	Including wet ice
	−3	0.8	0.33	0.2 to 0.5	
		2.5	0.5	0.3 to 0.4	
	−6	0.8	0.5	0.35 to 0.5	
8 in. standard (synthetic)	0	44	0.01		Without pouring water on ice
	0 to −1	44	0.08 to 0.2	0.04 to 0.09	Dry ice
		44	0.08	0.03	Wet ice
	−2 to −3	44	0.23	0.14	Dry ice
	−2	44		0.03	Wet ice
	−6	44	0.25	0.11 to 0.16	Dry ice

DISCUSSION OF RESULTS

When a tire is deflected, the volume gets slightly smaller and the inflation pressure rises. If, however, it could be arranged by means of some device to keep the inflation pressure the same for all loads, and if the strength of the wall were negligible, the value of p in Thirion's equation $1/\mu = a + bp$ would be constant, and since a and b are numerical constants depending on the sample, μ would remain constant; the friction-force-versus-load relation would then be linear. The results on the model tires show, however, that this is only approximately true: actually p increases with load and so the sliding-friction-force-versus-load curve should bend towards the load axis at high loadings—and this is what it does. One may, therefore, conclude that the sliding-friction results on the model tires do not conflict with Denny's conclusion that Thirion's

Law is widely applicable. Fig. 8 supports this conclusion: the straight line represents the equation $1/\mu = 1.85+2.7p$; the points are reciprocals of sliding-friction values taken from the graph in Fig. 4 corresponding to the 6 in. model tire at $-3°$ C.

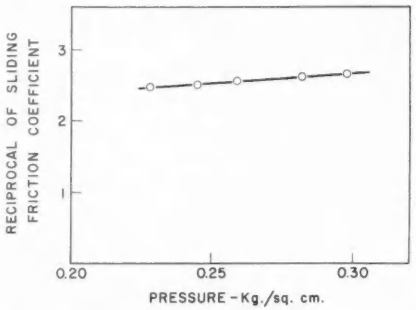

Fig. 8. Verification of the applicability of Thirion's Law to sliding friction by using values as given by the graph in Fig. 4 referring to the 6 in. inflated model tire at $-3°$ C.

However, what is of much greater importance is the fact that the rolling-friction results can never be expected to fit Thirion's equation because the curvature—such as there is—is away from the load axis at high loadings: in other words as p increases, $1/\mu$ gets smaller, a condition which cannot be made to fit the equation if b is positive.

The application of Thirion's Law to the 8 in. wheels cannot be discussed because the accuracy of the contact-area measurements was not good enough.

On the graph for the 6 in. model tire at $-1°$ to $0°$ C. (see Fig. 4) the two "broken-line" curves show widely differing results on sliding friction for dry ice: one of them is near the curve for wet ice and the other near the curve shown on an adjacent graph for dry ice at $-3°$ C. A small change in temperature is believed to have caused this, since evidence which will be discussed below in connection with Fig. 6 indicates that the friction properties of ice change markedly somewhere between $0°$ and $-1°$ C.

At $-3°$ C., the sliding and rolling frictions of each of the model tires were comparable. A series of low points on the graph for the 6 in. model tire at $-3°$ C. may have been due to tiny ice crystals on the surface, because that particular series of readings happened to have been taken on newly machined ice. Sliding friction can be higher than rolling friction under some circumstances. This could be verified visually if it were assumed that slow rolling friction is static friction (Taborex 1957), because the force necessary to balance the sliding friction when the table was turning slowly would draw the arm back as soon as the table stopped. This small detail suggests a peculiarity about rubber possibly connected with the fact that the braking coefficient of a tire on cement rises at first, quite sharply, with small percentage of slip before falling off at greater percentages (Förster 1956; Milwitzky *et al.* 1955).

Fig. 5 shows that the friction of the standard tires was lower than that of the model tires. The hardness of the standard tires was partly responsible for

this; in addition they were made of synthetic rubber, while the model tires were made of natural rubber. The two synthetic tires had comparable friction values except near 0° C. but since small changes in temperature have a large effect near that temperature according to other evidence, this difference need not be stressed. For the hard synthetic tires, rolling friction obeyed very nearly a straight-line relation while the sliding friction did not, the curves bending toward the load axis.

The results shown in Fig. 6 are entirely different from those in Fig. 5 and it is the difference in temperature which caused this. (The tire was so strong and hard that it deflected little even under a load of 44 kg. either at 0 or at 30 p.s.i. inflation pressure.) The results in Fig. 6 were obtained before it was decided to work always at a temperature slightly below 0° C., and they refer to ice which was almost melting.

It was only after the experimental work had been discontinued and the apparatus disconnected and removed from the cold room that the significance of these results was appreciated: they show that something happens between 0° and −1° C. which is of far greater consequence as far as friction is concerned than anything which happens between −1° and −6° C. The explanation of this result is almost self-evident if one accepts the modern theory that the surface of a solid is covered with asperities and that friction is due to adhesion to these asperities. In this instance the ice is to be regarded as covered with asperities composed of water molecules held together by strong molecular forces, so long as the temperature is below 0° C. As soon as the temperature rises above 0° C. these forces let go and the rubber is then adhering to something which has ceased to be solid; one would accordingly expect the friction to drop. In other words, since the freezing point of water is sharp, one would expect a discontinuity in the value of the friction at or very near −0° C.

The results of the investigation under the controlled conditions of the cold room can be applied to confirm and explain driving experience on ice. The coefficient of rolling friction is either constant (Amontons' Law) or it increases at high loading for temperatures definitely below 0° C. The coefficient of sliding friction on the other hand decreases with load particularly near 0° C. These facts explain why some drivers believe that heavy vehicles have more friction than light ones until sliding starts, because rolling friction *force* is either proportional to or better than proportional to the load on the tire, and so, if the load is unevenly distributed over the wheels, this force will appear small on the driven wheels when they carry less than their share of the load—a condition often found with light vehicles—and large, if they carry more than their share of the load—a condition often found with loaded trucks. There is at present insufficient evidence to say that the rolling-friction *coefficient* of an automobile tire on ice increases with load although the results on the model tires suggest this as a remote possibility. These tires were, however, deflected to a far greater extent than would be tolerated for the canvas-reinforced automobile tire. When the ice is exactly at 0° C. the work indicates that a heavily loaded hard tire should grip the road even less in proportion than a lightly loaded one, either rolling or sliding.

Low-pressure natural-rubber tires seem to grip well on ice. The rolling friction

of rubber tires on ice—even on wet ice—at a temperature as mild as $-1°$ C. is by no means negligible. When friction is low, torque should be applied gently to avoid spinning as this causes a temporary reduction of friction; gentle braking is likewise desirable. The really difficult driving condition appears to arise when the ice is at exactly 0° C., and because it is critical to have the ice temperature at 0° C., impossible driving conditions occur relatively rarely. The overruling danger factor in driving on ice is not so much that the friction is so low as that it is exceedingly variable, changing unexpectedly, yet considerably, because of very slight change in temperature near 0° C. or because water or loose ice particles happen to be on the surface or because the surface is not of uniform smoothness.

The important conclusion to draw from Table I is that 0.1 is not a safe coefficient to take for the rolling friction of a rubber tire on ice if the worst weather conditions are to be considered; 0.01 is nearer to the figure for safety in engineering design, at any rate for a hard tire. However, the hardness of the tire, the load, and the apparent contact area are such very important factors that until full-scale tests are made on an ice surface controlled at close to 0° C.—much like the tests made on a concrete surface at the Langley impact basin (Milwitzky, Linguist, and Potter 1955)—a precise minimum cannot be placed on the rolling friction for an inflated rubber tire. The time is well overdue to provide facilities for such tests in Canada because a small turntable cannot give all the answers; experience on the turntable has shown, however, that large-scale tests would be of little value unless the runway and ambient air temperature could be controlled to a temperature extremely close to 0° C.; at $-1°$ C. the runway would no longer be at the danger temperature.

ACKNOWLEDGMENTS

The author is grateful to Miss T. Stock for making the planimeter measurements on the apparent surface-contact areas, to Dr. R. A. Hayworth of the Goodyear Tire and Rubber Company of Canada, and to Mr. C. H. Lutman of the Model Shop, Newcastle-upon-Tyne, England, for information regarding the rubber in the sample tires. The author also expresses his appreciation of the interest and suggestions of Mr. J. J. Samolewicz and Mr. T. R. Ringer of the Low Temperature Laboratory, National Research Council, Ottawa, during the work.

REFERENCES

Conant, F. S., Dum, J. L., and Cox, C. M. 1949. Ind. Eng. Chem. **41**, 120.
Denny, D. F. 1953. Proc. Phys. Soc. (London), B, **66**, 721.
Förster, B. 1956. Natl. Advisory Comm. Aeronaut. Tech. Mem. No. 1416.
Gough, M. N., Sawyer, R. H., and Trant, J. P., Jr. 1956. Tire-runway braking coefficients. Agard Rept. No. 51.
Hadekel, R. 1952. Brit. Min. of Supply S & T Memo No. 10/52.
Hample, W. G. 1955. Natl. Advisory Comm. Aeronaut. Tech. Note. No. 3294.
Milwitzky, B., Linguist, D. C., and Potter, D. M. 1955. Natl. Advisory Comm. Aeronaut. Rept. No. 1248.
Niven, C. D. 1954. Can. J. Phys. **32**, 782.
Pfalzner, P. M. 1950. Can. J. Research, F, **28**, 468.
Pike, E. C. 1949. J. Roy. Aeronaut. Soc. **53**, 1085.
Taborex, J. J. 1957. Machine Design, **29**, No. 11, 60.
Thirion, P. 1946. Rev. gén. caoutchouc, **23**, 101.

THE SOMMERFELD MODEL AND THE HEAT OF SOLUTION OF AN ALLOY[1]

W. G. Henry

ABSTRACT

An approximately self-consistent method, using a Sommerfeld model, and incorporating an approximation to the second-order perturbation energy (Lennard-Jones 1930), is used to calculate the heat of solution of both monovalent–monovalent and monovalent–polyvalent alloy systems. The heat of solution, as given by the second-order approximation, varies directly with the square of the perturbing potential, and inversely with the mean total energy of the free electrons in the solvent. Varley's (1954) result resembles this, except that his expression varies inversely with the mean kinetic energy of the free electrons in the pure solute. The first-order approximation to the energy of the alloy system is identical, except for a change of sign, with the expression suggested by Friedel (1952, 1954) for the heat of solution. The charge accumulation about a solute site is found to vary directly with the strength of the perturbation, and inversely with the mean energy of the free electrons in the solvent. Varley obtained a comparable expression; however, his function varies inversely with the mean kinetic energy of the free electrons in the pure solute. The calculated charge accumulations in the copper–silver system, and for gold dissolved in silver, agree qualitatively with those of Arafa (1949) and Huang (1948).

1. INTRODUCTION

Oriani (1956) made a general survey of the calculations of the heats of solution of alloys. The calculations which are relevant are those of Huang (1948), Arafa (1949), Friedel (1952, 1954*a*, *b*), Varley (1954), and Shinohara (1955).

Shinohara (1955) attempted a self-consistent calculation of the heat of solution of a polyvalent solute in a monovalent solvent. It was assumed that the perturbing potential due to a solute atom was of the screened Coulomb type, and the perturbation calculation was carried out to second order. The fact that the calculated heats of solution were 30 to 40 times too large was ascribed to a deficiency in the method. Varley (1954), who used a "two-band" model, treated both monovalent–monovalent and monovalent–polyvalent systems. The form of the expression for the heat of solution obtained by Varley (1954) is similar to that of the present calculation. Friedel (1952, 1954*a*, *b*), on the basis of a cyclic process, derived an expression for the heat of solution of a polyvalent solute in a monovalent solvent which, on the basis of the present calculation, appears to be not related to the actual heat of solution. Arafa (1949) applied a cellular method to the copper–silver system, and obtained agreement with the heats of solution determined from the phase diagram. This method has not been applied to a monovalent–polyvalent system.

Huang (1948) assumed a square-hole potential, and treated the case of gold

[1]Manuscript received in original form July 5, 1957, and as revised February 28, 1958.
Contribution from the Division of Applied Chemistry, National Research Council, Ottawa, Canada.
Issued as N.R.C. No. 4700.

dissolved in silver by a self-consistent Thomas–Fermi method. After applying a large correction to take account of the kinetic energy associated with the rapid change of potential of the potential hole, he obtained good agreement with experiment. In the same paper he made an exact, non-self-consistent, quantum-mechanical calculation for the square-hole potential, and obtained -0.69 ev. per atom of gold for the heat of solution. The present approximately self-consistent calculation is an approximation to the exact square-hole potential problem, and is of more general applicability. It is a perturbation calculation which is carried out to second order, and in that respect it is similar to that of Shinohara. The method of carrying out the calculation, however, is quite different, in that an approximation to the second-order energy (Lennard-Jones 1930) is used in contrast to Shinohara's attempt to evaluate exactly the second-order terms.

The heats of solution of binary metal systems show the following *general* characteristics. The heats of solution of monovalent–monovalent systems and monovalent–polyvalent systems are of the same order of magnitude. There are no apparent systematic valence effects. The heat of solution is negative when either B is dissolved in A or vice versa. The present calculation attempts to relate the *general* features of the heat of solution to a simple model. The accumulation of charge at a solute site is also discussed.

In Sections 2 and 3 the non-self-consistent calculation is given. In Section 4 the self-consistent calculation is discussed. In Section 5 the problem of the polyvalent solute is discussed.

2. THE FIRST-ORDER APPROXIMATION

The integral heat of solution ΔH for N atoms of solution, where N is Avogadro's number, is defined as the difference in the heat content of the solution and of the components from which it is made. The integral heat of solution for small concentrations may be represented by the first term of a series

$$\Delta H = \Delta H'(0)n/N, \tag{2.1}$$

where n is the number of solute atoms and $\Delta H'(0)$ is the slope of the integral heat of solution curve at zero concentration, which is equal to the heat of solution per gram-atom of solute at zero concentration. In the following sections, the difference between the heat content of a solution formed from $N-1$ atoms of species A and one atom of B, and the heat content of the unalloyed components, is calculated. The difference according to (2.1) is equal to $\Delta H'(0)/N$.

In the Sommerfeld (1928) model of a one-dimensional pure metal the unperturbed wave functions ψ_k° are

$$\psi_k^\circ = (2/L)^{\frac{1}{2}} \sin(k\pi x/L), \tag{2.2}$$

and the energy associated with a level is given by the relation

$$W_k^\circ = V^\circ + \frac{h^2k^2}{8mL^2}. \tag{2.3}$$

L is the length of the metal, $h^2k^2/8mL^2$ is the kinetic energy of the kth level, and V° is the Sommerfeld potential which is independent of x. The total energy of the system of electrons W° is given by the expression

$$W^\circ = \sum \left[V^\circ + \frac{h^2k^2}{8mL^2} \right], \tag{2.4}$$

where the summation is over all occupied levels. The zero level of energy is taken to be the energy of all ions and electrons at infinite separation.

If it is assumed that one solute atom of species B, of the same valence and atomic length as the solvent A, may be represented by a perturbation (Fig. 1) of length $\delta = L/N$ and of strength V_p° equal to the difference in the Sommerfeld potentials of the free electrons in the pure components, then the change in energy of the system may be calculated by perturbation methods. The limit of the applicability of the method is discussed in Appendix 1. Since the energy levels of the one-dimensional unperturbed system are non-degenerate, the perturbation theory for non-degenerate systems may be applied. In three dimensions, it is assumed that the neglect of any near-degeneracy is not serious.

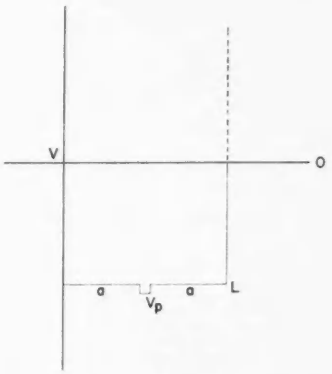

FIG. 1. The perturbed potential in a one-dimensional metal of length L.

The first-order approximation to $W_k^{(1)}$, the energy of the kth level, is (Henry and Rogers 1956)

$$\begin{aligned} W_k^{(1)} &= W_k^\circ + \frac{2}{L}\int \sin^2 \frac{k\pi x}{L}\, V_p^\circ\, dx \\ &= W_k^\circ + V_p^\circ \left[\frac{\delta}{L} + \frac{1}{k\pi} \sin\left(k\pi - \frac{k\pi\delta}{L} \right) \right]. \end{aligned} \tag{2.5}$$

By considering the levels in pairs, it may be shown (Appendix 2) that the mean energy of a level is changed by an amount $V_p^\circ\delta/L$. The result in three dimensions, which is discussed in Appendix 2, is $V_p^\circ\delta_x\delta_y\delta_z/L_xL_yL_z$.

For a binary system of monovalent metals with no volume change, the first approximation to the total energy of the perturbed system is

$$\sum W_k^{(1)} = NV_A^\circ + NV_p^\circ \frac{\delta}{L} + \sum \frac{h^2k^2}{8mL^2} = (N-1)V_A^\circ + V_B^\circ + N\mathfrak{E}_A^\circ, \tag{2.6}$$

since $\delta = L/N$ and $V_p^\circ = V_B^\circ - V_A^\circ$, the difference in the Sommerfeld potentials of pure A and B. $\mathfrak{E}_A^\circ$ is the mean kinetic energy of an electron in the solvent. The right-hand side of (2.6) is, however, identical with the total energy W_p of the pure components. Thus, the difference in heat content between the solution and the components from which it is made is zero, according to this approximation. That is, the first-order perturbation gives only the energy of a phase mixture of the pure components, and indicates no term favoring the formation of a solution.

For a binary system of monovalent metals with a volume change, there is an additional negative contribution to the heat of solution arising from the change in the kinetic energy. The total kinetic energy of the solution containing one solute atom is

$$\sum \frac{h^2k^2}{8m(L_A+\Delta)^2} = N\mathfrak{E}_A^\circ - \frac{2\Delta N\mathfrak{E}_A^\circ}{L_A} + 3\left(\frac{\Delta}{L_A}\right)^2 N\mathfrak{E}_A^\circ + \ldots, \tag{2.7}$$

where $\Delta = (L_B - L_A)/N$. The mean kinetic energy of an electron in the pure solute is

$$\frac{1}{N}\sum \frac{h^2k^2}{8m(N\Delta+L_A)^2} = \mathfrak{E}_A^\circ - \frac{2\Delta N\mathfrak{E}_A^\circ}{L_A} + 3\left(\frac{\Delta N}{L_A}\right)^2 \mathfrak{E}_A^\circ + \ldots. \tag{2.8}$$

The kinetic energy of the phase mixture $\mathscr{E}_p$ is therefore

$$\mathscr{E}_p = (N-1)\mathfrak{E}_A^\circ + \mathfrak{E}_A^\circ - \frac{2\Delta N\mathfrak{E}_A^\circ}{L_A} + 3\left(\frac{\Delta N}{L_A}\right)^2 \mathfrak{E}_A^\circ + \ldots. \tag{2.9}$$

The difference between the kinetic energy of the solution and the phase mixture is approximately $-3(L_B - L_A)^2\mathfrak{E}_A^\circ/L_A^2$. This is also valid for the three-dimensional model, where L_A and L_B are now the cube edges of a gram-atom of solvent and solute respectively. If, for example, L_B and L_A differ by 10%, and $\mathfrak{E}_A^\circ$ is 3.3 ev., then the contribution to the heat of solution is 0.1 ev. If the length of the perturbation is assumed to be equal to $1/N$ of the length of the solution, then there is no additional contribution from this source. In the remainder of the paper it will be assumed that the volume of the solute equals the volume of the solvent.

3. THE SECOND-ORDER APPROXIMATION

The second-order approximation to the energy of a level $W_k^{(2)}$ is given by the expression

$$W_k^{(2)} = W_k^{(1)} + \sum_l{}' \frac{H'_{lk}H'_{kl}}{W_k^\circ - W_l^\circ}, \tag{3.1}$$

where the dash indicates that the sum is over all values except $l = k$. H' is the formal representation of the perturbation. The sum may be rearranged (Lennard-Jones 1930; Pauling and Wilson 1935), to permit an approximate value to be found,

$$\sum_l{}' \frac{H'_{lk}H'_{kl}}{W_k^\circ - W_l^\circ} = \frac{(H'^2)_{kk}}{W_k^\circ} - \frac{(H'_{kk})^2}{W_k^\circ} + \sum_l{}' \frac{W_l^\circ}{W_k^\circ} \frac{H'_{lk}H'_{kl}}{W_k^\circ - W_l^\circ}. \tag{3.2}$$

The approximation consists in omitting the sum. The approximation is discussed in Appendix 3.

For a binary system of monovalent metals with no volume change, the first term on the right-hand side of (3.2) becomes

$$\begin{aligned} \frac{(H'^2)_{kk}}{W_k^\circ} &= \frac{2}{W_k^\circ L} \int \sin^2 \frac{k\pi x}{L} \, V_p^{\circ 2} \, dx \\ &= \frac{V_p^{\circ 2}}{W_k^\circ L} \left[\frac{\delta}{L} + \frac{1}{k\pi} \sin\left(k\pi - \frac{k\pi\delta}{L} \right) \right]. \end{aligned} \tag{3.3}$$

A comparison with (2.5) shows that the mean energy of a level is lowered by an additional amount $V_p^{\circ 2}\delta/W_k^\circ L$. The total energy change of the system resulting from this term is

$$\sum \frac{(H'^2)_{kk}}{W_k^\circ} \approx V_p^{\circ 2} \frac{\delta}{L} \frac{N}{V^\circ + \mathfrak{E}^\circ}, \tag{3.4}$$

where the sum is over all occupied states. N is the total number of electrons per gram-atom of alloy; $V^\circ + \mathfrak{E}^\circ$ is the mean energy of an electron in the solvent.

The second term may be evaluated and yields

$$\begin{aligned} \frac{(H'_{kk})^2}{W_k^\circ} &= \frac{1}{W_k^\circ} \left[\frac{2}{L} \int \sin^2 \frac{k\pi x}{L} \, V_p^\circ \, dx \right]^2 \\ &= \frac{V_p^{\circ 2}}{W_k^\circ} \left(\frac{\delta}{L} \right)^2. \end{aligned} \tag{3.5}$$

This term is small in comparison with the term which contains δ/L to the first power.

The total energy of the perturbed system is given by the second approximation to be

$$\sum W_k^{(2)} = N\bar{W}_A^\circ + N V_p^\circ \frac{\delta}{L} + N \frac{V_p^{\circ 2}}{\bar{W}_A^\circ} \frac{\delta}{L}, \tag{3.6}$$

where $\bar{W}_A^\circ = V_A^\circ + \mathfrak{E}_A^\circ$. The first two terms on the right-hand side of (3.6) are, by (2.6), the energy of the phase mixture. Therefore the heat of solution per atom at zero concentration is

$$\Delta H'(0)/N = V_p^{\circ 2}/\bar{W}_A^\circ. \tag{3.7}$$

It may be concluded from the form of (3.7) that: (1) $\Delta H'(0)/N$ is negative when either B is dissolved in A or vice versa; (2) the magnitude of $\Delta H'(0)/N$ depends on whether B is dissolved in A or vice versa.

The result expressed in (3.7) may be compared with an exact calculation. Huang (1948) made an exact calculation of the square-hole potential problem using numerical methods for the single case of gold dissolved in silver. He obtained -0.69 ev. per atom for the heat of solution. For monovalent metals the Sommerfeld potential is approximately equal to the negative value of the sum of the absolute values of the sublimation energy Λ, the first ionization energy $I^{(1)}$, and the mean kinetic energy $\mathfrak{E}$. If the atomic volumes are equal, the difference in the Sommerfeld potentials is also equal to the difference in the mean energies of the electrons. The atomic volumes of silver and gold are approximately equal. The mean energies of the electrons in gold and silver, as determined from their heats of sublimation and first ionization energies, are -13.1 ev. and -10.5 ev. respectively. Equation (3.7) yields

$$\Delta H'(0)/N = (-2.6)^2/(-10.5) = -0.64 \text{ ev.}, \tag{3.8}$$

which is in reasonable agreement with the exact calculation.

It is of interest to compare $\Delta H'(0)/N$, as given by equation (3.7), with the result obtained by Varley (1954) using a "two-band" model. For simplicity, the comparison will be made for a binary system of monovalent metals with no volume change. The change in the mean interaction energy of the electrons and the change in the ground state energy, which result from the transfer of charge, will be neglected. In the notation of the present paper, Varley's result for the difference in the energy between the solid solution and the phase mixture $\Delta H(n/N)$ is

$$\Delta H(c) = -\frac{c(1-c)V_p^{\circ 2}}{\frac{10}{3}[c\mathfrak{E}_A^{\circ}+(1-c)\mathfrak{E}_B^{\circ}]}, \tag{3.9}$$

where $c = n/N$. The heat of solution per atom, at zero concentration, is given by the relation

$$\Delta H'(0)/N = -\tfrac{3}{10}\, V_p^{\circ 2}/\mathfrak{E}_B^{\circ}. \tag{3.10}$$

It is thus seen that the "two-band" model, to which it is somewhat difficult to give a physical interpretation, yields a result which is very similar in form to that of the present calculation.

4. SELF-CONSISTENT CALCULATION

Before the calculation may be made approximately self-consistent, it is necessary to calculate the amount of extra charge which accumulates in the volume occupied by the solute atom. Lennard-Jones (1930) has shown that the wave function which corresponds to the approximation (3.2) has the form

$$\psi_k = \psi_k^{\circ}\left(1-\frac{H'_{kk}}{W_k^{\circ}}\right)+\frac{H'}{W_k^{\circ}}. \tag{4.1}$$

This is also the normalized wave function if terms in $1/W_k^{\circ 2}$ are neglected.

The extra charge which accumulates in the length δ is given by the expression

$$\Sigma\left[\int_a^{L-a}\psi_k^{\,2}dx-\int_a^{L-a}\psi_k^{\circ 2}dx\right] \approx \frac{2V_p^{\circ}}{\bar{W}_A^{\circ}}. \tag{4.2}$$

This result also holds for three dimensions. As may be seen from the form of the wave function, the accumulated charge comes uniformly from the whole lattice, and *each* wave function contributes to the localized charge. Since the denominator is negative, charge is accumulated about the solute when V_p° is negative, and is attracted from the solute to the solvent when V_p° is positive. Arafa (1949) also concluded that the charge comes uniformly from the lattice.

To make the calculation self-consistent, an attempt is made to make q and V_p compatible. The extra charge q which accumulates is given by the relation

$$q = \frac{2(V_p^\circ + f(q))}{|\bar{W}_A^\circ|} = \frac{2V_p}{|\bar{W}_A^\circ|}, \tag{4.3}$$

where V_p is the self-consistent potential. If it is assumed that the change in potential is equivalent to that of the charge q in a spherical shell at a radius r_0 equal to the radius of a sphere of equivalent atomic volume, then $f(q)$ is equal to q/r_0.

Since the accumulated charge comes uniformly from the whole lattice, then it is reasonable to assume that the potential of the $N-1$ solvent electrons is lowered by an amount equal to $q/(N-1)r_0$. The total energy of the perturbed lattice is now

$$\begin{aligned}\sum W_k^{(2)} &= N\bar{W}_A^\circ + N(V_p^\circ + q/r_0)\frac{\delta}{L} \\ &\quad + \frac{N(V_p^\circ + q/r_0)^2}{|\bar{W}_A^\circ|}\frac{\delta}{L} - (N-1)\frac{q}{(N-1)r_0} \\ &= N\bar{W}_A^\circ + NV_p^\circ\frac{\delta}{L} + N\frac{V_p^2}{|\bar{W}_A^\circ|}\frac{\delta}{L}.\end{aligned} \tag{4.4}$$

Thus the heat of solution per solute atom is, as before,

$$\Delta H'(0)/N = V_p^2/|\bar{W}_A^\circ|, \tag{4.5}$$

where V_p is the self-consistent potential.

Gold in silver will be again used as an example. V_p° is equal to -2.6 ev. The mean energy of the electrons in silver is -10.5 ev. The potential per unit of charge at 1.59 Å, the equivalent atomic radius, is 9.0 ev. The charge accumulated is therefore given by (4.3),

$$q = 2(-2.6)/[-10.5-2(9.0)] = 0.18 \text{ unit of charge.} \tag{4.6}$$

Therefore, the heat of solution is

$$\Delta H'(0)/N = (-2.6+0.18\times 9.0)^2/(-10.5) = -0.10 \text{ ev.}, \tag{4.7}$$

which is of the correct order of magnitude.

The field outside the region of the solute atom which results from the accumulated charge has been neglected thus far. This is difficult to handle by the methods developed in this paper. The magnitude of this effect may possibly be estimated by finding the polarization energy of the 12 nearest

neighbors in a field of qe/r^2. If it is assumed that the polarizability of the neighboring atoms is of the order of the polarizability of argon, for example, then the polarization energy $-\alpha q^2e^2/2r^4$ amounts to approximately $-2.0\,q^2$ ev. This term is always negative. For gold dissolved in silver the polarization energy is -0.03 ev., which is less than $V_p^2/\mathfrak{W}_A^\circ$.

It is not to be expected that the results of the calculation as a whole can be compared directly with experiment, since at least one important term which may be significant in many cases, namely the change in the energy of both the solute and solvent ions, cannot be treated by this model.

In terms of the self-consistent potential, the charge accumulated is given by

$$q = V_p/\mathfrak{W}_A^\circ. \tag{4.8}$$

Agreement in form is again obtained with the result calculated by Varley (1954). In the notation of the present paper, his result is

$$q = -\tfrac{9}{10}V_p^\circ/\mathfrak{S}_B^\circ. \tag{4.9}$$

Arafa (1949) found a charge accumulation of 0.32 unit round a copper ion in a silver lattice, and a diminution of 0.29 unit round a silver ion in a copper lattice. The present calculation yields an accumulation of 0.11 unit and a diminution of 0.10 unit. Huang (1948) derived, by using an approximately self-consistent Thomas–Fermi method, a charge accumulation of about 0.5 unit round a gold ion in a silver lattice and a diminution of charge in the immediate neighborhood of equal magnitude. The present calculation gives an accumulation of 0.18 unit.

5. POLYVALENT SOLUTES

A polyvalent solute has $Z+1$ electrons outside a closed shell. The discussion will be restricted to monovalent–polyvalent systems. In general, the heats of solution of monovalent–polyvalent systems and monovalent–monovalent systems are of the same order of magnitude, and are negative, when either B is dissolved in A or vice versa. A special feature of the systems with a polyvalent solute is the absence of clearly defined valence effects, such as those inferred by Hume-Rothery, Mabbot, and Channel-Evans (1934) from the equilibrium diagrams of the alloy systems. Kleppa (1956), who investigated systematically the heats of formation of a number of polyvalent solutes in copper, silver, and gold, found no definite systematic valence effect. A study of the collected data of Kubaschewski and Catterall (1956) confirms these general conclusions.

According to the present model, the heat of solution in monovalent–monovalent systems results primarily because the energy levels of the conduction band of the solvent are perturbed by the presence of the solute atom (see (2.5) and (3.3)). A polyvalent solute with Z either even or odd will also cause a perturbing of the conduction band, and thus there will again be a heat of solution arising from the same source.

When $Z = 2$, it will be assumed that the Sommerfeld model may be applied

to the lone electron. If the self-consistent calculation were carried out with a well corresponding to an ion with a charge of three, the charge accumulation would cause the perturbing potential to be small, and the perturbation method could be applied. It is also plausible that, on the average, two of the electrons would merely be bound, that is, have almost the same average potential and kinetic energy as in the pure solute. At the same time, only the energy of one electron of the solute, which replaces the electron of the solvent, would be altered appreciably. The trend in the sublimation energies, in the two series copper, zinc, gallium and silver, cadmium, indium, suggests that the pair of s electrons may contribute only a small amount to the binding of a trivalent element, and hence their energy should not depend markedly on their surroundings. The sublimation energies are 3.54, 1.37, 2.5 and 3.00, 1.16, 2.56 ev. per atom respectively.

If the change in the energy of the two s electrons is assumed to be small, and only the change in energy of the N electrons in the system is considered, it follows by analogy with (4.4) that the energy of the system is given by the relation

$$\sum W_k^{(2)} = N\bar{W}_A^\circ + N V_p^\circ \frac{\delta}{L} + N \frac{V_p^2}{\bar{W}_A^\circ} \frac{\delta}{L}, \tag{5.1}$$

where $V_p^\circ = V_B^\circ - V_A^\circ$ and V_B° is the potential energy of the electron replacing the solvent electron in the pure solute.

If the volumes of the solute and solvent metals are equal, then the heat of solution per solute atom is

$$\Delta H'(0)/N = V_p^2/\bar{W}_A^\circ, \tag{5.2}$$

which is the same as for the monovalent–monovalent systems. For a monovalent solute in a trivalent solvent, the same assumptions lead to the result that the heat of solution is equal to $V_p^2/\bar{W}_B^\circ$. The heat of solution is thus negative if either B is dissolved in A or vice versa. Any change in the average potential and kinetic energy of the s electrons will make a direct contribution to (5.2). V_p° may be evaluated approximately (see Section 3) by treating a trivalent metal as a monovalent metal. It is found, for example, that for the copper–gallium system V_p° is approximately 2.7 ev., which is almost the same as for the silver–gold system. In general this should be true, and it may account for the fact that the heats of solution of monovalent–monovalent systems are similar to those of monovalent–trivalent systems.

There is a relationship between the first two terms of (5.1) and the expression suggested by Friedel (1952, 1954 *a*, *b*) for the heat of solution. The first two terms by themselves are the first-order non-self-consistent approximation. The first two terms of (5.1) represent the energy of a phase mixture containing one atom of solute. Hence the change in the energy of a phase mixture, when an atom of solvent is removed from the system and a solute atom is added, is equal to V_p°. If the trivalent solute is treated as a monovalent metal of equal volume for the purposes of calculating V_p°, then it is given by (see Section 3) the relation

$$V_p^\circ = -[|\Lambda_B|+|I_B^{(1)}|-|\Lambda_A|-|I_A^{(1)}|]. \tag{5.3}$$

Friedel suggested the same expression as (5.3) for the heat of solution but with opposite sign.

A cycle such as Friedel uses yields correctly $\Delta H'(0)/N$, provided all the terms are included. The two terms which Friedel assumes to have approximately equal absolute values, namely, the energy required to remove an A^+ ion from neutral A, and the energy gained on the addition of a B^+ ion to negatively charged A forming a neutral alloy, could, in fact, differ by several electron volts per atom, and should not be neglected. Friedel considered that the change in energy of the conduction band can be neglected, but, as was shown in Section 3, where the second-order approximation was discussed, the perturbing of the conduction band resulting from the substitution of a different species with a different associated potential field leads to a contribution to the heat of solution of the order of magnitude of the observed heats of solution.

For $Z = 1$, a difficulty arises because of the equivalence of the valence electrons. The effective nuclear charge of neutral trivalent elements (Slater 1930) is greater than that of monovalent elements. This suggests that: (1) the levels of the solvent lattice will be lowered, that is, V_p° is negative; (2) the energy of the two electrons of the solute will be raised because of increased screening. If it is assumed that neither electron enters the band and that the volume of the solute atom may be excluded for the purposes of calculating $\mathfrak{E}_A^\circ$, then the energy of the system is given by

$$\sum W_k^{(2)} = (N-1)\bar{W}_A^\circ+2(\bar{W}_B^\circ+g(q))+V_p^\circ+\frac{V_p^{\,2}}{\bar{W}_A^\circ}, \tag{5.4}$$

where V_p° cannot be well defined in terms of the present model and $g(q)$ is the change in energy per electron of the pair due to the charge accumulation. The heat of solution per solute atom has the form

$$\frac{\Delta H'(0)}{N} = \frac{V_p^{\,2}}{\bar{W}_A^\circ}+V_p^\circ+2g(q). \tag{5.5}$$

All that can be said is that the last two terms, which are of opposite sign, will tend to cancel.

In order to avoid the occurrence of large positive terms which would result from the forcing of electrons to occupy levels at the top of the band, it is necessary to assume that not all of the valence electrons of trivalent and divalent solutes enter the band.

6. SUMMARY

An attempt is made to calculate the heat of solution at zero concentration for monovalent–monovalent and monovalent–polyvalent systems using a "Sommerfeld-like" model for an alloy. The calculated heats of solution are of the correct order of magnitude. The model consists of a small rectangular well representing the solute, inside a large rectangular well representing the solvent. The non-self-consistent first-order perturbation calculation gives the energy of a phase mixture. The first-order approximation is identical in form to

the expression suggested by Friedel (1952, 1954 *a*, *b*) for the heat of solution of a polyvalent solute except for a change of sign. The non-self-consistent second-order perturbation problem is solved by means of an approximation due to Lennard-Jones (1930). The second-order calculation gives, in addition to the energy of a phase mixture, a negative term which is identified as the heat of solution. The approximation was checked and found to be in good agreement with an exact calculation of Huang (1948).

According to the present model the heat of solution arises primarily because the energy levels of the conduction band are perturbed by the potential associated with the solute atom. The heat of solution for monovalent–monovalent systems varies directly as the square of the difference in the Sommerfeld potentials of the pure components, and inversely with the mean energy of the solvent electrons. For monovalent–polyvalent systems the heat of solution varies in a like manner, although the idea of the Sommerfeld potential must be modified. Varley (1954), who used a "two-band" model, found an expression for the heat of solution which varies directly as the square of the difference in the Sommerfeld potentials, but inversely with the mean kinetic energy of the solute.

The calculation is refined by making it approximately self-consistent. The main reason for making the calculation self-consistent is to allow for the modification of the perturbing potential which results from the movement of charge. The movement of charge decreases the perturbing potential and hence the heat of solution. It is shown that the charge accumulation about a solute atom varies directly as the difference in the Sommerfeld potentials of the pure components, and inversely with the mean energy of the solvent electrons. For the copper–silver system and for gold dissolved in silver, the present calculations of the charge accumulation are in qualitative agreement with those of Arafa (1949) and Huang (1948) respectively.

For polyvalent solutes it is argued that all of the valence electrons must not enter the conduction band, for the heats of solution would then be positive.

Since the change in energy of both the solute and solvent ions cannot be treated by this model, it is not to be expected that the results of this calculation may be compared quantitatively with experiment. The model does, however, reproduce qualitatively the general properties observed experimentally.

The author wishes to express his appreciation to Mr. R. Talman for discussions.

APPENDIX

1. The Applicability of the Perturbation Method

Rojansky (1946) points out that a general rule for the convergence of the perturbation method is that the change in the energy of a level should be small in comparison with the separation between levels. The separation between the levels ΔW in the Sommerfeld model of a metal is equal to the inverse of the density of states $N(\mathfrak{E})$ which is given by Mott and Jones (1936), for example, and hence

$$\Delta W = \frac{4\pi^2}{\Omega}\left(\frac{\hbar}{2m}\right)^{3/2}\mathfrak{E}^{-1/2}, \tag{A.1}$$

where Ω is the volume and $\mathfrak{E}$ is measured from the bottom of the band. For copper the maximum value of $\mathfrak{E}$ is 7.1 ev. and hence, in a gram-atom of copper, the minimum separation of the levels is, by equation (A.1), 14×10^{-24} ev.; about two per cent of the levels have a separation twice as great as this. At the bottom of the band the spacing is of the order of 1×10^{-15} ev. In three dimensions, the first-order perturbation change in the energy level is

$$V_p\frac{\omega}{\Omega}=\frac{11.7}{7.1\times10^{24}}V_p=1.5\times10^{-24}V_p, \tag{A.2}$$

where ω and Ω are the volume per atom and volume per gram-atom of copper respectively. It is, therefore, to be expected that for perturbations of a few electron volts, reasonable results will be obtained for levels near the top of the band. For levels at the bottom of the band, quite large perturbations may be treated by this method. Since the ratio of the first-order perturbation to the separation between the levels is independent of the volume of the metal, these conclusions hold irrespective of the size of the metal specimen.

2. Evaluation of $W_k^{(1)}$ and the Generalization to Three Dimensions

Equation (2.5) shows that

$$W_k^{(1)}=W_k^{\circ}+V_p^{\circ}\left[\frac{\delta}{L}+\frac{1}{k\pi}\sin\left(k\pi-\frac{k\pi\delta}{L}\right)\right]. \tag{A.3}$$

If the levels are considered in pairs, so that $k=2m$ and $k=2m+1$, then

$$\begin{aligned}\frac{W_{2m}+W_{2m+1}}{2}&=\tfrac{1}{2}[W_{2m}^{\circ}+W_{2m+1}^{\circ}]+\frac{V_p^{\circ}}{2}\left[\frac{\delta}{L}+\frac{\delta}{L}-\frac{1}{2m}\frac{2m\pi\delta}{L}+\frac{1}{2m+1}\frac{(2m+1)\pi\delta}{L}\right.\\&\left.+\frac{1}{2m\pi}\left(\frac{2m\pi\delta}{L}\right)^3\frac{1}{3!}-\frac{1}{(2m+1)\pi}\left(\frac{(2m+1)\pi\delta}{L}\right)^3\frac{1}{3!}+\cdots\right]\\&\approx\tfrac{1}{2}[W_{2m}^{\circ}+W_{2m+1}^{\circ}]+V_p^{\circ}\frac{\delta}{L}.\end{aligned} \tag{A.4}$$

Thus, if the levels are taken in pairs, the mean energy of a level is altered by $V_p^{\circ}\delta/L$.

In two dimensions

$$V_p^{\circ}=V_p^{\circ}(x)\,.\,V_p^{\circ}(y) \tag{A.5}$$

and the normalized wave functions are

$$\psi_{kl}^{\circ}=\left(\frac{4}{L_xL_y}\right)^{\frac{1}{2}}\sin\frac{k\pi x}{L_x}\sin\frac{l\pi y}{L_y}, \tag{A.6}$$

where L_x and L_y are not in the ratio of integers, which ensures no degeneracy in the system. The first-order perturbation treatment involves products of integrals of the form

$$H'_{kl}=\frac{4}{L_xL_y}\int\sin^2\frac{k\pi x}{L_x}\,V_p(x)dx\int\sin^2\frac{l\pi y}{L_y}\,V_p(y)dy. \tag{A.7}$$

If the integrals are arranged in a two-dimensional array

$$\begin{matrix} 11 & 12 & 13 & \cdots & 1(N/2)^{\frac{1}{2}} \\ 21 & 22 & 23 & \cdots & \\ \vdots & & & & \vdots \\ (N/2)^{\frac{1}{2}}1 & & & & (N/2)^{\frac{1}{2}}(N/2)^{\frac{1}{2}} \end{matrix} \quad , \tag{A.8}$$

and the integrals then summed first horizontally and then vertically, it is seen, by equations (A.4) and (2.5), that the change in energy of the $N/2$ levels is given by $NV_p^{\circ}\delta_x\delta_y/L_xL_y$. The average change in energy of a level is thus $V_p^{\circ}\delta_x\delta_y/L_xL_y$. Similarly, in three dimensions, it is found that the average change in energy of a level is $V_p^{\circ}\delta_x\delta_y\delta_z/L_xL_yL_z$.

3. Discussion of the Approximation (3.2)

For $|W_l^{\circ}| < |W_k^{\circ}|$, that is, for levels above W_k°,

$$\sum_l{}' \frac{H'_{lk}H'_{kl}}{W_k^{\circ}-W_l^{\circ}} = \sum_l{}' \frac{H'_{lk}H'_{kl}}{W_k^{\circ}}\left[1+\frac{W_l^{\circ}}{W_k^{\circ}}+\left(\frac{W_l^{\circ}}{W_k^{\circ}}\right)^2+\cdots\right]. \tag{A.9}$$

For $|W_l^{\circ}| > |W_k^{\circ}|$, that is, for levels below W_k°,

$$\sum_l{}' \frac{H'_{lk}H'_{kl}}{W_k^{\circ}-W_l^{\circ}} = -\left\{\sum_l{}' \frac{H'_{lk}H'_{kl}}{W_l^{\circ}}\left[1+\frac{W_k^{\circ}}{W_l^{\circ}}+\left(\frac{W_k^{\circ}}{W_l^{\circ}}\right)^2+\cdots\right]\right\}. \tag{A.10}$$

The Lennard-Jones approximation is equivalent to neglecting all the terms in both equations (A.9) and (A.10) except

$$\sum_l{}' \frac{H'_{lk}H'_{kl}}{W_k^{\circ}} = \frac{(H'^2)_{kk}}{W_k^{\circ}} - \frac{(H'_{kk})^2}{W_k^{\circ}}. \tag{A.11}$$

This is also equivalent to neglecting W_l° in the denominator of

$$\sum_l{}' H'_{lk}H'_{kl}/(W_k^{\circ}-W_l^{\circ}). \tag{A.12}$$

Inspection shows that

$$\left|\sum_{l>k}{}' \frac{H'_{lk}H'_{kl}}{W_k^{\circ}}\right| < \left|\sum_{l>k}{}' \frac{H'_{lk}H'_{kl}}{W_k^{\circ}-W_l^{\circ}}\right| \tag{A.13}$$

and both terms are negative. Thus

$$\sum_{l>k}{}' H'_{lk}H'_{kl}/W_k^{\circ} \tag{A.14}$$

is a lower limit for the complete expression. It is also true that, near W_k°,

$$\left|\sum_{l<k}{}' \frac{H'_{lk}H'_{kl}}{W_k^{\circ}}\right| < \left|\sum_{l<k}{}' \frac{H'_{lk}H'_{kl}}{W_k^{\circ}-W_l^{\circ}}\right|, \tag{A.15}$$

where the term on the right-hand side is positive and the term on the left, which is to be added to the term on the left-hand side of the relation (A.13),

is negative. The question now arises as to whether or not this latter term can make

$$\text{(A.16)} \qquad \left| \sum_i{}' H'_{ik}H'_{ki}/W_k^\circ \right| > \left| \sum_i{}' H'_{ik}H'_{ki}/(W_k^\circ - W_i^\circ) \right| .$$

The result obtained by Huang (1948), and referred to in Section 3, indicates that for the Sommerfeld model of a monovalent metal it does not, and thus the approximation is reasonable.

REFERENCES

ARAFA, M. K. I. 1949. Proc. Phys. Soc. **62**, 238.
FRIEDEL, J. 1952. Phil. Mag. **43**, 153.
——— 1954*a*. Ann. phys. **9**, 158.
——— 1954*b*. Advances in Phys. **3**, 446.
HENRY, W. G. and ROGERS, J. L. 1956. Phil. Mag. **1**, 237.
HUANG, K. 1948. Proc. Phys. Soc. **60**, 161.
HUME-ROTHERY, W., MABBOT, G. W., and CHANNEL-EVANS, K. M. 1934. Phil. Trans. Roy. Soc. London, **233**, 1.
KLEPPA, O. J. 1956. J. Phys. Chem. **60**, 846, 852, 858.
KUBASCHEWSKI, O. and CATTERALL, J. A. 1956. Thermochemical data of alloys (Pergamon Press, New York).
LENNARD-JONES, J. E. 1930. Proc. Roy. Soc. (London), A, **129**, 598.
MOTT, N. F. and JONES, H. 1936. The theory of the properties of metals and alloys (Clarendon Press, Oxford), p. 55.
ORIANI, R. A. 1956. Acta. Met. **4**, 15.
PAULING, L. and WILSON, E. B. 1935. Introduction to quantum mechanics (McGraw-Hill Book Co., Inc., New York), pp. 204, 206.
ROJANSKY, V. 1946. Introductory quantum mechanics (Prentice-Hall Inc., New York), p. 204.
SHINOHARA, S. 1955. J. Fac. Sci., Hokkaido Univ., Ser. II, **4**, 377.
SLATER, J. C. 1930. Phys. Rev. **36**, 57.
SOMMERFELD, A. 1928. Z. Physik, **47**, 1.
VARLEY, J. H. O. 1954. Phil. Mag. **45**, 887.

NOTES

SHOCK-INDUCED PHYSICAL AND CHEMICAL SURFACE CHANGES ON OXIDE POWDERS

R. W. Nicholls and W. H. Parkinson

The shock tube is a very convenient source of transient high temperatures ($\sim 10^4$° K.) with which to excite spectra of solids which are difficult to excite in more conventional ways. A recent study of the luminosities produced in the shock excitation of about 20 inorganic oxides (Nicholls and Parkinson 1957) (using helium-driven shock waves in argon up to Mach 7.5) showed that 'clean', entirely molecular spectra of, for example, BO, AlO, VO, and WO were produced at the lowest Mach numbers (4), mixed molecular and atomic spectra occurred at medium Mach numbers, and entirely atomic spectra occurred at the highest attainable Mach numbers (7.5). Subsequent experiments, using time-resolved emission and time-resolved flash absorption spectroscopy, have established that the reflected shock wave (from the quartz window at the end of the tube) is largely responsible for the excitation.

It is the purpose of this communication to comment briefly upon unusual physical and chemical changes produced upon the surfaces of the shock-treated powder particles of α-hematite (Fe_2O_3), litharge (PbO), and metatungstic acid ($H_2W_4O_{13}$).

The most obvious gross change is in color. Fe_2O_3 turned from red to black, the intensity of the apparent blackening increasing with repeated shock treatment. PbO turned from yellow to gray, and $H_2W_4O_{13}$ turned from yellow to blue. Microscopic examination showed that the seat of the color change was on the grain surface, either a uniform change across the whole surface (PbO, $H_2W_4O_{13}$) or a localized change at sporadic points upon the surface (Fe_2O_3). Microscopic evidence of severe ablation of the surfaces is seen in the case of Fe_2O_3.

Fe_2O_3

Figures 1(*a*) and 1(*b*) are microphotographs of typical Fe_2O_3 grains before and after shock treatment at about 5700° K. (calculated temperature of the reflected shock wave) for about 2 milliseconds. The black spherical inclusions of about 10 μ diameter upon the ablated surface of the shocked grain are responsible for the color change. Further, repeated moderate shock treatment ($M_{\text{incid}} = 5$) was found to be more effective in increasing the surface density of the black inclusions than repeated treatment by stronger shock waves ($M_{\text{incid}} = 7.5$). The luminosity arising from the mild shock excitation was almost entirely of FeO, *A* and *B* band systems (Pearse and Gaydon 1950), while the luminosity arising from the stronger shock treatment was almost entirely of FeI lines. The shocked powder was also magnetically quite active.

A number of the black spheres were detached from parent grains and found to be the seat of magnetic activity. X-Ray powder photographs of the black spheres showed them to be Fe_3O_4 (magnetite or ferrosoferric oxide $FeO.Fe_2O_3$). This was confirmed by a wet chemical analysis, which established the presence of the ferrous ion in the spheres.

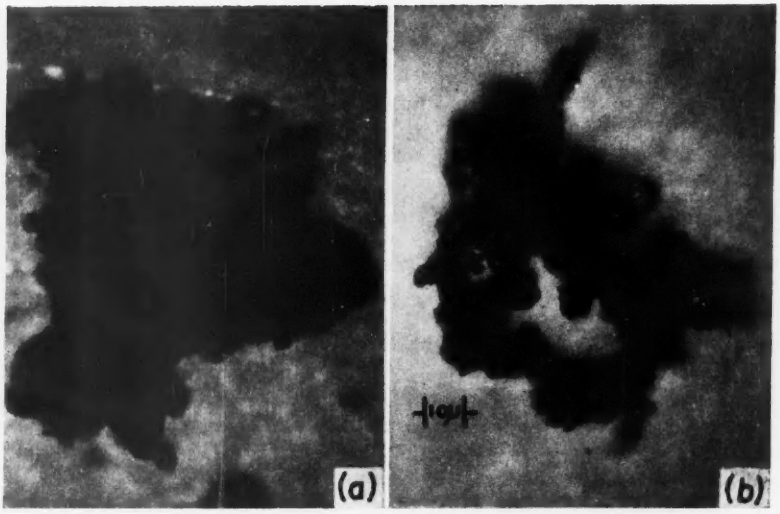

FIG. 1. Microphotographs at equal magnification of α-Fe_2O_3 grains before and after shock treatment. (*a*) Unshocked α-Fe_2O_3 grain. (*b*) Shocked (at Mach 5) α-Fe_2O_3 grain showing ablation and the black spherical inclusions of Fe_3O_4.

It is tempting to speculate that the Fe_3O_4 spheres were formed by a condensation of FeO radicals (which are certainly copiously present in the luminous vapor produced by the shock excitation as shown by the spectrum) upon the Fe_2O_3 surface with the formation of $FeO.Fe_2O_3$. Whether the FeO radicals were ablated from the grains by mild shock waves or whether individual atoms (Fe, O) were ablated and later combined to form FeO is a matter for further investigation. Similar observations were made upon ilmenite ($FeTiO_3$); the spectrum consisted of FeO (*A* and *B* systems) and TiO (alpha and beta systems) bands (Pearse and Gaydon 1950). Fe_3O_4 was again present on the grain surface after shock treatment. These observations may have some application to paleomagnetism.

PbO

Shock excitation of PbO powder at about $M_{\text{incid}} = 5$ (reflected temperature = 5700° K.) gave rise to luminosity which consisted almost entirely of the $A^1\Sigma^+ — X^1\Sigma^+$ and $B^1\Sigma^+ — X^1\Sigma^+$ band systems of PbO (Pearse and Gaydon 1950). Even under these relatively mild excitation conditions a few PbI lines were present and the observed band systems were weak. A color change from

yellow to gray was produced. Microscopic observation showed that the yellow grains of PbO (100 μ diameter) had been replaced by small spheres of 10 μ diameter of two types: shiny gray and fused yellow. The latter were probably fused PbO. X-Ray powder photographs of the former showed that they were either Pb or Pb+PbO (Sidgwick 1950). In this case the transient heating caused by the reflected wave evidently caused significant dissociation in addition to excitation.

$H_2W_4O_{13}$

Repeated mild shock treatment ($M_{\text{incid}} = 5$) of this compound caused a color change from yellow to blue. The spectrum of luminosity consisted almost entirely of a complex system of bands attributed to WO (Pearse and Gaydon 1950; Gatterer and Krishnamurthy 1952). The grains appear to be uniformly blue after shock treatment, and it seems likely that one of the higher tungsten oxides, e.g. W_4O_{11}, has been formed.

The work is proceeding, particular attention being paid to the quantitative aspects of ablation. Particle size and shape measurements which may have application to meteor physics are in progress.

ACKNOWLEDGMENTS

This work has been supported in part by the Defence Research Board of Canada through grant D.R.B.C. 5001-15 and in part by the Ontario Research Foundation. One of us (W.H.P.) is also indebted to the Ontario Research Foundation for a scholarship.

Gatterer, A. and Krishnamurthy, S. G. 1952. Nature, **169**, 543.
Nicholls, R. W. and Parkinson, W. H. 1957. J. Chem. Phys. **26**, 423.
Pearse, R. W. B. and Gaydon, A. G. 1950. The identification of molecular spectra (Chapman and Hall, Ltd., London).
Sidgwick, N. V. 1950. The chemical elements and their compounds (Clarendon Press, Oxford), p. 624.

Received January 16, 1958.
Department of Physics, University of Western Ontario,
London, Ontario.

THERMOELECTRICITY AT LOW TEMPERATURES
V. THE SUITABILITY OF LEAD AS A STANDARD REFERENCE MATERIAL[1]

J.-P. Jan,[2] W. B. Pearson, and I. M. Templeton

INTRODUCTION

In discussing the determination of an absolute scale of thermoelectric power at low temperatures, Pearson and Templeton (1955, III in this series) con-

[1]Issued as N.R.C. No. 4718.
[2]National Research Council Postdoctorate Fellow. Now at Laboratoire Suisse de Recherches Horlogères, Neuchâtel, Switzerland.

cluded that lead was probably the most suitable conductor to adopt as a standard reference metal. A redetermination of this scale for lead will be published shortly (Christian *et al.* 1958, VI in this series). However, before this redetermination of the absolute thermoelectric power was undertaken, it was necessary to establish that small amounts of common impurities in lead did not give rise to a large anomalous thermoelectric power at low temperatures. (The thermoelectric power of copper and gold at low temperatures is, for instance, very strongly affected by traces of certain impurities; as an example, the presence of only ~ 0.002 wt.% of iron changes the absolute thermoelectric power of copper from ~ 0 to -9 μv. per degree at 15° K.) It was also considered advisable, in view of the work reported by Preston-Thomas (1952), to establish that the presence of small amounts of impurities in the lead did not appreciably modify the thermoelectric properties in zero magnetic field in the temperature region immediately above the superconducting transition temperature. The present paper gives a brief account of these investigations.

EXPERIMENTAL MEASUREMENTS AND DISCUSSION

Measurements of the thermoelectric force, as a function of temperature, of dilute lead alloys containing bismuth, tin, indium, or cadmium in solid solution, shown in Figs. 1 and 2, were made by an improved form of the method already described by MacDonald and Pearson (1953, 1954). The thermoelectric force was measured relative to "spec-pure" lead (Johnson, Matthey & Co.) from which also the alloys were prepared. Alloys containing ~ 0.1 at.% Pd, or Au

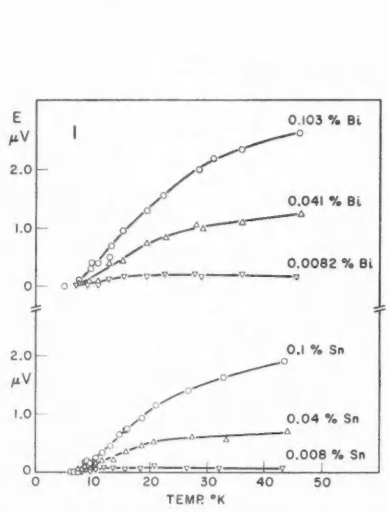

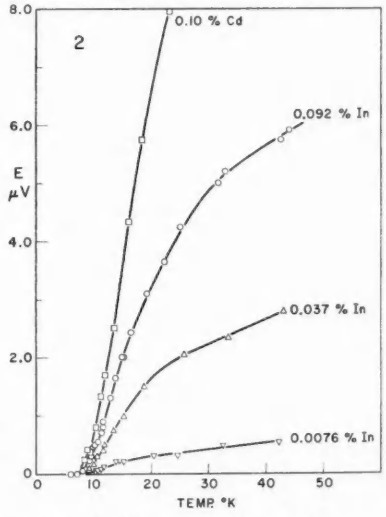

FIG. 1. Thermoelectric force of dilute Pb–Sn and Pb–Bi alloys relative to lead. Abscissa: temperature of "hot" junction; "cold" junction at 4.2° K.

FIG. 2. Thermoelectric force of dilute Pb–In and Pb–Cd alloys relative to lead. Abscissa: temperature of "hot" junction; "cold" junction at 4.2° K.

showed practically no net thermoelectric force relative to pure lead, but 'residual' resistance measurements ($R_{8°K}/R_{295°K}$), which were made as a check on the nominal compositions of all specimens, indicated that very little of these solutes actually entered into solid solution in the lead.

In order to search for any evidence of "foreshadowing" of the superconducting transition point, samples containing 0.04 at.% Bi and 0.04 at.% Cd were selected so that alloys were examined in which the electron concentration of lead had been both increased and decreased. Careful thermoelectric and resistivity measurements were made throughout the transition region (Figs. 3, 4, and 5), the absolute thermoelectric measurements being made against the superconducting alloy Nb_3Sn by the method described in Christian *et al.* (1958).

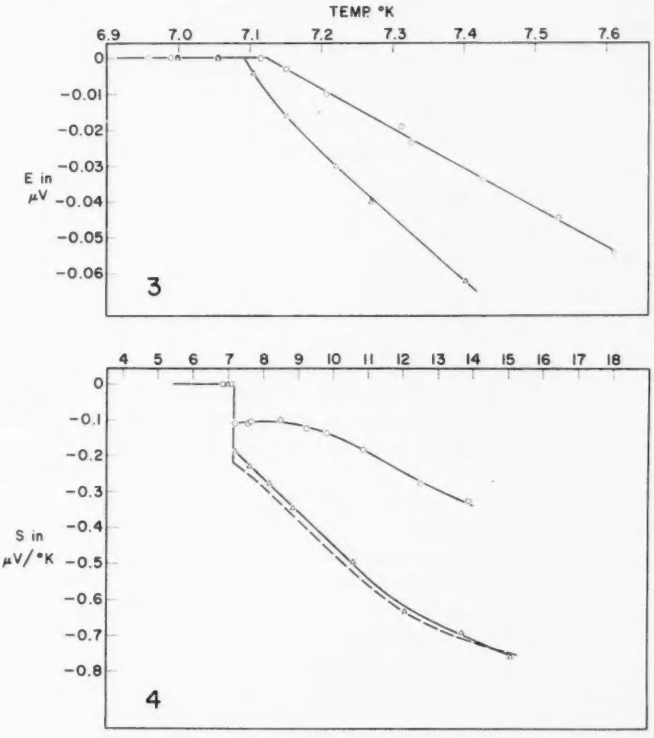

FIG. 3. Observed absolute thermoelectric force of a Pb – 0.04 at.% Bi alloy (△) and a Pb – 0.04 at.% Cd alloy (○) in zero field in the region of the superconducting transition temperature. Independent measurements of the transition temperatures of these alloys by an inductive method show that they actually transform at the same temperature as pure lead, i.e. $7.17_5 \pm 0.010°$ K.

FIG. 4. Absolute thermoelectric power of a Pb – 0.04 at.% Bi alloy (△) and a Pb – 0.04 at.% Cd. alloy (○) measured against the superconductor Nb_3Sn. – – – Absolute thermoelectric power of Johnson, Matthey and Co. Ltd. "spec-pure" lead from which the alloys were made.

The data shown in Figs. 1 and 2 indicate that small amounts of common impurities dissolved in lead do *not* give rise to any notable anomalous variation of thermoelectric power as a function of composition or of tempera-

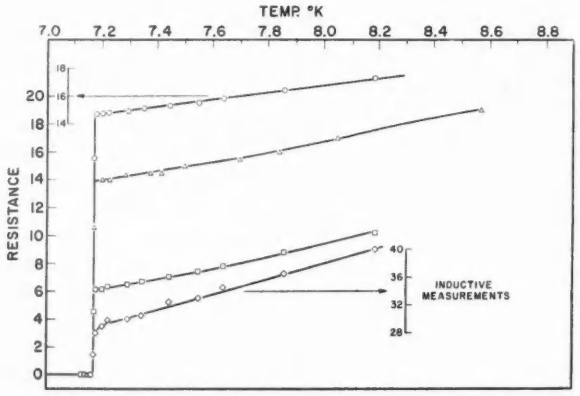

FIG. 5. Resistive and inductive measurements of zone-purified lead and dilute alloys in the vicinity of the superconductive transition.

□ zone-purified lead
△ Pb – 0.04 at.% Bi alloy
○ Pb – 0.04 at.% Cd alloy
} resistive measurements, current 1 or 2 ma.

◇ zone-purified lead — inductive measurements

ture, and only in the alloy containing 0.1 at.% Cd does the thermoelectric power relative to pure lead become fairly large, being about 0.6 μv./° C. between 10° and 20° K. It is thus clear that in the amounts in which these metallic impurities are present in *pure* lead (readily obtainable in a purity exceeding 99.99%), they should have no noticeable effect on its observed absolute thermoelectric power. Furthermore the impurities which we have chosen to examine are representative of elements lying in Groups I to V and VIII. The other common impurities of Groups II to V, if they enter solid solution in lead, would be expected to behave similarly to the elements we have studied, while the Group I elements and transition metals probably do not dissolve in lead. The data given in Figs. 3, 4, and 5 do not reveal any serious "foreshadowing" effects above the superconducting transition temperature, although a small effect may exist in the Pb–Bi alloy. We can therefore conclude (see also Pearson and Templeton 1955) that lead seems to be a most suitable reference material against which measurements of the absolute thermoelectric power of metals and alloys can be made.

We are grateful to Dr. D. K. C. MacDonald for his interest, and for discussions of this work.

REFERENCES

CHRISTIAN, J. W., JAN, J.-P., PEARSON, W. B., and TEMPLETON, I. M. 1958. Proc. Roy. Soc. (London), A (to be published).
MACDONALD, D. K. C. AND PEARSON, W. B. 1953. Proc. Roy. Soc. (London), A, **219**, 373.
——— 1954. Proc. Roy. Soc. (London), A, **221**, 534.
PEARSON, W. B. AND TEMPLETON, I. M. 1955. Proc. Roy. Soc. (London), A, **231**, 534.
PRESTON-THOMAS, H. 1952. Can. J. Phys. **30**, 626.

RECEIVED FEBRUARY 3, 1958.
DIVISION OF PURE PHYSICS,
NATIONAL RESEARCH COUNCIL,
OTTAWA, CANADA.

THE VALENCE STATE OF METALLIC LEAD[1]

W. B. PEARSON

A connection between cohesion and the effective sizes of the atoms in elemental metals has long been recognized by metallurgists; it provides, for instance, the basis for the conclusion that lead is divalent rather than quadrivalent in the metallic state (cf. Hume-Rothery and Raynor 1954). The failure of metallic lead to ionize the two electrons in "6*s* orbitals" is assumed from the abnormally large increase in the diameter of the metallic atoms found at Pb (and Tl) on proceeding along the Third Long Period of the Periodic Table. Such a conclusion is also consistent with the chemical evidence that the divalent state of lead is more stable than the quadrivalent state, and that lattice-spacing measurements of lead alloys (Tyzack and Raynor 1954) do not give any indication that the anomalous size of the metallic lead atom can, as in the case of aluminum, be interpreted in terms of "Brillouin zone effects" (Axon and Hume-Rothery 1948).

It appears to us difficult, however, to reconcile this view with the electrical properties of some dilute lead alloys, containing Cd, In, Sn, or Bi as solutes, which were examined at low temperatures. If the $6s^2$ electrons (of the free atom) remain bound in the solid state and are not concerned with cohesion (i.e. do not take part in the formation of resonating metallic bonds) we would expect lead to behave as if only two electrons were ionized when it is considered as an electrical conductor. From our experience of the behavior of heterovalent solutes in copper, silver, and gold (cf. Linde 1932) we would in these circumstances expect a homovalent impurity for lead to be one which also ionized two electrons. The data shown in Fig. 1, which are taken from thermoelectric and resistive measurements of dilute lead alloys containing various solute proportions (Jan *et al.* 1958), indicate that a homovalent impurity in lead is an atom lying in Group IV, not in Group II, since the electron scattering increases with valence difference on proceeding from Group IV to higher or lower groups. It seems worth while to draw attention to this fact,

[1]Issued as N.R.C. No. 4719.

particularly as the data of Fig. 1 were derived from alloys which contained only 0.008 to 0.1 at.% of each solute, and so it is unlikely that the electronic structure of the lead will have been changed by alloying.

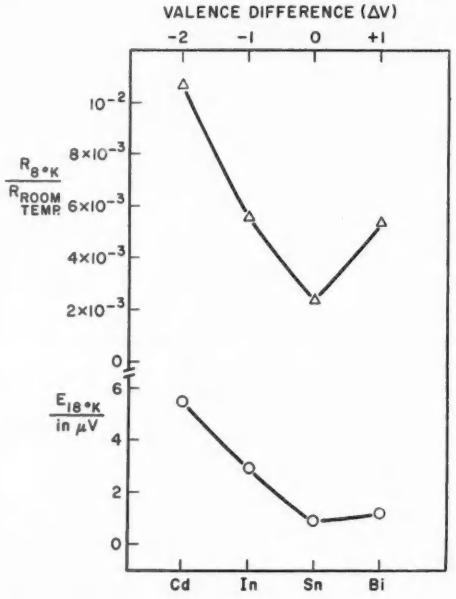

FIG. 1. Resistance ratio ($R_{8°\,K.}/R_{room\ temp.}$) and thermoelectric force generated against pure lead between 4.2° and 18° K. ($E_{4.2°\ to\ 18°\,K.}$) for dilute lead alloys containing 0.1 at.% Cd, In, Sn, or Bi.

AXON, H. J. and HUME-ROTHERY, W. 1948. Proc. Roy. Soc. (London), A, **193**, 1.
HUME-ROTHERY, W. and RAYNOR, G. V. 1954. The structure of metals and alloys (The Institute of Metals, London).
JAN, J.-P., PEARSON, W. B., and TEMPLETON, I. M. 1958. Can. J. Phys. **36**, 627.
LINDE, J. O. 1932. Ann. phys. [5], **15**, 219.
TYZACK, C. and RAYNOR, G. V. 1954. Acta Cryst. **7**, 505.

RECEIVED FEBRUARY 7, 1958.
DIVISION OF PURE PHYSICS,
NATIONAL RESEARCH COUNCIL,
OTTAWA, CANADA.

THE RATIO OF THE NUCLEAR *g*-FACTORS FOR B^{11} AND B^{10}[1]

W. BROUWER[2] AND H. E. PETCH

The nuclear magnetic resonance (n.m.r.) and atomic hyperfine structure

[1]The research for this paper was supported by the Defence Research Board of Canada, under Grant No. 9510-08.
[2]Holder of a National Research Council of Canada Bursary, 1957–58.

methods for the measurement of a nuclear g-factor depend upon the interaction of the nuclear magnetic moment with an applied external magnetic field or with an internal atomic field, respectively. In the n.m.r. method the ratio of the resonance frequencies for two isotopes gives the ratio of their nuclear g-factors directly since the applied external field cancels in the ratio. However, for some pairs of isotopes the terms containing the effects of the internal fields differ slightly. In such cases, the ratio of the A's, the internal interaction constants, obtained by the atomic hyperfine structure method is not exactly equal to the ratio of the g's. Deviations between the values determined by the two methods, which lead to the so-called h.f.s. anomalies, have been interpreted (Bohr and Weisskopf 1950) as due, at least in part, to the effect of the finite size of the nucleus.

It was recently pointed out to us that, to establish the h.f.s. anomaly for boron, a more precise value is needed for the ratio of the nuclear g-values of B^{11} and B^{10}. The value for the ratio of the A's calculated from a hyperfine structure measurement by Title (1957) is

$$A(B^{11})/A(B^{10}) = 2.9867 \pm 0.0002.$$

This value is to be compared with Bitter's (1949) n.m.r. value of

$$g(B^{11})/g(B^{10}) = 2.9861 \pm 0.0009.$$

The ratio of the A's agrees with that of the g's to within the latter's rather large limits of error so that there appears to be no h.f.s. anomaly. The object of this work was to obtain, using n.m.r. techniques, a more precise value of the ratio of the g's for B^{11} and B^{10} with which to compare the value for the ratio of the A's obtained from h.f.s. measurements.

The ratio of the nuclear g-factors for a pair of isotopes is given directly by the ratio of the resonance frequencies of the two nuclear species in an externally applied magnetic field. The g-factor ratio can often be determined to a much greater accuracy than either of the g-factors alone because the frequency ratio for isotopic pairs is not subject to several corrections which normally have to be applied. To obtain the greatest possible accuracy, the experimental arrangement was designed to permit simultaneous measurement of the two resonance frequencies. Two radio-frequency coils were wound, with their axes mutually perpendicular, on a spherical container which held 2 cc. of sample. Each coil formed the inductive branch of the tank circuit of a separate marginal oscillator. Resonance conditions were made repetitive by modulating the steady magnetic field with an amplitude greater than the signal width and a frequency of 60 c./sec. The recurrent resonance signals from the two marginal oscillators were, after detection and amplification, simultaneously displayed on a Dumont Type 322-A double-beam oscilloscope. The horizontal traces of the oscilloscope were driven by the same sinusoidal signal that modulated the steady magnetic field. The frequency of the marginal oscillator used to detect the B^{11} resonance was maintained constant at 20 Mc./sec.; it was continuously checked against the 20 Mc./sec. output from a General Radio unit time/frequency calibrator Type No. 1213-C which in turn was periodically calibrated by means of the 10 Mc./sec. signal from

WWV. The steady magnetic field was then adjusted ($H_0 \approx 14{,}640$ gauss) until the B^{11} signal from the 20 Mc./sec. oscillator was at the mid-point of one of the oscilloscope traces. The frequency of the second marginal oscillator was then adjusted until the B^{10} resonance signal appeared at the mid-point of the second oscilloscope trace. When exact matching of the signals had been attained, the frequency (6.69728 Mc./sec.) of the B^{10} marginal oscillator was measured with a Hewlett-Packard frequency counter Model 524A. This instrument was also checked against WWV at 10 Mc./sec.

In a preliminary investigation, the boron isotopes were studied in a supersaturated aqueous solution of $NaBO_2$. Matching of the two signals was difficult because of the large disparity in intensity caused by the low natural abundance and small g-factor of B^{10} relative to B^{11}. A specimen was therefore prepared by allowing powdered boron, enriched in B^{10}, to react with fused NaOH. A supersaturated aqueous solution of the reaction product gave good B^{10} and B^{11} signals of nearly equal intensities and total widths of approximately 1.9 gauss and 0.9 gauss respectively. At the same position the field inhomogeneity limited the proton line width to about 0.3 gauss.

The mean ratio of the resonance frequencies, obtained by three different observers in this laboratory, is

$$f(B^{11})/f(B^{10}) = g(B^{11})/g(B^{10}) = 2.98629 \pm 0.00002.$$

The calculated probable error corresponds to a matching of the two signals to within about one-tenth of the B^{11} line width which seems quite reasonable in view of the difficulty of exactly matching two signals of different widths. No evidence of systematic errors was found. This more precise value of the ratio of the g-factors of B^{11} and B^{10} is in good agreement with the value previously determined by n.m.r. methods by Bitter (1949) but it differs from the ratio of Title's (1957) A's by an amount which is probably significant. Confirmation of this point must await a more precise measurement of the hyperfine structure.

The writers are grateful to Dr. Hin Lew of the National Research Council of Canada who suggested this problem and supplied the sample of B^{10}. We are also obliged to Drs. Duckworth, Graham, and Kleerekoper, all of McMaster University, whose contributions of advice or equipment materially aided the progress of this work. We are happy to have this opportunity to acknowledge the generous contribution made by the Ontario Research Foundation for the purchase of the large electromagnet.

Bitter, F. 1949. Phys. Rev. **75**, 1326.
Bohr, A. and Weisskopf, V. F. 1950. Phys. Rev. **77**, 94.
Title, R. S. 1957. Private communication of a preliminary value obtained at the National Research Laboratories, Ottawa.

Received February 5, 1958.
Departments of Physics and of Metallurgy and Metallurgical Engineering,
Hamilton College,
McMaster University,
Hamilton, Ontario.

COSMIC-RAY INTENSITY VARIATIONS AT SEA LEVEL DURING MAGNETIC-STORM PERIODS

G. RAMASWAMY* AND S. D. CHATTERJEE

In this paper we will discuss some of the geophysical aspects of cosmic radiation in the light of ion-chamber measurements taken at Ottawa during February–May, 1951 (Chatterjee and Bloom 1955). This period was chosen for two reasons. Firstly, though the year 1951 was relatively quiet magnetically, the magnetic activity was higher during the first half than in the second half. Secondly, during the same period, intensity measurements were made at Berkeley, California, by Chasson using wide-angle triple-coincidence-counter telescopes, and an analysis of magnetic-storm effects on these intensity variations has been reported (Chasson 1954). Since both data were obtained at sea level, some comparison could be validly attempted.

It is well known that the time variations in cosmic radiation are due in major part to the changes in the distribution of atmospheric mass. By application of what is known as 'barometric correction' to the sea-level intensity much of the effects of these changes can be removed and the corrected intensity may then be examined for possible magnetic-storm effects.

Figure 1 shows the variations of cosmic-ray intensity during February–May, 1951, when corrected for barometric pressure. The intensity variations are plotted as daily percentage deviations from the prestorm average. This

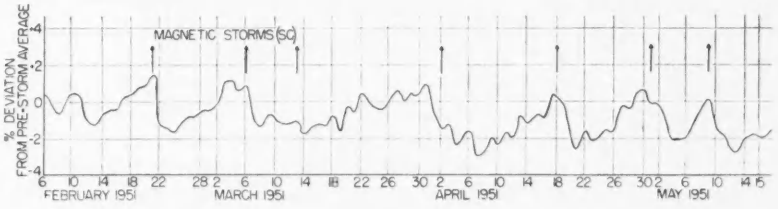

FIG. 1. Variations in cosmic-ray intensity corrected for barometric pressure.

type of continuous plotting of variations is preferable to short-interval charts used by some earlier investigators like Hess (1940). For, one cannot say from short-interval charts whether the intensity changes are but part of the general pattern of variations or are different from it. A most noticeable feature of this curve is the general irregular pattern in the variations. Whether this feature can be attributed to the pressure–altitude effect (due to decay of μ-mesons) cannot be answered with definiteness. However, as Chasson (1954) has observed, a simple barometric correction would give a set of corrected intensities reliable enough to be used in examining for magnetic-storm effects.

*Now at Standard Vacuum Oil Co., Producing Operations, Calcutta, India.

Cosmic-ray intensity decreases, immediately after the commencement of magnetic storms, are observable from February 21, March 6, April 18, and May 9. It might be said that these decreases are not within the general pattern of variations and are therefore physically real. These decreases can therefore be called simultaneous decreases and might be explained as being due to the magnetic storms. The decrease from May 1 is not sufficiently clear to be ascribed to the storm commencing May 1. The storm of March 13 does not seem to have an effect on the intensity, except probably to maintain the decrease for some days to come. The variation during the storm period commencing April 2 is interesting, for the decrease in intensity begins on March 31 itself and continues for several days up to April 7. To call this phenomenon an example of prestorm effect may not be wrong, if the marked irregularities of the curve during this period are considered as being due to other factors or to random causes.

Of the four cosmic-ray effects associated with magnetic storms, viz., (1) prestorm decrease, (2) simultaneous decrease, (3) delayed decrease, and (4) null effect, the most noticeable in our data appears to be the simultaneous decrease. However, examples of the other effects are also present in our data. Because of these exceptions no precise relationship of magnetic-storm variations can be attempted. Chasson's data give examples of all these effects and his results are more inconclusive than ours. Consideration of our results with those of Chasson shows that there is no good agreement between these results. It is of interest to note that correlating the time variations and cosmic-ray intensity (corrected for barometric effect) with the corresponding indices of geomagnetic activity (obtained from Agincourt Observatory) gives an inverse relationship in the sense that their correlation coefficient is highly negative (its value being -0.81). This negative correlation suggests that there is a tendency for relatively lower cosmic-ray intensity on magnetically disturbed days than during quiet periods. This same conclusion was obtained by Forbush (1938) in an earlier analysis of Huancayo data by comparing the cosmic-ray intensity for quiet and disturbed days, averaged for several months.

As yet, no theory constructed has been successful in explaining the behavior of cosmic-ray intensity during magnetic-storm periods. However, from a comparison of our results and the studies of several others it can be said that in a majority of cases there is a decrease in cosmic-ray intensity associated in some manner with the magnetic storms and their sudden commencement. Whether this decrease is simultaneous or whether this is characterized by any lag or lead in time can not be adequately described with a knowledge of current studies.

The measurements were taken while one of us (S. D. C.) was holding a National Research Council Postdoctorate Fellowship at Ottawa. The writers wish to acknowledge with thanks the generous help given by Dr. D. C. Rose, in whose laboratory the measurements were taken.

ALTMANN, G. O., WALKER, H. N., and HESS, V. F. 1940. Phys. Rev. **58**, 1011.
CHASSON, R. L. 1954. Phys. Rev. **96**, 1116.
CHATTERJEE, S. D. and BLOOM, J. N. 1955. Can. J. Phys. **33**, 577.
FORBUSH, S. E. 1938. Terrestrial Magnetism and Atmospheric Elec. **43**, 203.

RECEIVED FEBRUARY 7, 1958.
JADARPUR UNIVERSITY,
CALCUTTA, INDIA.

LETTERS TO THE EDITOR

Under this heading brief reports of important discoveries in physics may be published. These reports should not exceed 600 words and, for any issue, should be submitted not later than six weeks previous to the first day of the month of issue. No proof will be sent to the authors.

Nuclear Orientation of Mn^{54} in Antiferromagnetic Single Crystals

It has been suggested by various people that nuclei might be aligned in an antiferromagnetic single crystal at low temperatures (e.g. Daunt 1951; Gorter 1957). In all the cases so far reported, interactions in general, and antiferromagnetism in particular, appear to reduce nuclear orientation rather than to enhance it. For example, the anisotropy of γ-rays from Mn^{54} in cerium magnesium nitrate is much reduced on account of interactions, and is reduced still further below 0.003° K., the Néel temperature of the salt (Grace *et al.* 1954). We wish to report that we have used the interactions in an antiferromagnetic single crystal to produce nuclear alignment, and claim that this represents a significant extension of the class of substances in which nuclear alignment can be produced.

Three single crystals of $MnCl_2.4H_2O$, with a total weight of about 250 mg., containing about 3 microcuries of Mn^{54} were mounted in parallel crystallographic orientation in a demagnetization cryostat. They were sandwiched between cylinders of compressed potassium chrome

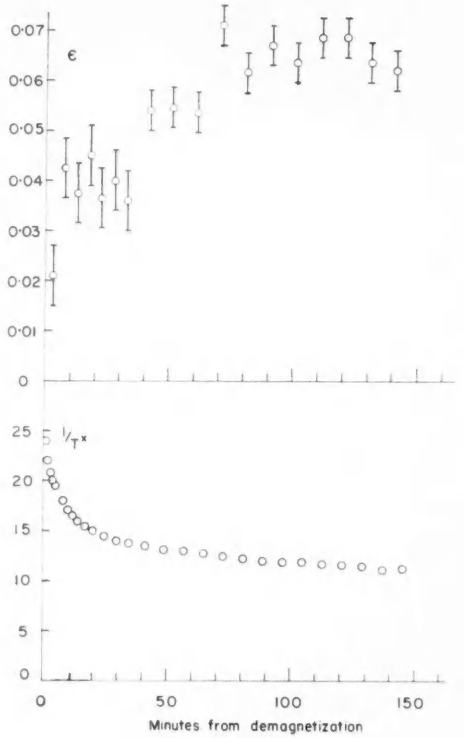

FIG. 1.

alum, and the space between was filled with a sludge of alum powder and Apiezon oil B. The whole sample was cooled by adiabatic demagnetization, and observations were made as the specimen warmed up over a period of $2\frac{1}{2}$ hours. No external magnetic field was applied during this time. Manganese chloride crystallizes in the monoclinic system, and its external morphology has been described by Groth (1906), whose nomenclature we use. According to Gijsman (1957) the direction of easy magnetization is the crystallographic c-axis, and the next preferred axis is the b-axis. We placed scintillation counters along the crystallographic b and c axes and counted the γ-rays emitted in those directions. Mn^{54} decays by K capture followed by the emission of an $E2$ gamma ray of 835 kev. energy (Grace *et al.* 1954). We can define an anisotropy of γ-ray emission ϵ, by the equation $\epsilon = (I_b - I_c)/I_b$ where, for example, I_b is the intensity of γ-ray emission along the b-axis. Measurements were also made of T^*, the magnetic temperature of the chrome alum, during the warm-up period. Figure 1 shows ϵ and $1/T^*$ as functions of time from demagnetization.

It is noticed that the manganese nuclei were in fact aligned along the c-axis. The magnetic moment of Mn^{54} is so far unknown, so we are unable to estimate the internal field acting on the manganese nuclei. The time required for the anisotropy to develop, about half an hour, is not inconsistent with estimates of the spin–lattice relaxation time, made according to the theory of Moriya (1956).

A similar effect is seen in $MnBr_2.4H_2O$, and the results of an exactly similar experiment are shown in Fig. 2. The axis of preferred orientation in this salt is also the c-axis (Bolger 1955; Gijsman 1955).

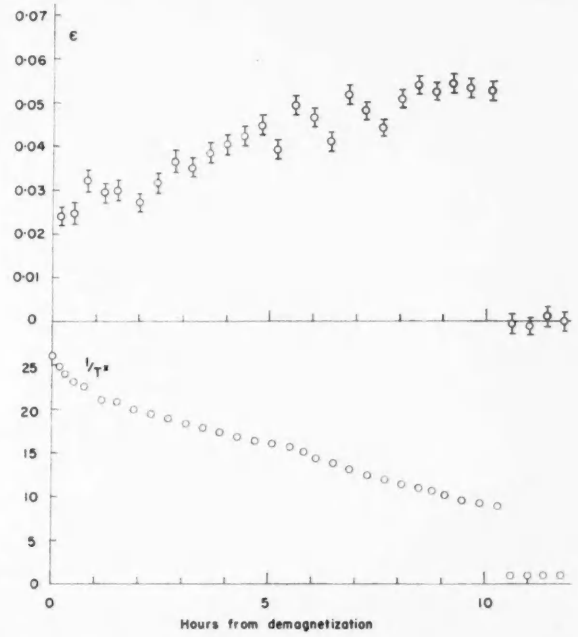

FIG. 2. The salt was warmed up to the temperature of the helium bath after 10.6 hours, to take a normalization count. The normalization count is included on this figure to indicate the stability of the counters. The relaxation time in $MnBr_2.4H_2O$ is longer than in $MnCl_2.4H_2O$, probably because the Néel temperature of $MnBr_2.4H_2O$ is higher than that of $MnCl_2.4H_2O$.

This work was carried out under contract from Atomic Energy of Canada Ltd., to whom grateful acknowledgment is made. One of us (M.A.R.L.) acknowledges the award of a National Research Council Studentship.

BOLGER, B. 1955. Communications du Conférence de Physique des Basses Températures, Paris (Institut International du Froid), p. 244.
DAUNT, J. C. 1951. Proceedings of an International Conference on Low Temperature Physics at Oxford, p. 157.
GIJSMAN, H. M. 1955. Communications du Conférence de Physique des Basses Températures, Paris (Institut International du Froid), p. 202.
GIJSMAN, H. M. 1957. Private communication.
GORTER, C. J. 1957. Proceedings of an International Conference on Low Temperature Physics at Oxford, p. 158.
GRACE, M. A., JOHNSON, C. E., KURTI, N., LEMMER, H. R., and ROBINSON, F. N. H. 1954. Phil. Mag. **45**, 1192.
GROTH, P. 1906. Chemische Krystallographie, Vol. 1 (Verlag von Wilhelm Engelmann, Leipzig), p. 245.
MORIYA, T. 1956. Progr. Theoret. Phys. (Kyoto), **16**, 641.

RECEIVED FEBRUARY 19, 1958.
DEPARTMENT OF PHYSICS,
UNIVERSITY OF BRITISH COLUMBIA,
VANCOUVER, B.C.

J. M. DANIELS
M. A. R. LEBLANC

Long τ_2 Lifetimes from Positronium Annihilations in Liquid Argon and Liquid Nitrogen*

The time spectra of positron decays in liquid argon and liquid nitrogen have been investigated using a standard coincidence circuit (Bell, Graham, and Petch 1952). The source was a finely deposited layer of $Na^{22}Cl$ on 1.6 mg./cm.^{2} aluminum foil and was placed in a monax cryostat of $\frac{3}{4}$ in. external diameter. Two-inch-thick NaI(Tl) phosphors in conjunction with RCA 6342 photomultipliers were used as detectors. The resolving time, $2\tau_0$, of the circuit was 3.4×10^{-9} sec. at 60% coincidence efficiency, and 5.2×10^{-9} sec. at 90% coincidence efficiency, with mean drop-off rates of 8×10^{-10} sec. In this way over 1000 true coincidences per minute were detectable without using a source so strong as to overwork the photomultipliers at the very high operating voltages necessary for such high resolution (~2400 volts).

Measurements revealed τ_2 components, such as are normally associated with the formation of triplet positronium, in both liquids; see Fig. 1 and Table I. The values of I_2 in Table I were calculated making an allowance for the absorption of positrons in the source materials.

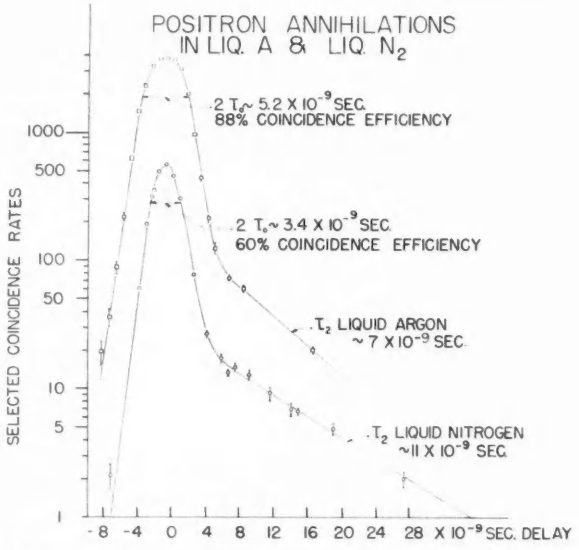

FIG. 1. Time spectra for positron decays in argon and nitrogen liquids of 99.99% purity.

*This work has been assisted in part by the Defence Research Board of Canada under Grant No. 9510-11.

this allowance was measured experimentally. A calculated correction for backscattering into the source materials is also included: the backscattering causes less than 10% of all positrons to annihilate in the source.

TABLE I

TRIPLET POSITRONIUM ANNIHILATION DATA

Substance	Lifetime τ_2, 10^{-9} sec. units	Intensity I_2, %	Temperature, °K.
Liquid argon 99.99% purity	6.9±0.7	7±1	87.55±0.15
Liquid nitrogen 99.99% purity	11.3±0.5	15±2	77.5 ±0.1

Errors in τ_2 are 2×standard deviation+an allowance for calibration errors.
Errors in I_2 are merely estimates.

No observable temperature effect was found in liquid argon, but this substance is only liquid over a range of 4 centigrade degrees.

These τ_2 components are interesting on account of their long mean-life which is far in excess of values reported for any other liquids except liquid helium (see Table II). De Benedetti and Siegel (1954) state that the number of three-quantum annihilations in liquid nitrogen is "of the same order as that expected from an equal number of positrons stopping in a solid metal". This observation is in agreement with previous observations of R. L. Graham and myself (1955, 1956, unpublished) who observed no τ_2 component in liquid nitrogen, indicating that either positronium was not formed or the triplet lifetime was highly quenched. These earlier results can now be understood if one assumes a small percentage of oxygen (a very common impurity in commercial nitrogen) to have been present in both de Benedetti's and our samples of liquid nitrogen. The effect of the oxygen is to reduce the τ_2 lifetime by converting triplet positronium to singlet; this arises as a result of the magnetic moment of the oxygen molecule. Recent experiments at this laboratory (1957) with commercial grade liquid nitrogen again revealed no τ_2 component.

TABLE II

TRIPLET POSITRONIUM ANNIHILATION IN PURE LIQUIDS

Liquid	Temp., °K.	τ_2, 10^{-9} sec. units	I_2, %	Reference
Isopropyl alcohol	293	2.3±0.4	~30	Bell and Graham (1953)
Water	293	1.7±0.2	~30	Bell and Graham (1953)
Water	293	1.8±0.1*	21±5*	Green and Bell (1957)
Benzene	293	2.67±0.08	31±3	Berko and Zuchelli (1956)
p-Dioxane	293	2.67	36±7	Green and Bell (1957)
Naphthalene	353–373	2.68	29	Landes, Berko, and Zuchelli (1956)
Ethylenediamine	293	1.8±0.2		Hogg, Sutherland, Paul, and Hodgins (1956)
Ammonia	193	1.7±0.2		Hogg, Sutherland, Paul, and Hodgins (1956)
Helium I	4.2	120±20	16±2	Wackerle and Stump (1957)
Helium I	4.2	91±3†	15.5±2.5‡	Paul and Graham (1957)
Helium II	1.4	84.5±4†	15.5±2.5	Paul and Graham (unpublished)

*Authors specified that these are standard errors.
†Errors are 2×standard deviation (statistical)+allowance for calibration errors.
‡The value published by Paul and Graham was 13% but was in error owing to an arithmetical mistake.

Deutsch (1952), working with argon gas, observed that oxygen would induce ortho–para conversion in positronium with a molecular cross-section $\sigma = 4\times10^{-19}$ cm.^{2} This value will have been determined by assuming that positronium was in thermal equilibrium with the gas, and substituting the appropriate value of v, the positronium velocity, in

$$\sigma v = 3.1\times10^{-12} \text{ cm.}^3/\text{sec.}$$

The product σv will be referred to as the "volume rate". A study of the effect of oxygen in liquid argon has been made using a new five-channel adaptation of the circuit of Bell, Graham, and Petch (1952). With this circuit the counting rates at five points on the τ_2 "tail" of a liquid argon resolution curve are simultaneously observed. Figs. 2 and 3 show some results. The quenching effect of oxygen is evidence that the τ_2 component is due to the formation of triplet positronium. The value for the "volume rate" due to oxygen in liquid argon is computed from Fig. 3 to be $\sigma v = 9.7\times10^{-12}$ cm.^{3}/sec. per molecule, more than three times Deutsch's value. While there is no a priori reason why these two observed volume rates should agree, they would have the same value if σ varied inversely with positronium velocity. If therefore a simple gas kinetic picture for positronium collisions in liquid argon is justifiable, it can be concluded that σ does not follow a $1/v$ law. Volume rates have been compared here instead of cross sections in order to avoid making any assumption about thermalization of positronium in liquid argon.

The wide difference in the two volume rates would be clarified by an investigation of the variation of σ with v. Measurements on the quenching of triplet positronium by oxygen in argon gas over a range of temperatures, say 100° K. to 270° K., would yield σ as a function of v, at least over a limited range of positronium velocities.

Measurements on liquid nitrogen are being continued at this laboratory.

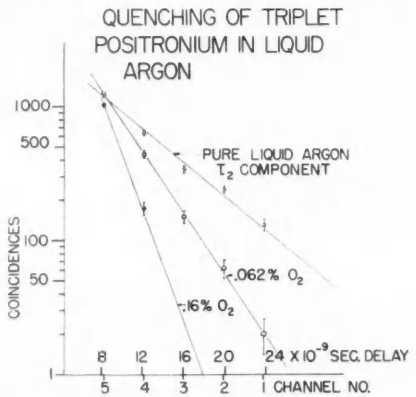

FIG. 2. τ_2 components of delayed annihilations in liquid argon, each obtained in a single run using a five-channel circuit. These results were obtained with one filling of the Dewar with liquid argon.

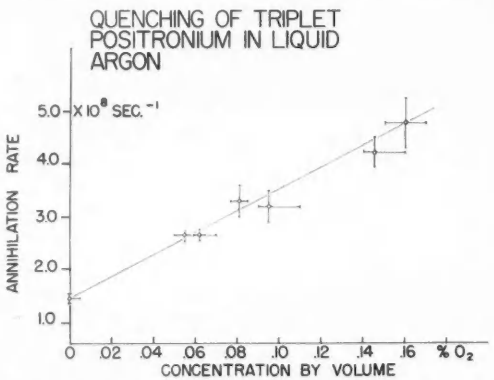

FIG. 3. Plot of reciprocal of τ_2 in liquid argon against % volume of liquid oxygen added.

I am indebted to Atomic Energy of Canada Limited, Chalk River, for the continued loan of some equipment, and to the Physics Department, Queen's University, for a similar loan. I would also like to thank Dr. B. G. Hogg and Dr. D. H. Rogers for the interest they have shown in this work, and for helpful discussions.

BELL, R. E. and GRAHAM, R. L. 1953. Phys. Rev. **90**, 644.
BELL, R. E., GRAHAM, R. L., and PETCH, H. E. 1952. Can. J. Phys. **30**, 35.
BERKO, S. and ZUCHELLI, A. J. 1956. Phys. Rev. **102**, 724.
DE BENEDETTI, S. and SIEGEL, R. 1954. Phys. Rev. **94**, 955.
DEUTSCH, M. May, 1952. Mass. Inst. Technol. L.N.S.E. Progress Report, p. 174.
GREEN, R. E. and BELL, R. E. 1957. Can. J. Phys. **35**, 398.
HOGG, B. G., SUTHERLAND, T. H., PAUL, D. A. L., and HODGINS, J. W. 1956. J. Chem. Phys. **25**, 1082.
LANDES, H. S., BERKO, S., and ZUCHELLI, A. J. 1956. Phys. Rev. **103**, 828.
PAUL, D. A. L. and GRAHAM, R. L. 1957. Phys. Rev. **106**, 16.
WACKERLE, J. and STUMP, R. 1957. Phys. Rev. **106**, 18.

RECEIVED MARCH 3, 1958.
D. A. L. PAUL
DEPARTMENT OF PHYSICS,
ROYAL MILITARY COLLEGE,
KINGSTON, ONTARIO.

CANADIAN JOURNAL OF PHYSICS

Notes to Contributors

Manuscripts

(i) **General.** Manuscripts, in English or French, should be typewritten, double spaced, on paper 8½×11 in. **The original and one copy are to be submitted.** Tables and captions for the figures should be placed at the end of the manuscript. Every sheet of the manuscript should be numbered.

Style, arrangement, spelling, and abbreviations should conform to the usage of recent numbers of this journal. Names of all simple compounds, rather than their formulas, should be used in the text. Greek letters or unusual signs should be written plainly or explained by marginal notes. Superscripts and subscripts must be legible and carefully placed.

Manuscripts and illustrations should be carefully checked before they are submitted. Authors will be charged for unnecessary deviations from the usual format and for changes made in the proof that are considered excessive or unnecessary.

(ii) **Abstract.** An abstract of not more than about 200 words, indicating the scope of the work and the principal findings, is required, except in Notes.

(iii) **References.** References should be listed **alphabetically by authors' names,** unnumbered, and typed after the text. The form of the citations should be that used in current issues of this journal; in references to papers in periodicals, titles should not be given and only initial page numbers are required. The names of periodicals should be abbreviated in the form given in the most recent *List of Periodicals Abstracted by Chemical Abstracts.* All citations should be checked with the original articles and each one referred to in the text by the authors' names and the year.

(iv) **Tables.** Tables should be numbered in roman numerals and each table referred to in the text. Titles should always be given but should be brief; column headings should be brief and descriptive matter in the tables confined to a minimum. Vertical rules should not be used. Numerous small tables should be avoided.

Illustrations

(i) **General.** All figures (including each figure of the plates) should be numbered consecutively from 1 up, in arabic numerals, and each figure referred to in the text. The author's name, title of the paper, and figure number should be written in the lower left corner of the sheets on which the illustrations appear. Captions should not be written on the illustrations (see Manuscripts (i)).

(ii) **Line Drawings.** Drawings should be carefully made with India ink on white drawing paper, blue tracing linen, or co-ordinate paper ruled in blue only; any co-ordinate lines that are to appear in the reproduction should be ruled in black ink. Paper ruled in green, yellow, or red should not be used. All lines should be of sufficient thickness to reproduce well. Decimal points, periods, and stippled dots should be solid black circles large enough to be reduced if necessary. Letters and numerals should be neatly made, preferably with a stencil (**do NOT use typewriting**) and be of such size that the smallest lettering will be not less than 1 mm. high when reproduced in a cut 3 in. wide.

Many drawings are made too large; originals should not be more than 2 or 3 times the size of the desired reproduction. Whenever possible two or more drawings should be grouped to reduce the number of cuts required. In such groups of drawings, or in large drawings, full use of the space available should be made; the ratio of height to width should conform to that of a journal page (4⅝×7⅛ in.), but allowance must be made for the captions.

The original drawings and one set of clear copies (e.g. small photographs) are to be submitted.

(iii) **Photographs.** Prints should be made on glossy paper, with strong contrasts. They should be trimmed so that essential features only are shown and mounted carefully, with rubber cement, on white cardboard, with no space between them. In mounting, full use of the space available should be made to reduce the number of cuts required (see Illustrations (ii)). Photographs or groups of photographs should not be more than 2 or 3 times the size of the desired reproduction.

Photographs are to be submitted in duplicate; if they are to be reproduced in groups one set should be mounted, the duplicate set unmounted.

Reprints

A total of 50 reprints of each paper, without covers, are supplied free. Additional reprints, with or without covers, may be purchased at the time of publication.

Charges for reprints are based on the number of printed pages, which may be calculated approximately by multiplying by 0.6 the number of manuscript pages (double-spaced typewritten sheets, 8½×11 in.) and including the space occupied by illustrations. An additional charge is made for illustrations that appear as coated inserts. Prices and instructions for ordinary reprints are sent out with the galley proof.

Any reprints required in addition to those requested on the author's reprint requisition form must be ordered officially as soon as the paper has been accepted for publication.

Contents

Printed in Canada *by* University of Toronto Press